Aerobraking Analysis for the Orbit Insertion Around Jupiter

a project presented to
The Faculty of the Department of Aerospace Engineering
San José State University

in partial fulfillment of the requirements for the degree
Master of Science in Aerospace Engineering

by

Neerja Nisha Bangar

May 2018

approved by

Prof. Jeanine Hunter
Faculty Advisor

San José State
UNIVERSITY

Table of Contents

Chapter 1: Aerobraking Analysis for Jupiter Orbit Insertion

1.1 Introduction 04
1.2 Motivation 06
1.3 Literature Review 07
1.3.1 Hiten 07
1.3.2 Magellan 08
1.3.3 Mars Global Surveyor 09
1.3.4 Mars Odyssey 11
1.3.5 Mars Reconnaissance Orbiter 12
1.3.6 Venus Express 12
1.4 Project Proposal 13
1.5 Methodology 14
1.6 Conclusion 14
1.7 References 16

Chapter 2: Jupiter's Atmosphere

2.1 Introduction 19
2.2 Chemical Composition 20
2.3 Vertical Structure of the atmosphere 23
2.4 Belts and zones 25
2.5 Hot-spots 27
2.6 Winds 28
2.7 Deep and Shallow Atmospheric Models 30
2.8 Distinct Features 31
2.8.1 Great Red Spot 31
2.8.2 Oval BA 32
2.8.3 Cyclones 32
2.8.4 Lightning 32
2.9 Temperature, Pressure, and Density Profiles 33
2.10 Conclusion 37
2.11 References 39

Chapter 3: Jupiter's Magnetosphere and its effect on the spacecraft

3.1 Introduction 42
3.2 Jovian Magnetosphere 43
3.2.1 Bow Shock 44
3.2.2 Magnetosheath 45
3.2.3 Magnetopause 46
3.2.4 Magnetotail 46
3.2.5 Io torus 47
3.2.6 Plasma sheet 47
3.2.7 Current sheet 48
3.3 Inner magnetosphere 48
3.4 Middle magnetosphere 50

3.5 Outer magnetosphere 50
3.6 Radiation belts 51
3.7 Rings 52
3.8 Hazards to the spacecraft 54
3.9 Possible protection techniques 56
3.10 Conclusion 57
3.11 References 58

Chapter 4: Aerobraking Analysis and Results

Nomenclature 62
4.1 Introduction 64
4.2 Theory 64
4.3 Assumptions 65
4.4 Procedure 65
4.4.1 : Determination of state vector 66
4.4.2 Dynamics 67
4.4.3 : Aerobraking phases 68
4.4.4 : Propellant savings 68
4.4.5 : Cost analysis 69
4.5 Results 69
4.6 Discussion 75
4.7 Conclusion 77
4.8 References 78
4.9 Appendices 79
4.9.1 Appendix A - MATLAB code 79
4.9.1.1 Main script 79
4.9.1.2 Differential equation 80
4.9.1.3 Density calculation function at each point 81
4.9.2 Appendix C – Aerobraking at different altitudes 82

Chapter 5: Heat Transfer Analysis on the Spacecraft During Aerobraking

Nomenclature 87
5.1 Introduction 88
5.2 Theory 88
5.3 Assumptions 91
5.4 Procedure 92
5.5 Results 93
5.6 Discussion 94
5.7 Conclusion 96
5.8 References 97
5.9 Appendix 98

Chapter 6: Viability of Aerobraking Technique for the Orbit Insertion Around Jupiter

6.1 Introduction 100

6.2 Summary of aerobraking and heat analysis results 100
6.2.1 Aerobraking analysis results 100
6.2.2 Heat analysis on the spacecraft during the atmospheric pass 102
6.3 Discussion 103
6.4 Conclusion 104

Chapter 1 - Aerobraking Analysis for Jupiter Orbit Insertion

1.1 Introduction

Aerobraking is a process of circularizing or making the orbit smaller in shape without performing the propulsive burn, instead, making use of atmospheric drag of the planet as a brake. To reduce the eccentricity and period of the orbit, the spacecraft passes through planet's atmosphere several times to achieve the desired orbit. Each pass slows down the spacecraft and shrinks the orbit of the spacecraft because of atmospheric drag. Aerobraking results in the fuel and cost savings by removing the need for large propulsive burn requirement for orbit modifications.

The spacecraft encounters the target planet on an open orbit (hyperbolic or parabolic) on which it has a higher velocity compared to the velocity needed for the closed orbit (circular or elliptical) around the planet. Reduction in velocity is required to slow down the spacecraft so that it does not escape the planet after encountering it on a parabolic or hyperbolic trajectory. Initially, the spacecraft is captured in a large elliptical orbit. The highly elliptical orbit is circularized using aerobraking by making the spacecraft pass through the atmosphere of the planet. The friction of the atmosphere makes the orbit smaller and smaller. In this manner, aerobraking contracts the orbit using drag.

Aerobraking can be divided into three main stages: walk-in, main phase, and walk-out phase. The walk-in phase pertains to the initial stage where spacecraft is making atmospheric passes in large elliptical orbits and adjusting itself to the planet’s environment. The engineers use walk-in phase to understand the response of the spacecraft during the atmospheric pass. After ensuring that the spacecraft is safe and performing according to the implemented adjustments during the walk-in phase, the main phase is initiated. The main phase deals with the majority of the passes made by the orbiter, and the shape of the orbit becomes smaller and closer to the target orbit during this phase. During the walk-out phase, the periapsis is raised up from the atmosphere of the planet to terminate the action of the drag force on the spacecraft. At the end of these three phases involving aerobraking, the spacecraft is captured into the required orbit.

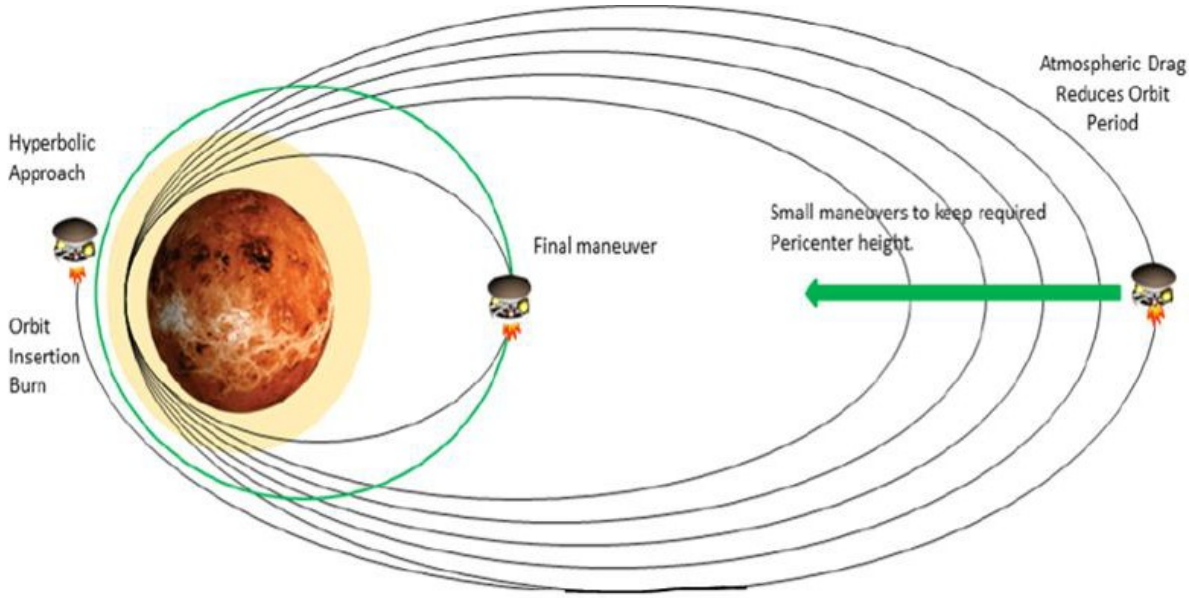

Fig. 1: Aerobraking visualization [27]

Besides fuel saving benefit associated with aerobraking, the technique also encompasses several complications which necessitate careful mission planning and design of the spacecraft. For instance, aerobraking involves challenges with distant navigation control of the spacecraft, increased load of aerodynamic forces due to perturbations, and heat transfer to the spacecraft body during atmospheric passes. As spacecraft is controlled by navigation engineers from Earth, there is a time gap between the exchange of commands from the mission team and feedback from the spacecraft. The delay in receiving and sending commands from Earth-based stations pose difficulties to the process in case of frequent response is needed from the spacecraft. In addition, the occurrence of storms at the planet affects the atmospheric density. The variation in density can have adverse effects on the spacecraft performance. If density at aerobraking altitude becomes higher, the spacecraft could encounter a large drag force acting on it which could be greater than the maximum load the spacecraft is capable of handling. Consequently, spacecraft may encounter excessive forces acting on it which can destabilize the spacecraft. The atmospheric entry generates heat because of the interaction of spacecraft moving at high speed with the atmosphere. Therefore, atmospheric passes cause extreme heat transfer to the body of the spacecraft. These challenges can be overcome by careful planning of the mission, robust

design of the spacecraft, and by performing adjustments to the spacecraft trajectory during the mission.

Several missions have managed the risks associated with aerobraking via thorough mission and spacecraft design and have benefitted from the procedure. Missions to the moon, Mars, and Venus proved the viability of aerobraking and have set the road for future economical missions. Despite the challenges involved in aerobraking technique, fuel saving resulted from the process outweighed the risks which are manageable through careful planning of the mission.

1.2 Motivation

Instead of burning fuel, aerobraking uses the atmospheric drag of the target planet to put the spacecraft into the mission orbit. If a propulsive burn was used instead of aerobraking, a large amount of propellant would be needed which could be a significant portion of the total spacecraft mass. Many missions have benefitted from aerobraking and reduced overall mass and cost of missions via fuel savings. For instance, nearly half of the mass was fuel for the Odyssey spacecraft which was used up in about the first 20 minutes during orbit insertion around Mars [1]. Odyssey achieved its final orbit for the mission by making use of aerobraking. If the final mission orbit for Odyssey was attained with the propulsive burn, additional fuel would be needed to store in the spacecraft which would have resulted in the larger and heavier spacecraft [1]. Like Odyssey, other missions to Mars have also used aerobraking method to achieve their required orbit around Mars. Fuel savings and ΔV savings resulting from aerobraking for Mars missions are listed in table 1 below which shows that Mars missions saved 320 to 580 kg of fuel by making use of aerobraking in place of the propulsive burn.

Table 1: Aerobraking comparison for past Mars missions [26]

	Pre-Aerobraking Orbit			Post Aerobraking Orbit			ΔV Savings, m/s	Propellant Savings, kg
	h_p, km	h_a, km	P, hrs	h_p, km	h_a, km	P, hrs		
Magellan	170	8450	3.2	200	540	1.6	1220	490
MGS	120	54200	45	110	430	1.9	1220	330
Odyssey	110	26200	18	120	540	2.0	1090	320
MRO	110	44000	34	120	500	1.9	1190	580

The orbit insertion via pure propulsive burn is not only expensive, the spacecraft also becomes much heavier due to higher fuel requirement; therefore, a limited number of experimental instruments can be taken onboard. Aerobraking reduces fuel dependence of the mission which leads to lighter spacecraft, and additional science equipment for data sampling can be incorporated in the probe. Furthermore, transporting payload to space is highly expensive. According to NASA, the cost to put 1 lb. of payload to Earth orbit can be more than $10,000 [28]. If fuel requirement for the mission can be lessened, the cost of launching the spacecraft can be also be reduced. Hence by utilizing aerobraking technique, less amount of fuel is needed for the mission which leads to increase in the useful mass of the spacecraft.

1.3 Literature Review

The benefits of aerobraking have been observed in several missions and have resulted in space missions saving both mass and money. There have been several missions to Mars which used aerobraking to capture the spacecraft into the required orbit. Prior to Mars missions, aerobraking has been successfully demonstrated by Lunar and Venusian missions. Thus, aerobraking is an established technique to make the space exploration missions more efficient. The following sections present a brief overview of missions which used aerobraking as an orbit insertion method.

1.3.1 Hiten

Aerobraking was first performed by Hiten satellite around Earth. The Hiten spacecraft was launched by the Japanese Space Agency, Institute of Space and Astronautical Science (ISAS) on January 24, 1990 [4]. It was originally called Muses-A and was named Hiten during the mission. The five main goals of the mission were: 1) to study technologies for precise orbit design and control along with fast and effective data transmission, 2) to insert the spacecraft into lunar orbit, 3) to investigate a lunar swing-by 4) examination of aerobraking around Earth, and 5) to measure cosmic dust particles between Earth and moon in collaboration with Munich Technical University [4]. During the mission, two additional mission goals were introduced. The regression of Lagrange points of the Earth-moon system and hard landing on moon’s surface were studied as follow up goals [5]. Due to complications during launch, the spacecraft had 50 m/s lower injection velocity than the nominal velocity. As a result, Hiten acquired the orbit the with the

apogee of 290,000 km which was much smaller than the targeted apogee of 476,000 km. Consecutive correction maneuvers extended apogee back to the aimed value. On March 8, 1990, it made its first flyby of the moon and released a small payload spacecraft named Hagoromo [5].

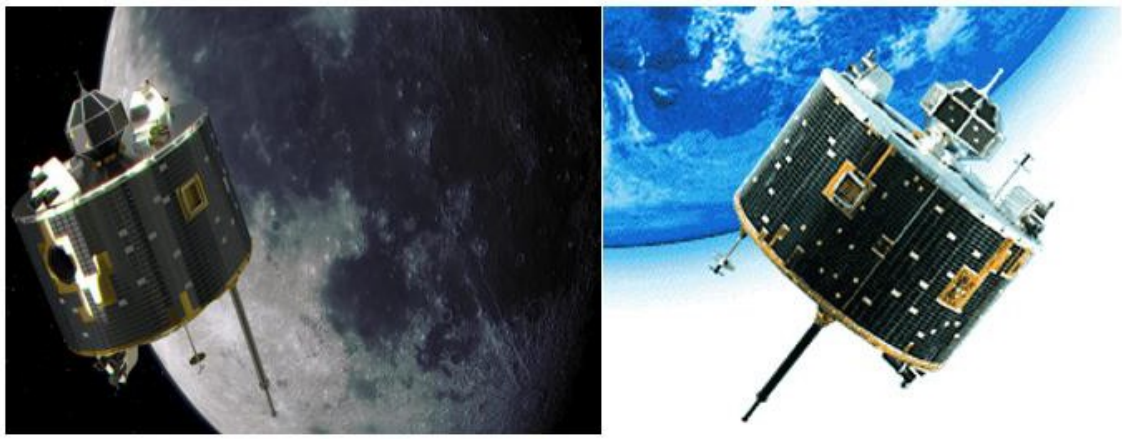

Fig. 2: Hiten spacecraft near moon [6] and earth [7]

After performing several close flybys of the moon, Hiten started the aerobraking process which was the first ever attempt to employ this technique. Hiten carried out the aerobraking experiment around Earth between March 19 and March 30, 1991 [8]. Hiten made its first pass into Earth's atmosphere on March 19 at 11 m/s velocity with the perigee altitude of 125.5 km. The spacecraft velocity was reduced by 1.712 m/s and the apogee altitude was lowered by 8,665 km due to atmospheric drag. On March 30, Hiten successfully concluded the aerobraking experiment with the atmospheric pass at 120 km perigee altitude and drag slowed it down by 2.8 m/s and shrunk the apogee altitude by 14,000 km [5]. In addition to achieving the aerobraking objective, Hiten was able to attain its rest of the mission goals successfully.

1.3.2 Magellan

The Magellan spacecraft studied Venus and mapped the entire planet. Magellan was launched on May 4, 1989, and it arrived at Venus on August 10, 1990. Magellan was put into a highly elliptical orbit and it was nearly a polar orbit at an inclination of 9.5 deg. N [9]. The initial orbit of Magellan had the period of 3 hrs. 15 minutes with the periapsis of 294 km and apoapsis of 8,543 km. The Magellan mission included four cycles of eight months (243 days) to study the planet [10]. During the first three cycles, it mapped approximately 98% of the Venus surface. In

the fourth cycle, Magellan captured data on the gravitational field of Venus. After completing its fourth orbital cycle around Venus, Magellan initiated aerobraking to investigate the planet in a greater detail. Magellan performed aerobraking around Venus between May 25, 1993 and August 3, 1993 [10]. By making successive passes through Venusian atmosphere, Magellan reduced its orbit to the periapsis of 180 km and apoapsis of 541 km with a period of 94 minutes [10].

At the completion of aerobraking, Magellan further dipped into the atmosphere of Venus to perform the “Windmill experiment”. During this experiment, solar panels of the spacecraft were oriented like a windmill blade configuration to measure the amount of restoring torque the spacecraft experiences in response to the destabilizing forces acting on the spacecraft at lower altitudes. The windmill experiment collected data on the molecular activity in the upper atmosphere of Venus [10]. The Magellan mission made use of orbital cycles along with aerobraking and windmill experiment to help construct surface and gravitational field map of Venus.

1.3.3 Mars Global Surveyor

Mars Global Surveyor (MGS), as the name of the spacecraft suggests, was a mission to Mars. MGS was launched on November 7, 1996 using McDonnell Douglas Delta II 7925A launch vehicle. The main objective of MGS was to perform global mapping of Mars by studying the Martian surface, atmosphere, gravitational field, and magnetic field [11]. MGS is a part of the Mars Surveyor program which proposed the launch of spacecraft pairs to Mars every twenty-six months, MGS was the first spacecraft built and launched to Mars of the first pair of planned satellites under the Mars Global Surveyor program [12]. MGS was inserted into Mars’ orbit via aerobraking.

The MGS mission was dependent on aerobraking because it was launched with a ΔV deficit of 1,250 m/s [11]. “This reduction in the spacecraft propulsive capability was necessary to permit the development of a spacecraft design that satisfied the payload capabilities of the Delta II launch vehicle during the Earth-to-Mars ballistic launch opportunities of November 1996” [11]. To make up for the ΔV deficit during launch, aerobraking was required in place of the propulsive

burn to reduce the period of 45 hrs to 2 hrs [11]. Thus, aerobraking was essential for MGS mission because the total weight of the spacecraft was limited by launch vehicle's payload capabilities.

The MGS mission involved several constraints due to uncertain atmospheric conditions at Mars and structural limits of the spacecraft. The aerobraking maneuver had to be able to withstand 90% change in density, of which 70% change was predicted because of atmospheric variability from one orbit to the successive orbit, and the remaining 20% change was due to navigational deterrence in case of unexpected magnetic field change [11]. The spacecraft needed to maintain 40% battery life when solar power is not available in situations like solar eclipse. Furthermore, a time limitation was also a part of MGS mission: "the duration of aerobraking is constrained by the time it takes the local mean solar time of the descending node upon arrival at Mars, which is near 5:45 PM, to transition to the desired 2:00 PM condition - a four and a half-month time period" [11]. The MGS spacecraft included two solar panels on each side. Unfortunately, one of the solar arrays failed to latch after launch. The damper shaft arm is believed to have stuck between the inner panel and the yoke, leading to the inability of the solar panel to latch properly [13]. The failure of the solar array deployment led to redesign of the spacecraft configuration during the mission to withstand aerodynamic forces. In addition, the aerobraking strategy was modified twice to accommodate time constraints and dynamic pressure limitations. The period of the spacecraft was reduced to 45 hrs. from 48 hrs. to match a 2 pm mapping orbit condition, and dynamic pressure control strategies were applied to stay within the targeted density pressure corridor [11]. Challenges faced during Mars Global Surveyor mission indicate the delicacy of the aerobraking maneuvers; therefore, onboard modifications to spacecraft operation and configuration during the mission are required based on the variability of many factors like atmospheric conditions, solar eclipse, the strength of storms, and so on.

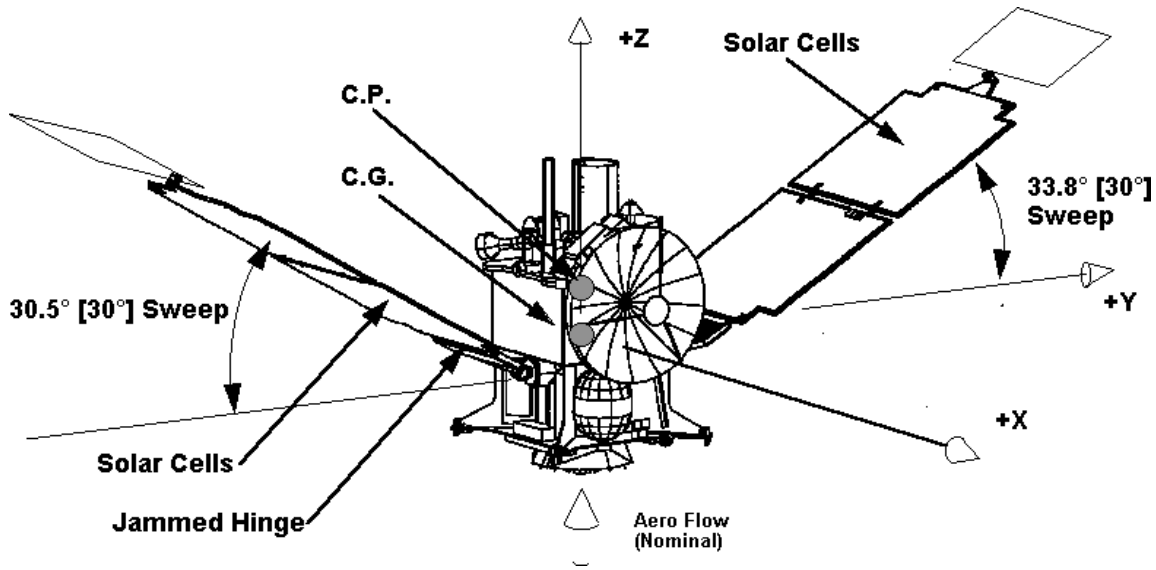

Fig. 3: Modified configuration of MGS [11]

Damaged solar panel and uncertain Martian atmospheric conditions posed several challenges to the mission which resulted in the revision of the mission design in addition to stopping and restarting of the aerobraking maneuvers. MGS was inserted into Martian orbit on September 12, 1997 with the periapsis altitude of 263 km and the orbital period of 45 hrs. [11]. The walk-in phase reduced the periapsis altitude in the consecutive passes to 110.5 km which marked the main phase of aerobraking. However, the reduction in density margin caused aerobraking to temporarily terminate and a maneuver was performed to raise the periapsis altitude to 172 km on October 12, 1997 [11]. Aerobraking was resumed on November 7, 1997 and altitude was lowered to 135 km. The main phase was initiated at 120.5 km. On November 23, 1997, aerobraking was once again stopped due to atmospheric disturbance resulted from dust storm, and periapsis altitude was raised to 132 km [11]. In late November, aerobraking was reinitiated which reduced the period from 45 hrs. to 2 hrs. with the apoapsis distance of 450 km [14]. MGS encountered many challenges during its mission; however, it was able to attain the targeted orbit through revisions in planning and spacecraft configuration with the aid of aerobraking.

1.3.4 Mars Odyssey

Mars Odyssey is a part of NASA's continued program to send missions to Mars every 26 months. Odyssey took advantage of the launch window with a minimum amount of energy required to transfer spacecraft to Mars. This launch opportunity (a Hohmann transfer window) is

available every 26 months due to the alignment of Earth and Mars orbits around Sun. Mars Odyssey was launched on April 7, 2001 and is expected to end in October 2030. The mission goal of Odyssey is to study the composition of minerals and elements present on the Martian surface [15]. Mars Odyssey used aerobraking to achieve the desired orbit around Mars which translated into the ΔV savings of 1.08 km/s [23]. After performing the burn to place Odyssey into highly elliptical orbit, the walk-in phase was executed which lowered the periapsis altitude to 130 km approximately. The main phase involved 336 passes in 75 days which brought the orbital period to 2 hrs. from the initial period of 19 hrs. Odyssey concluded aerobraking on January 11, 2002 with the end of walk-out phase which circularized the final orbit with the altitude of 400 km [2]. Aerobraking made the Mars Odyssey project cost effective by providing an alternative to the fuel burn required to reduce its period from 19 hrs. to 2 hrs.

1.3.5 Mars Reconnaissance Orbiter

Mars Reconnaissance Orbiter (MRO) is another chapter in NASA's exploration of Mars. It was launched on August 12, 2005 from Cape Canaveral Air Force Station, Florida in the search of water on Mars. It used close-up photography in addition to other sampling instruments to analyze minerals found on Mars surface, traces of water in the atmosphere, and any marks of shorelines or dried lakes [16]. It is the largest spacecraft launched to Mars to date with the mass of 1,400 kg approximately. MRO completed aerobraking in 145 days by performing 26 aerobraking maneuvers [17]. The walk-in phase was performed with 5 consecutive atmospheric passes which lasted for a week. The main phase was completed through 500 orbits in five and half month duration while the walk-out phase took five days involving 64 orbits to readjust the periapsis to the desired altitude. Aerobraking reduced MRO's period from an initial orbital period of 35 hrs. to 2 hrs. and reshaped the orbit to circular at 450 km altitude [16]. The MRO mission saved 400 kg of fuel by using the aerobraking technique instead of a propulsive burn for orbit insertion [24]. MRO became another successful example of a mission which benefited from aerobraking.

1.3.6 Venus Express

Venus express marked the European Space Agency's first mission to Venus. Its main motive was to study the plasma environment and atmosphere of Venus which was used to form meteorological maps. The data from Venus Express suggested that volcanic activities existed at

Venus nearly three million years ago, and it provided clues that Venus might be geologically active at present [18]. Venus Express was launched on November 9, 2005 and reached Venus on April 11, 2006 [19]. The initial orbit of Venus Express had a period of 24 hrs. with the periapsis of 250 km and the apoapsis altitude of 66,000 km at the North Pole. Aerobraking was kept as a backup plan for Venus Express mission. Venus Express executed aerobraking to extend its mission in the months of June and July of 2014 [25]. Venus Express was running low on fuel at the end of its mission; however, it was able to survey Venus for additional six months with the help of aerobraking maneuvers [25]. During the aerobraking period, Venus express could carry out science operations also because of well-designed operations which did not interfere with aerobraking maneuvers [25]. Through aerobraking, Venus Express reduced its orbit by 135 km approximately to study Venus in a greater detail. Aerobraking was ended with the final orbit of periapsis at 460 km and 63,000 km apoapsis altitude [20]. Thus, aerobraking extended Venus Express' mission life which provided additional valuable information about the planet.

1.4 Project Proposal

Aerobraking is economical and provides the opportunity to expand the data collection and experimentation of a mission by allowing larger room for science equipment. Orbit insertion around Jupiter can be done through aerobraking instead of using a propulsive burn. Jupiter's moon Europa is an important candidate in NASA's quest for finding the habitable world other than Earth. Europa is thought to have a large ocean beneath its icy crust as indicated by Hubble telescope and Galileo mission [21]. The core of Europa is suspected to resemble Earth's core. Europa is thought to have an iron core with a rocky mantle and a salty water ocean hidden under its icy surface [21]. Europa's special characteristics make it one of the most attractive targets in the search of the habitable world. Future missions are focused on verifying predictions about Europa's composition along with the further exploration of the Jovian moon for more evidence that it might be a habitable world. Future missions to Jupiter are currently in their planning phase. For example, NASA's Europa Clipper mission will specifically study Europa for its habitability conditions. The Europa Clipper spacecraft will orbit Jupiter while making 40-45 flybys of Europa to make observations and take data [22]. As mission planning to Jupiter is ongoing, aerobraking can be used to make the missions cost-effective through fuel savings.

Jupiter is the largest planet in the solar system. It has extreme radiation belts and a highly powerful magnetosphere surrounding the planet. Aerobraking has never been performed at Jupiter. The extreme conditions at Jupiter will pose numerous challenges to aerobraking maneuvers. It is important to study the effectiveness and viability of aerobraking at Jupiter to determine if this technique is advantageous for Jovian missions. Hence, aerobraking at Jupiter will be analyzed through this project to explore the benefits and drawbacks of the procedure for a Jovian mission.

1.5 Methodology

As aerobraking depends upon atmospheric entry, the atmospheric modeling of the planet is crucial. Hence, density modeling of Jupiter's atmosphere will be performed as a first step in the process of aerobraking simulation. In-depth understanding of the Jovian magnetosphere is very important so that highly unfavorable surroundings and their effect on the spacecraft during maneuvers can be studied. Next, modeling of three aerobraking phases will be performed, and challenges involved in the process around Jupiter will be assessed. The walk-in phase includes the first few passes through the atmosphere to better understand the first response of the spacecraft during atmospheric entries. Optimization of the spacecraft trajectory is performed as necessary. The walk-in phase will be used to perform the initial adjustments to the orbit. The main phase involves the majority of the orbit reshaping by lowering apoapsis. Next, the walk-out phase will be analyzed to conclude the aerobraking by making the last necessary adjustments to the orbit. The assessment of the resulting ΔV will be performed to evaluate the effectiveness of aerobraking for Jovian missions. Heat analysis will be performed to investigate the high-temperature effects on the spacecraft body during the atmospheric pass at high speed. Finally, the evaluation of the cost savings and high temprature effects on the spacecraft will be performed to conclude the viability of aerobraking technique for Jovian missions.

1.6 Conclusion

Orbit insertion around a planet with the atmosphere through aerobraking which will make the mission economical and lighter, thereby, saving fuel and money along with providing more room for data collection instruments. This project will focus on the orbit insertion of the spacecraft around Jupiter through the aerobraking technique. The project will also optimize the mission by

lowering overall ΔV and will investigate if there are any drawbacks associated with the technique in the presence of extreme conditions at Jupiter.

1.7 References

[1] “Aerobraking, part 2”, Mars Odyssey 2001, NASA [online], https://mars.nasa.gov/odyssey/mission/timeline/mtaerobraking/aerobraking2/ [retrieved 10 Apr. 2017].

[2] Takashima N., and Wilmoth, R. G., “Aerodynamics of Mars Odyssey,” AIAA Paper 2002-4809 [online], 5-8 Aug. 2012, https://ntrs.nasa.gov/archive/nasa/casi.ntrs.nasa.gov/20030010282.pdf .

[3] Prince, J., Powell, R., and Murri, D., “Autonomous Aerobraking: A Design, Development, and Feasibility Study,” AAS 11-473 [online], https://ntrs.nasa.gov/archive/nasa/casi.ntrs.nasa.gov/20110014523.pdf [retrieved 8 May 2017].

[4] “Hiten Spacecraft”, Insitute of Space and Astronautical Science [online], http://www.isas.jaxa.jp/en/missions/spacecraft/past/hiten.html [retrieved 29 Aug. 2017].

[5] “Hiten” NASA NSSDCA/COSPAR ID: 1990-007A [online], https://nssdc.gsfc.nasa.gov/nmc/spacecraftDisplay.do?id=1990-007A [retrieved 05 Sept. 2017].

[6] “Hiten-Hagoromo (MUSES-A)”, [online] https://www.flickr.com/photos/nyaisas/6878930639 [retrieved 10 Sept. 2017].

[7] “Hiten”, [online], http://www.daviddarling.info/encyclopedia/H/Hiten.html [retrieved 8 Sept. 2017].

[8] Shizgal, B. D., and Weaver, D. P., “Numerical Analysis of Aerothermodynamic Environment of HITEN Spacecraft Aerobrake Experiment,” Rarefied Gas Dynamics: Space Science and Engineering [online], Progress in Astronautics and Aeronautics, AIAA, 1994, https://arc.aiaa.org/doi/10.2514/5.9781600866326.0012.0024.

[9] Williams, D. R., “Magellan Mission to Venus”, 28 Feb. 2005, https://nssdc.gsfc.nasa.gov/planetary/magellan.html.

[10] “Magellan Summary Sheet” Jet Propulsion Laboratory [online], https://www2.jpl.nasa.gov/magellan/fact1.html [retrieved 12 Sept. 2017].

[11] Johnson, M. D., Esposito, P. B., Alwar, V., Demcak, S. W., Graat, E. J., and Mase, R. A., “MARS Global Surveyor Aerobraking at Mars”, AAS 98-112 [online], Jet Propulsion Laboratory, California Institute of Technology, [retrieved 20 Sept. 2017] .

[12] Shane, R., Tolson, R., Rault, D., Shane, R., Tolson, R., and Rault, D., “Mars Global Surveyor aerodynamics for maneuvers in Martian atmosphere,” 32nd Thermophysics Conference [online], Jul. 1997, https://ntrs.nasa.gov/archive/nasa/casi.ntrs.nasa.gov/20040095949.pdf .

[13] Lyons, D. T., Beerer, J. G., Esposito, P., Johnston, M. D., and Willcockson, W. H., “Mars Global Surveyor: Aerobraking Mission Overview,” Journal of Spacecraft and Rockets [online], Vol. 36, No. 3, 1999, pp. 307-313, https://doi.org/10.2514/2.3472 .

[14] “Mars Global Surveyor Successfully Completes Aerobraking”, Jet Propulsion Laboratory, California Institute of Technology [online], Feb. 1994, https://www.jpl.nasa.gov/news/news.php?feature=5077 .

[15] “Overview - Mars Odyssey 2001,” NASA [online], https://mars.nasa.gov/odyssey/mission/overview/ [retrieved 28 Aug. 2017].

[16] “Overview - Mars Reconnaissance Orbiter,” NASA [online], https://mars.nasa.gov/mro/mission/overview/ [retrieved 25 Aug. 2017].

[17] Prince, J., and Streipe, S., “Mars Reconnaissance Orbiter Operational Aerobraking Phase Assessment”, AAS 07-244 [online], https://ntrs.nasa.gov/archive/nasa/casi.ntrs.nasa.gov/20070010460.pdf [retrieved 10 Sept. 2017].

[18] Mai, T., “Venus Express,” NASA [online], 16 May 2014, https://www.nasa.gov/directorates/heo/scan/services/missions/solarsystem/VenusExpress.html .

[19] Serra, S. V., Bonnamy, O., Witasse, O., and Camino, O., “Venus Express Aerobraking,” IFAC Proceedings Volumes [online], Vol. 44, 2011, pp. 715–720 https://doi.org/10.3182/20110828-6-IT-1002.02433 .

[20] “An Analysis of Aerobraking at Mars,” An Analysis of Aerobraking At Mars | Historical Aerobraking, [retrieved 12 Aug. 2017].

[21] “Europa - In Depth | Planets - NASA Solar System Exploration,” NASA [online], https://solarsystem.nasa.gov/planets/europa/indepth [retrieved 15 Sept. 2017].

[22] Greicius, T., “NASA's Europa Flyby Mission Moves into Design Phase,” NASA [online], 21 Feb. 2017, https://www.nasa.gov/feature/jpl/nasas-europa-flyby-mission-moves-into-design-phase.

[23] Smith J. C., and Bell, J. L., “2001 Mars Odyssey Aerobraking", Journal of Spacecraft and Rockets [online], Vol. 42, No. 3, 2005, pp. 406-415, https://doi.org/10.2514/1.15213 .

[24] Zurek, R. W., and Smrekar S. E., “An overview of the Mars Reconnaissance Orbiter (MRO) science mission”, Journal of Geophysical Research [online], Vol. 112, E05S01, 12 May 2007, https://agupubs.onlinelibrary.wiley.com/doi/pdf/10.1029/2006JE002701 .

[25] Spencer, D. A., and Tolson R., “Aerobraking Cost/Risk Decisions”, Deep Space Systems [online], GT-SSEC.C.6, http://citeseerx.ist.psu.edu/viewdoc/download?doi=10.1.1.884.7708&rep=rep1&type=pdf [retrieved 15 Sept. 2017].

[26] Merritt, D. R., "Venus Express: Aerobraking and Post-Aerobraking Science Operations", AIAA SPACE 2015 Conference and Exposition, AIAA SPACE Forum, (AIAA 2015-4447), 2015, https://doi.org/10.2514/6.2015-4447 .

[27] Eismont, N., Ledkov, A., Nazirov, Dunham, D., and Chumachenko, E., “Spacecraft Transfer from Interplanetary to Low Near Planet Orbit by Use of Aerobraking in Venus Atmosphere”, AIAA [online], 2012, https://www.researchgate.net/figure/Successive-aerobraking-maneuvers_fig3_269054818?_sg=TAxGBISZoIxhHdEusIfjJUCZYsuJum9PhGM4VkkxmkOER1TyTWy3PZkON9JbUQEjNIrn1heMB5-a6DaLKdwwUA .

[28] Zapata, E., “The State of Play US Space Systems Competitiveness”, Presentation to the Future In-Space Operations (FISO) Seminar [online], NASA, 11 Oct. 2017, https://ntrs.nasa.gov/archive/nasa/casi.ntrs.nasa.gov/20170009967.pdf

Chapter 2 - Jupiter's Atmosphere

28.1 Introduction

Jupiter is not only the largest planet in the solar system; it is also the fastest one as well. To design an aerobraking mission to Jupiter, the characterization of Jupiter's atmosphere is essential. Jupiter is mainly composed of helium and hydrogen, and a trace amount of other compounds such as ammonia (NH_3), methane (CH_4), hydrogen sulfide (H_2S), and water (H_2O) are present in the lower atmosphere. As Jupiter is a gaseous planet, there is no topological change present on the planet. Hence, the planet has a well-mixed atmosphere; differentiation between individual layers of the atmosphere is hard. Distinct layers of the Jovian atmosphere are indicated by the temperature gradient. Jupiter's atmosphere is primarily divided into four layers: troposphere, stratosphere, thermosphere, and exosphere. Jupiter radiates more heat than it receives from the sun, "The ratio of Jupiter's internal power to absorbed solar power is 0.7" [1]. The interior of Jupiter is at extremely high temperature and pressure.

Given that Jupiter is made up of fluid rather than of solid mass, the entire planet does not rotate at the same rate. The rotation period differs with latitude giving differential rotation to the different features of Jupiter. The differential rotation of Jupiter is defined by three distinct rotational systems known as system I, system II and system III. The standard rotation of Jupiter is characterized by the rotation of its magnetic field which is measured from radio emissions also known as the radio rotation period of the Jupiter. This radio rotation period of Jupiter is designated as the system III with the period of 9h 55m 29.67s [12]. The equatorial rotation system is named as the system I which has the period of 9h 50m 30s and is 5 minutes faster than system III. The mid-latitude rotation is defined as system II with a period of 9h 55m 41s. System II is 11 seconds slower than system III. Th bulk of Jupiter's mass exists in the fluid state (gaseous or liquid) which requires multiple rotation systems to describe the motion of the planet based on the latitude site.

Jupiter's atmosphere is divided into stripes that run across the planet parallel to the equator which gives the planet a colorful banded appearance. White bands are known as zones while darker rings are called belts. The zones move in anticyclonic fashion, and belts rotate in the

cyclonic direction [1]. Zones and belts are organized in the alternating pattern. Winds at the boundary of the zones and belts tend to be stronger. There is a great amount of uncertainty about color and dynamic appearance of zones and belts. Nonetheless, the color of zones is believed to be the result of ammonia clouds, and the darker color of belts seems to be caused by the combination of traces of organic compounds with sulfur and phosphorus. The banded structure of Jovian atmosphere includes distinct features such as major vortices which affect the dynamics of the atmosphere strongly. There are two major anticyclones located in the zones: Great Red Spot (GRS) and Oval BA. The GRS is located in the southern hemisphere, and it is approximately 32,000km long and 13,000 km wide [3]. The GRS is the largest vortex in the solar system; it is roughly equal to the 3.5 times the size of the Earth [4]. Thus, the atmosphere of Jupiter displays the colorful alternating pattern of belts and zones rotating in the opposite fashion to each other.

Jupiter does not have a hard surface because of gaseous nature of the planet. Moving down towards the center of Jupiter, pressure and temperature rise to extremely large values. With increasing depth, the gaseous hydrogen transitions to the liquid state through phase transformation under high temperature and pressure. “The internal heat flux (comparable in magnitude to the flux obtained from the sun on the surface of the planet) produces high temperatures in the interior of Jupiter, and the mixture is in a supercritical state throughout, above the hydrogen-helium interface” [13]. The liquid state of hydrogen is metallic and exhibits different properties than its gaseous form. For instance, the liquid state can conduct electricity and behaves like a metal unlike the gaseous state of hydrogen. The liquid state of hydrogen is believed to be the source of Jupiter’s strong magnetic field.

To understand the nature of Jupiter’s atmosphere, the study of composition and dynamics of the atmosphere along with its various features is essential.

28.2 Chemical Composition

Main constituents of Jupiter’s mass are hydrogen and helium; it contains approximately 86% hydrogen and 13.6% helium while other gases are present in small quantities. “The atmosphere of Jupiter is evidently well-mixed to a great depth, and the reasonable assumption that chemical

equilibrium is attained in the hot interior leads to the expectation that the common elements are all fully reduced by combination with hydrogen" [11]. Hence, other elements like carbon, oxygen, nitrogen, sulfur, and phosphorus are found in the form of hydrogen compounds: methane (CH_4), ammonia (NH_3), water (H_2O), hydrogen sulfide (H_2S), and phosphine (PH_3) [11]. The trace amounts of arsine (AsH_3) and germane (GeH_4) are also present in the Jovian atmosphere. The abundance of noble gases: argon (Ar), krypton (Kr), and xenon (Xe) is comparable to the amount of these gases present in the Sun except for neon (Ne) which is found in much less amount at Jupiter [9]. The ultraviolet radiations and charged particles from magnetosphere cause methane to form hydrocarbons such as acetylene (C_2H_2), diacetylene (C_4H_2), and ethane (CH_3) in the upper atmosphere. It is suspected that oxygen compounds like carbon monoxide (CO), carbon dioxide (CO_2), and water (H_2O) were imported to the upper atmosphere of Jupiter by the impact of comets [9]. Table 1 and 2 present the composition of Jupiter's atmosphere compared to the Sun using data collected from Galileo probe, ground-based measurements, and from Voyager 1 and 2.

Table 1: Elemental ratio in Jupiter from Galileo probe, Voyager 1 and 2, and ground data and comparison of abundance with Sun [11]

Elements	Elemental ratio for Jupiter	Jupiter/Sun
Ne/H	1.23×10^{-5}	0.1
Ar/H	9.06×10^{-6}	2.5
Kr/H	4.35×10^{-9}	2.7
Xe/H	4.37×10^{-10}	2.6
C/H	1.05×10^{-3}	2.9
N/H	4.03×10^{-4}	3.6
O/H	2.98×10^{-4}	0.35
P/H	3.06×10^{-7}	0.82
S/H	4.05×10^{-5}	2.5

Table2: Isotopic ratio in Jupiter from Galileo probe, Voyager 1 and 2, and ground data and comparison of abundance with Sun [11]

Isotopes	Isotopic ratio for Jupiter	Jupiter/Sun
$^{13}C/^{12}C$	0.0108	0.10
$^{15}N/^{14}N$	0.0023	0.82
$^{36}Ar/^{38}Ar$	5.6	0.97
$^{136}Xe/Xe$	0.076	0.96
$^{132}Xe/Xe$	0.0091	0.09
$^{134}Xe/Xe$	0.29	1.09
$^{131}Xe/Xe$	0.203	0.94
$^{130}Xe/Xe$	0.038	0.87
$^{129}Xe/Xe$	0.285	1.04
$^{128}Xe/Xe$	0.018	0.82
$^{20}Ne/^{22}Ne$	13	0.94

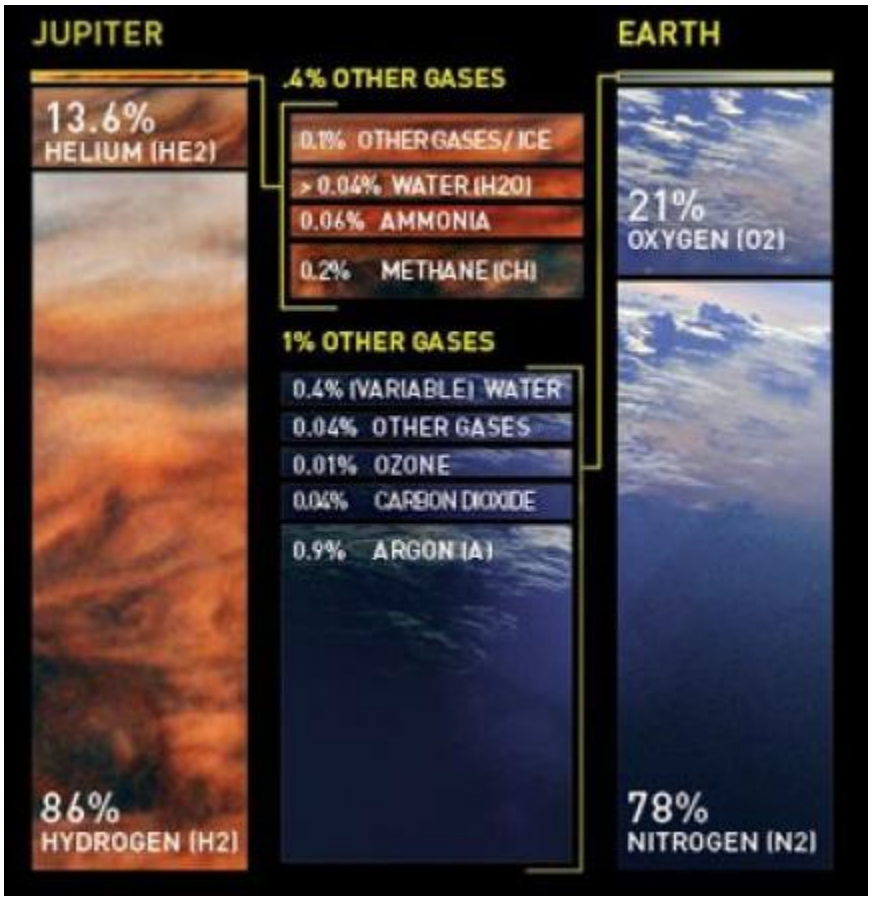

Fig. 1: Jupiter's chemical composition compared to Earth [10]

28.3 Vertical Structure of the atmosphere

Jupiter's atmosphere includes three main cloud layers with the cumulative span of 71 km (44 miles) approximately. It is believed that the outermost layer of clouds is composed of ammonia ice, the middle layer could be of ammonium hydrosulfide crystals, and the bottom layer can be of water vapor or ice [18]. The water clouds are believed to have the base at the pressure level of 6 - 7 bar, nearly 75 km below the colorful clouds [1]. It is assumed that the trace quantities of "elemental sulfur, phosphorus, and organic compounds could combine in trace amounts to form the muted colors'' to give a colorful appearance to Jupiter's atmosphere. The main components of the Jovian clouds such as water and ammonia are colorless; therefore, the combination of organic compounds with sulfur and phosphorus seems to be the possible explanation of the color of the Jovian clouds [1]. The clouds in the upper atmosphere are divided into zones and belts due to the fast rotation of Jupiter [18]. The visible atmosphere of Jupiter presents the alternating pattern of zones and belts.

To define individual the atmospheric layers of the Jovian atmosphere, the surface of the planet is taken to be the point where the pressure is equal to 1 bar at the temperature of 165K [17]. Galileo probe measured the atmospheric properties like temperature, pressure, and density from 1,029 km to -133 km (133 km below 1 bar assumed surface) [17]. In the upper atmosphere, the probe measured drop in the pressure and density and rise in temperature with height.

Pressure reach 1 μbar at the base of the thermosphere and further decreases when moving upwards towards exosphere. At 150 km from thermosphere, where the base of exosphere starts, the pressure gets to 2.5 pbar [2]. Two isothermal layers were detected by the Galileo probe, one layer is found above the tropopause and the second layer was in the stratosphere. In the upper atmosphere, temperature increases, specifically in the exosphere, temperature reaches 900 K approximately near the 1 nbar pressure level. The density calculations from Galileo probe data indicates the density values of the order of $10^{-11} kg/m^3$ in the exosphere [17]. From exosphere to outer space, there is a no clear boundary exists. The exosphere gradually merges to the outer space with the increasing height and decreasing density value.

Moving downwards, density, temperature, and pressure rise, and the gaseous hydrogen is condensed to the liquid state. The liquid hydrogen at Jupiter forms the largest ocean in the entire solar system [18]. Going further down, nearly halfway through the planet, extremely high temperature and pressure cause liquid hydrogen to lose the electrons. As a result, hydrogen exhibits metal-like properties and conducts electricity [18]. Therefore, liquid hydrogen generates huge current systems which are believed to be the source of the powerful magnetic field of Jupiter. At deeper levels, the state of Jupiter's core is unknown; it could be made up of dense fluid or of solid material (may be of iron or silicate minerals). The temperature at the core could be as high as $50{,}000^{\circ}C$ ($90{,}032^{\circ}F$) [18]. Hence, the state of the Jupiter's core is an open question.

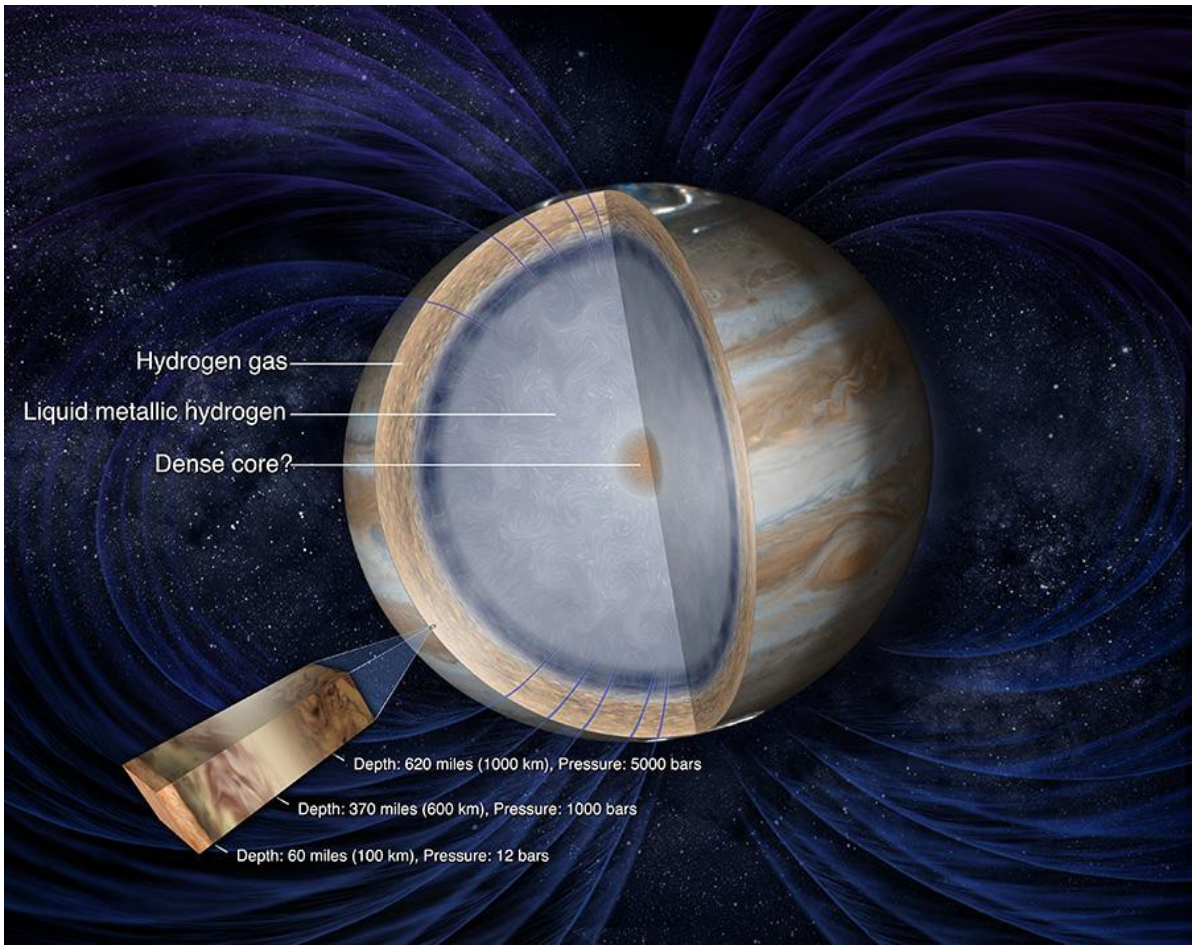

Fig. 2: Model of Jupiter's interior by Jet Propulsion Laboratory (JPL) [19]

28.4 Belts and zones

Belts and zones are the key features of Jupiter's visible atmosphere. They are the result of Jupiter's large periodicity which breaks the clouds into individual bands encircling the planet. At the boundary of zones and belts, the winds tend to be stronger compared to their inner regions. At the upper boundary (towards poles), zones have easterly winds, and they have westerly motion at the lower end (towards equator of the planet). Therefore, the overall motion of zones can be viewed as the anticyclonic pattern [1]. Similarly, belts move in the opposite fashion to that of the zones. Hence, the belts have westerly motion towards poles and easterly movement at the lower boundary. The rotational motion of the zones and belts change with latitude, and the variation in the rotational speed is ± 5 minutes from System III period [1]. The large features in zones show stability over time compared to the belts. The clouds in the zones are present at

higher altitudes than the clouds in belts which stay deeper in the atmosphere [1]. The features in the belts are more dynamic compared to zones.

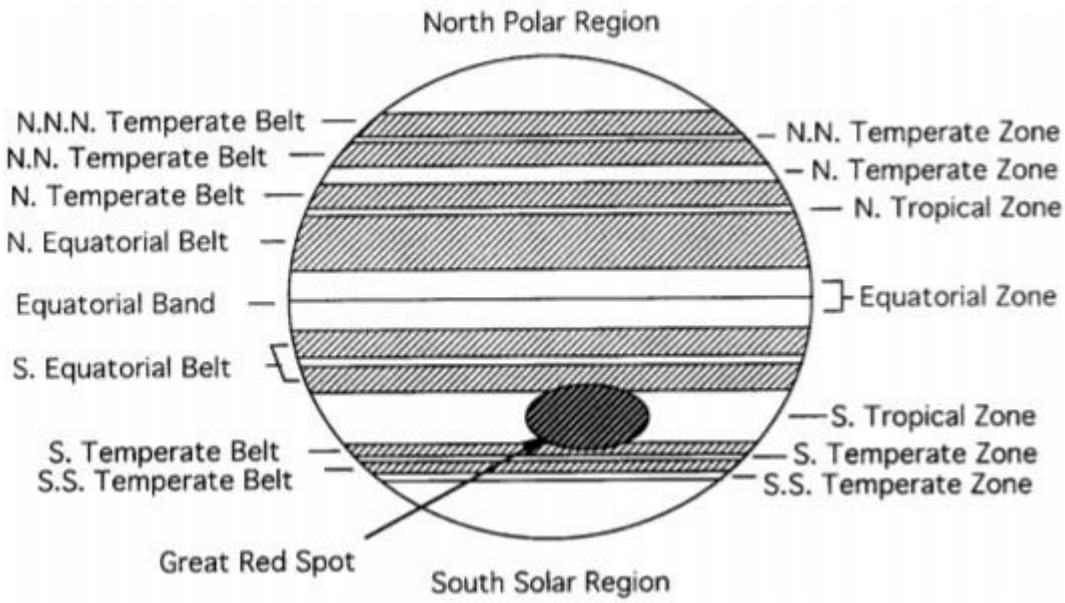

Fig. 3: Depiction of belts and zones of Jupiter [5]

The individual belts and zones are identified with specific names based on their location with respect to the equator of Jupiter as shown in figure 3. The equatorial zone (EZ) differs from the other zones because it contains a higher amount of haze compared to the neighboring latitudes which is revealed by methane band images [1]. Anticyclonic features in zones such as GRS expand to the adjacent belts towards equator which cause the smaller cyclonic cells to develop in between the two extended anticyclones from the zones [1]. This results in an appearance of a turbulent wake originating from west of the anticyclone. For instance, the Great Red Spot (GRS) extends into the South Equatorial belt (SEB), and a turbulent wake can be seen north of the GRS in figure 4. The extension of cyclones to the neighboring belts results in a disturbance in the vicinity of the region which appears as a wake.

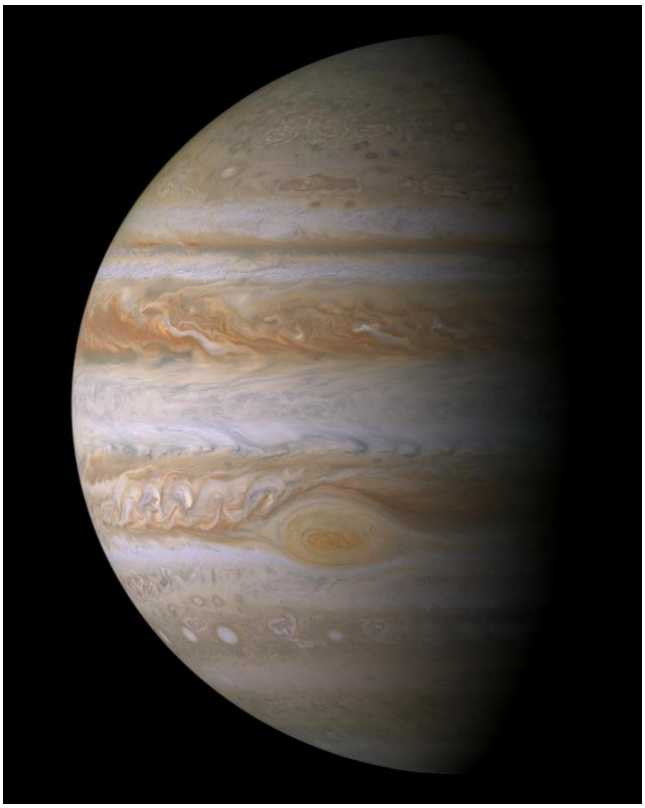

Fig. 4: Photo taken by Cassini [21]

28.5 Hot-spots

The hot-spots are puzzling but an important feature of the Jupiter's atmosphere. The hot-spots are the holes in the cloud deck which release radiations from the underlying warmer layers. The radiations can be detected more clearly in the narrow wavelength band of 5 μm without the interference of absorption lines from other gases in the spectrum [1]. Hot-spots are generally found in the belts where they sometimes originate as smaller hot-spots and become bigger with time to span the entire planet. The hot-spots provide valuable information about the dynamics of the Jovian atmosphere as they provide the view underneath the clouds.

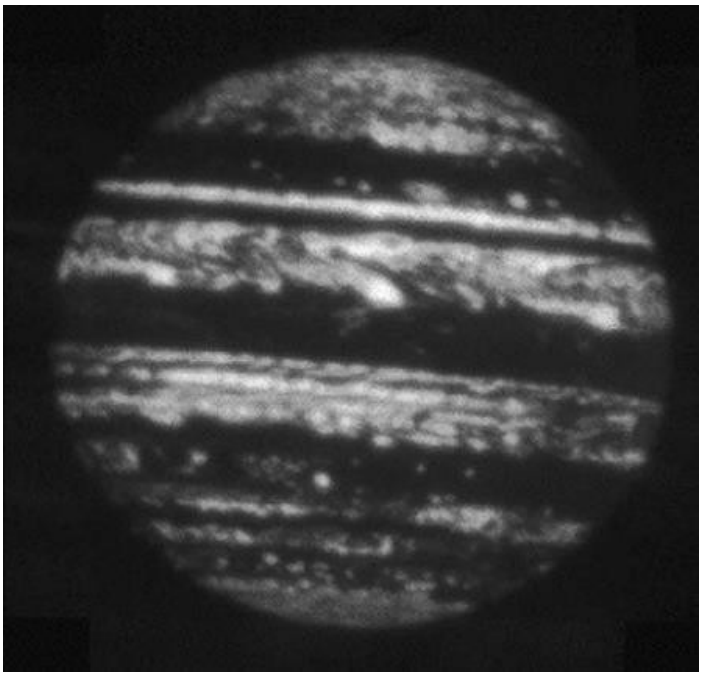

Fig. 5: Infrared image of Jupiter at $5\mu m$ wavelength indicating brightest spots as hot-spots [1]

The Galileo probe descended in the Jupiter's atmosphere at the southwest side in one of the equatorial hot-spot at 6.5°N latitude which was 5000 km wide. The Galileo probe was able to take data in the 150 km height range from 0.4 bar to 22 bar pressure level [1]. The formation of the hot-spots is not very well understood, and there are hypotheses to explain the existence of hot-spots. Many experts assume that hot-spots are the creation of "downdrafts that advect dry air from upper troposphere" to the deeper atmosphere based on the idea that unstable air tends to sink down [1]. This hypothesis is unable to explain the stability of the hot-spots as wind shear can make the hot-spots disappear in 1-2 days. Another hypothesis explains the hot-spots as the features of equatorial waves. "Air parcels that enter the hot spot from west (at 10's of ms^{-1}) are deflected downward; the parcels return to their original altitudes a few days later as they exit the hot-spot to the east" [1]. This model also has some issues. However, it is able to explain the layering structure of ammonia, hydrogen sulfide, and water, and it makes the hot-spot creation a local phenomenon [1]. The hot-spots provide a deeper look into the Jovian atmosphere.

28.6 Winds

The winds at Jupiter blow at the speed on the order of the hundreds of meters per second. The strength of winds at Jupiter is 3-4 times greater than the winds on Earth. The eastward jets can

reach the top speed of 150 m/s (approximately 335 mph) [1]. Despite the presence of dissipating factors like turbulence and convection, the data taken by Voyager 1 and 2, Galileo probe, Hubble Space Telescope, and Cassini show a small variation in the wind speed over the 21-year period, "Between 1979 and 1995 the eastward jet at 23° N slowed from 180 m/s to 140 m/s and then remained constant. The westward jet at 30° N and the jets between 40° N and 55° N also show significant (10–20 m/s) changes and small shifts in latitude" [1]. The stability in wind velocity is not clear yet [1]. The Jovian winds get much stronger near the equator compared to the jets that are closer to the poles. The wind strength is shown in figures 6 and 7 at different latitudes based on the data taken by visiting spacecraft.

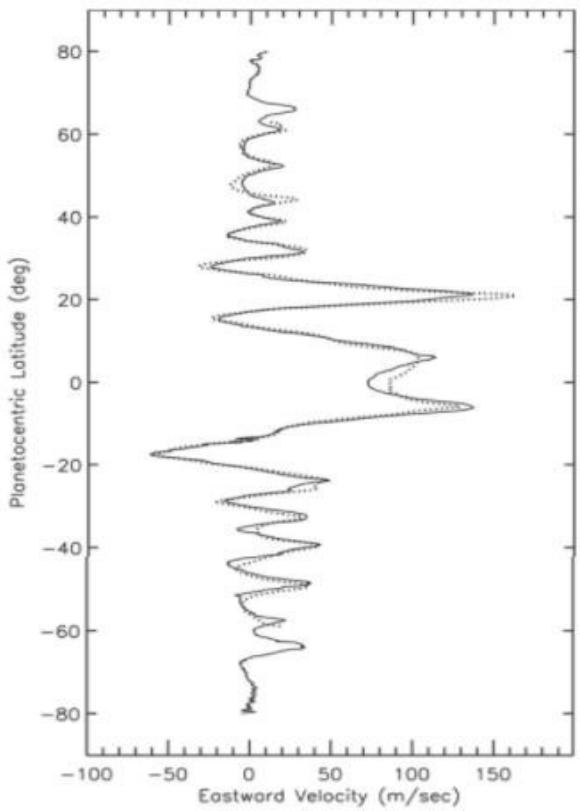

Fig. 6: Data taken by Voyager in 1979 (dashed line) and by Cassini in 2000 (solid line) [1]

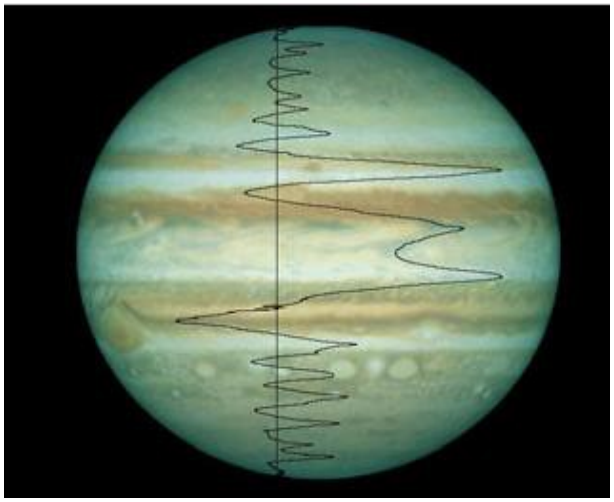

Fig. 7: Wind velocities with respect to zero velocity vertical line [6]

28.7 Deep and Shallow Atmospheric Models

As Jupiter is a gaseous planet, the dynamics of the atmospheric activities need to be explained in terms of fluid dynamics. The anticyclones are termed as the warm-core features having higher temperature compared to the surrounding air at the same pressure level. For warmer air, pressure decreases at a slower rate with respect to altitude; therefore, the vorticity of warm-core features become more anticyclonic. Similarly, the cold-core features become more cyclonic with increasing depth [1]. The existence of zones and belts is defined by looking at their vorticity. The shallow and deep models are two models which try to explain the atmospheric phenomenon at Jupiter.

The shallow model assumes that winds at Jupiter are weaker at the deeper levels. Therefore, this model is based on the idea that winds are weak in the deep atmosphere speed, and it assumes that the atmosphere is stable at greater depths. According to this model, warm-core features like anticyclonic zones tend to rise, and the cold-core features have the tendency to sink down. This view can explain the higher altitude of clouds in the zones and lower heights of clouds in the belts which is reinforced through the observation from hot-spots [1]. However, this model has problems justifying the stability of jets in the Jovian atmosphere. In addition, the Galileo probe found that the winds are present below water clouds, and the data show that winds do not seem to slow down even below the pressure level of 22 bar [1]. The data from Galileo probe contradicts with the shallow model.

The second model known as the deep model assumes that the winds at the outer layer of the atmosphere are the indication of much stronger winds at greater depths. This model explains zones and belts as concentric cylinders with respect to the rotational axis of the planet [1]. For a barotropic fluid which has a constant temperature at a constant pressure, the motion of the fluid can be defined as a movement in the form of columns which can be described by the Taylor-Proudman theorem. According to Taylor-Proudman theorem, “weak currents in a rotating homogeneous fluid are two-dimensional: the fluid moves about in columns whose axes are parallel to the rotation vector. Moreover, since the currents tend to be deflected around solid obstacles, those columns of fluid which intersect an obstacle are isolated from the rest of the flow” [20]. However, if temperature changes at constant pressure level, the model of zones and belts as a cylindrical fluid column in motion collapses because the fluid does not follow Taylor-Proudman theorem in this case, and the belts and zones do not rotate in columns [1]. The deep model assumes stronger winds at a greater depth of the planet but, it cannot explain the fluid motion at varying temperature for the given pressure value.

Both shallow and deep models fall short in explaining the atmospheric dynamics of Jupiter because of their simplified assumptions and the lack of data at the interior of the planet.

28.8 Distinct Features

There are several distinct features that dominate Jupiter’s visible atmosphere. The Great Red Spot (GRS), Oval (BA), smaller white ovals, and cyclonic regions are the major features of Jupiter’s atmosphere which are dominant in the visible atmosphere. The smaller white ovals are formed in zones occasionally which are anticyclonic in their vorticity. They sometimes merge together to become larger anticyclones. The cyclones are present in the belts. A brief description of these features is given below.

2.8.1 Great Red Spot

The Great Red Spot (GRS) in Jupiter’s atmosphere is the largest vortex in the solar system. It is the oldest known vortex as well. Its existence is known from more than 300 years. It is believed to have noticed by J.P. Cassini and others between 1665 and 1713 [1]. It spans from 17°S to

27.5°S with a maximum speed of 120m/s. The anticyclonic vorticity of the GRS is approximately 6 x 10^{-5} s^{-1} which is nearly one-third of the planetary vorticity locally [1]. The GRS consumes relatively smaller anticyclones which move towards it. In mid-2008, the GRS engulfed Baby Red Spot. Initially, the GRS split the Baby Red Spot into smaller pieces which circled GRS, and by August 2008, the Baby Red Spot was completely assimilated into the GRS [8]. Sometimes, the South Tropical Zone Disturbance (STZB) comes into existence which deflects smaller anticyclones southwards before their encounter the GRS. Occasionally, the GRS produces a white plume at 6° S in South Equatorial Belt (SEB) [1]. The GRS has shrunk over time and is becoming more circular from the elliptical shape.

2.8.2 Oval BA

The Oval BA is another major storm in the atmosphere of Jupiter. The Oval BA came into existence by the merger of three different vortices. In 1939, anticyclonic zone, STZ, split into three identical ovals: BC, DE, and FA [1]. In 1998, oval BC and DE merged together due to disturbance caused by deceleration of the Oval BC in the late 1990s. By 2000, the Oval FA and the new oval resulted from ovals BC and DE combined to make bigger oval BA [1]. The Oval BA is also an anticyclonic vortex.

2.8.3 Cyclones

Unlike anticyclonic storms, the cyclones tend to be chaotic and short living features. They disappear in a few year period. They are believed to be warmer at upper tropospheric altitudes. The cyclones also extend into the neighboring zones [1]. The cyclones and anticyclones have a symmetric pattern at Jupiter. For example, “the 12 compact anticyclonic white ovals at 41°S alternate in longitude with chaotic cyclonic patches that are a few degrees closer to the equator than the anticyclonic ovals” [1]. The cyclones tend to be elliptical in shape.

2.8.4 Lightning

The short-lived storms typically formed in the cyclonic regions that bring moisture from the deeper atmosphere to the upper troposphere. These storms last 3-4 days and generally extend up to 100 km in height with 5-7 bar pressure range [1]. These storms are accompanied by the lightning strikes. Cassini and Galileo detected several lightning strikes in the belts at night side

hemisphere by taking images closer to the westerly jets specifically at 51◦N, 56◦S and14◦S latitudes [9]. The strength of lightning at Jupiter is much stronger than at the Earth.

2.9 Temperature, Pressure, and Density Profiles

Each atmospheric layer of the Jovian atmosphere has a distinct temperature gradient. Deeper in the atmosphere, temperature, pressure, and density rise to higher values. The determination of temperature, pressure, density profiles is made by the data obtained from various sources including Earth observations such as spectroscopy, Voyager 1 and 2 flybys, Hubble telescope measurements, Cassini flyby, and Galileo probe descent. The molecular abundance of various gases in the atmosphere is estimated through the spectral lines of these gases. The $5\mu m$ hot-spots provide valuable data due to the transparency of Jupiter's atmosphere at these locations.

The temperature, pressure, and density profiles are constructed by Kerney in [14] through the development of equations of state (EOS) for the component gases of planet's atmosphere. The equations of state (EOS) relate the measured data like temperature and pressure with the fluid properties such as specific heat capacity to determine the profile of the atmospheric properties. The equations of state are derived based on the assumptions that the lower atmosphere is in the hydrostatic equilibrium and has dry adiabatic conditions. The gaseous composition data with respect to the height measured by Galileo probe was used in the computation of the equations of state for the mixture of gases at Jupiter [14]. Hydrostatic equilibrium indicates that when the external forces such as gravity acting on the fluid are balanced by the pressure gradient; the fluid maintains its condition of rest or of constant velocity at each point. The assumption of dry adiabatic conditions indicates that the rate of temperature change for ascending or descending air occurs without the addition or removal of heat.

Hydrostatic equation: $dp = -\rho g dz = -(\rho g/RT)dz$ [17]

The temperature, pressure, and density profiles of deeper atmosphere developed from equations of state are shown below.

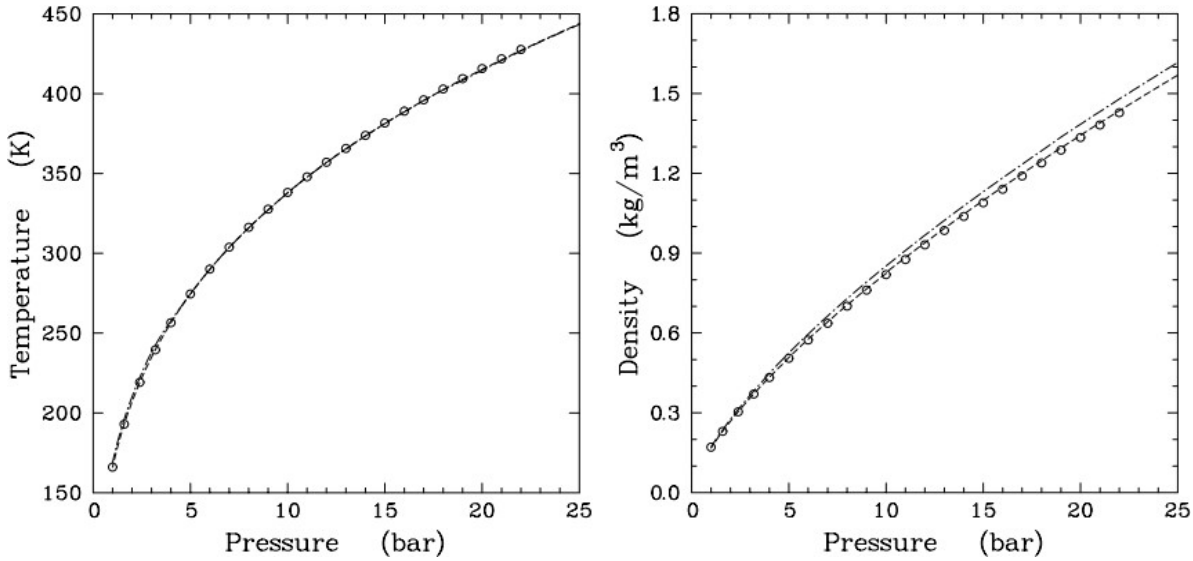

Fig. 8: Temperature and density profiles with respect to pressure in the lower atmosphere [14]

The plots indicate that rise in temperature and density with respect to pressure. The pressure increases with depth.

Roger et al. [15] modeled atmospheric properties using data available from spectroscopy, and UVS solar occultation. They compared three models: A, B, and C which differ by the temperature gradient. The models looked at the temperature and pressure trends from the upper atmosphere to the deeper levels. Roger et al [15] concluded that there is a higher temperature gradient which ranges between 3K/km to 10K/km in the pressure region of 0.1bar and 0.1μbar [15]. The pressure profile with respect to the temperature shown in figure 9 is calculated using different temperature gradients where model C agrees with the obtained data from UVS solar occultation.

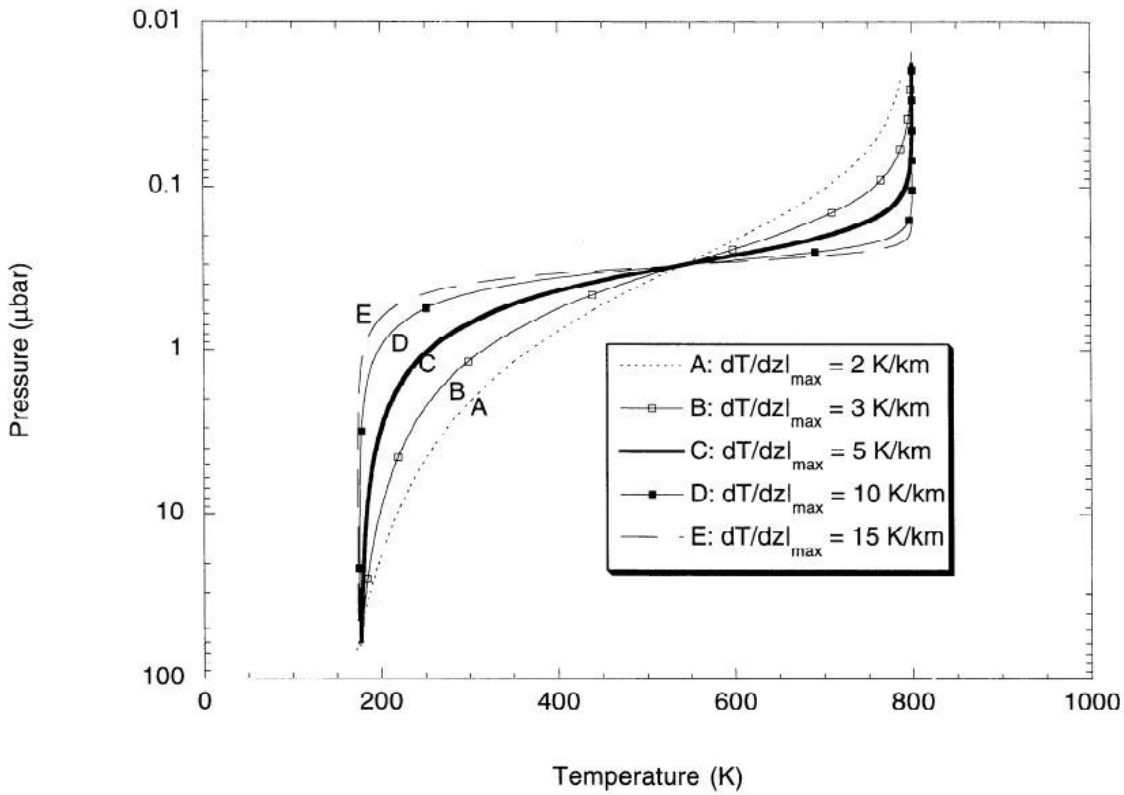

Fig. 9: Pressure vs. temperature for models A, B, and C [16]

According to the above plot, at temperatures of 176K and 800K, the atmosphere is isothermal (no temperature change) indicated by asymptotic behavior of the curves.

Seif et al [17] investigated the data obtained from the Galileo probe and constructed temperature, pressure, and density profiles, and they analyzed the changes occurring in the atmospheric properties. In addition, they compared the results with the Voyager 1 data to find the similarities and discrepancies between the two sets. The Voyager data agrees with the Galileo probe data for the upper atmosphere from 10 mbar to 1000 mbar, and both data sets indicate the exospheric temperature of 900 K at 1 nbar pressure level [17]. The Galileo probe measured atmospheric properties from 1029 km to -133 km. The two isothermal layers were also found in the stratosphere and above the tropopause. The first isothermal layer was detected from 290 km to 90 km with the temperature of 160K approximately [17]. This isothermal layer is also predicted by Roger et al [15] as shown in the figure 9. Moving down from this layer, the temperature changes with a temperature gradient of nearly 1.25 K/km. The second isothermal layer is found above the tropopause at 260 mbar pressure level and at a temperature of 112 K approximately

[17]. The gravity waves have a significant effect on the upper atmosphere. Therefore, the temperature in the upper atmosphere increases because gravity waves cause it to heat up. The dry adiabatic conditions were detected from 6 bars to 16 bars assuming the uncertainty of 0.1 K/km nearly. The density range was found to be between 10^{-1} kg/m^3 to 10^{-11} kg/m^3 from the lower atmosphere to the exospheric layer of the upper atmosphere. The atmospheric property profiles deduced from the Galileo data and from the equations of state are shown below:

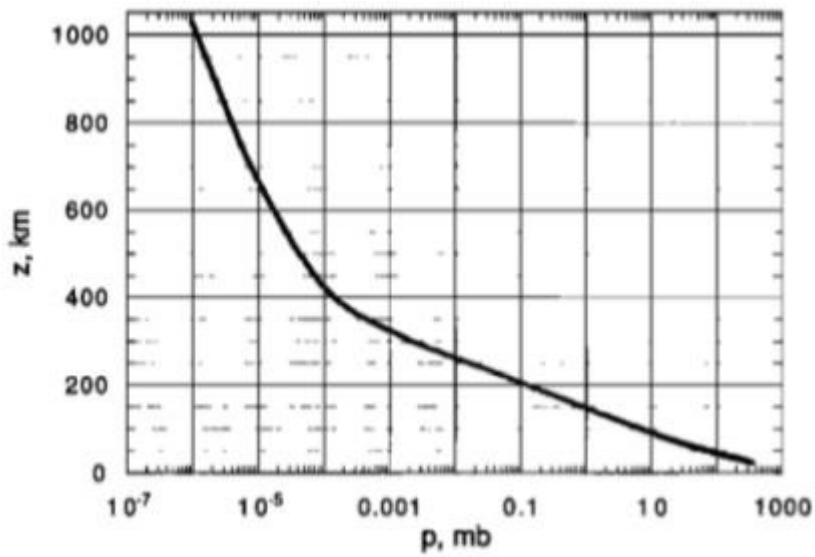

Fig. 10: Altitude vs. pressure based on Hydrostatic equation [17]

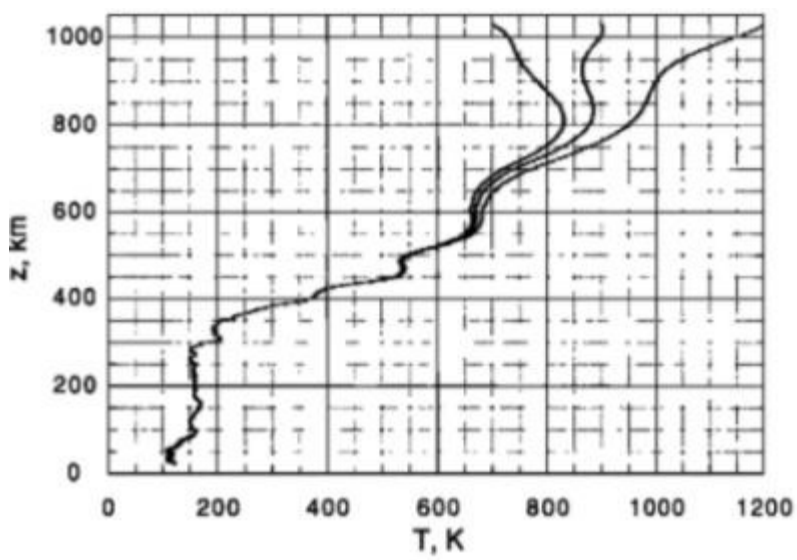

Fig. 11: Temperature vs. altitude the three curves indicate three different temperature assumptions at initial height [17]

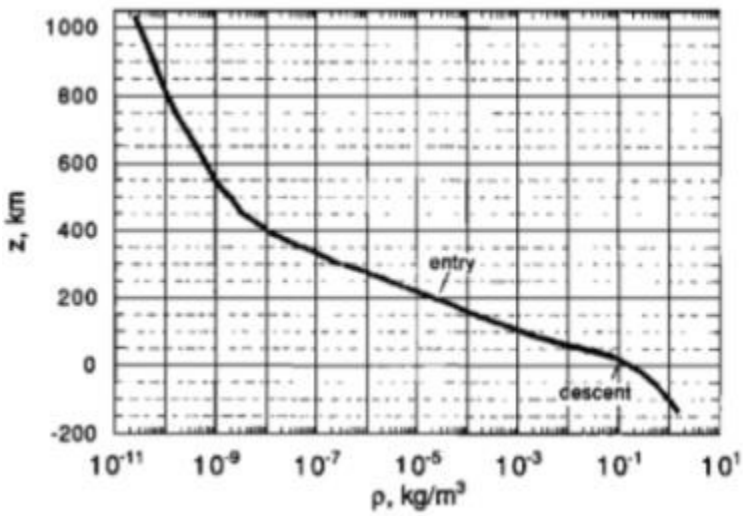

Fig. 12: Altitude vs. density profile [17]

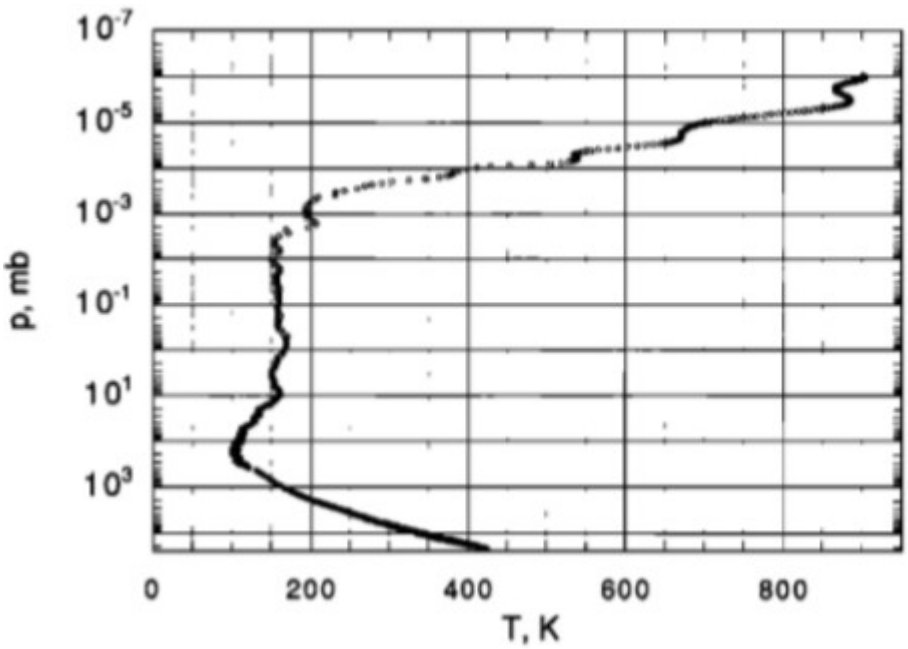

Fig. 13: Pressure vs. temperature [17]

The above plots show the trends of atmospheric properties, the pressure decline with height, temperature rises in the upper atmosphere, and figure 12 shows density drop with respect to the altitude.

2.10 Conclusion

The atmosphere of Jupiter is extremely active with the high-speed winds and the persistent atmospheric features like anticyclones. The Jovian atmosphere is analyzed by dividing it into

distinct layers and modeled using fluid flow properties. Jupiter's atmosphere is studied with the aid of various sources such as Cassini, Voyager 1 and 2 flyby data, spectroscopy, Hubble telescope observations, and with the atmospheric entry of the Galileo probe. The temperature, pressure, and density profiles are constructed using the data from the above sources which provide the understanding of Jupiter's atmospheric activities which is crucial for the design of future missions to Jupiter.

2.11 References

[1] Ingersoll, A. P., Dowling, T. E., Gierasch, P. J., Orton, G. S., Read, P. L., Sanchez-Lavega, A., Showman, A. P., Smion-Miller, A. A., and Vasavada, A. R., "Dynamics of Jupiter's Atmosphere", Jupiter: The Planet, Satellites and Magnetosphere, by Bagenal, F.; Dowling, T.E.; McKinnon, W.B., Cambridge University Press, 2004, http://www.lpl.arizona.edu/~showman/publications/ingersolletal-2004.pdf .

[2] Yelle, R. V., and Miller, S., "Jupiter's Thermosphere and Ionosphere', Jupiter: The Planet, Satellites and Magnetosphere, by Bagenal, F.; Dowling, T.E.; McKinnon, W.B., Cambridge University Press, 2004, http://www.lpl.arizona.edu/~yelle/eprints/Yelle04c.pdf .

[3] Lodders, K.,, "Atmospheric Chemistry of the Gas Giant Planets," Geochemical Society, [online], Dept. of Earth & Planetary Sciences and McDonnell Center for the Space Sciences, Washington University, Saint Louis MO 63130, 23 March 2010, https://www.geochemsoc.org/publications/geochemicalnews/gn142jan10/atmosphericchemistryoftheg/ .

[4] "What is Jupiter?', NASA [online], 10 Aug. 2011, https://www.nasa.gov/audience/forstudents/5-8/features/nasa-knows/what-is-jupiter-58.html .

[5] Patrick,G. J. I., "Cloud Structure and Composition of Jupiter's Atmosphere", Surveys in Geophysics [online], Vol. 20, Issue 6, Nov. 1999, pp. 505-535, https://doi.org/10.1023/A:1006662811248 .

[6] "Where Did You Get Those Stripes?", NASA, [online], https://www.nasa.gov/centers/goddard/multimedia/largest/atmosphere.html [retrieved 23 March 2017].

[7] Rogers, J.H, "The Giant Planet Jupiter", Practical Astronomy Handbook Series, Book 6, Cambridge University, 1995.

[8] Rogers, J. H., (August 8, 2008). "The collision of the Little Red Spot and Great Red Spot: Part 2". British Astronomical Association [online], 8 Aug. 2008, http://www.britastro.org/jupiter/2008report05.htm.

[9] Vasavada, A.R., and Showman, A., “Jovian Atmospheric Dynamics: An Update after Galileo and Cassini”, Planetary and Space Science [online], No. 51, 2003, pp. 105-112, http://citeseerx.ist.psu.edu/viewdoc/download?doi=10.1.1.492.2330&rep=rep1&type=pdf .

[10] “What is Jupiter’s Atmosphere Made?”, NASA [online], https://www.missionjuno.swri.edu/jupiter/atmosphere?show=hs_jupiter_atmosphere_story_what-is-jupiters-atmosphere-made-of [retrieved 24 April, 2017].

[11] Taylor, F. W., Atreya S.K., Encrenaz, Th., Hunten D.M., Irwin, P. G. J., and Owen, T.C., “The Composition of the Atmosphere of Jupiter”, [online], http://citeseerx.ist.psu.edu/viewdoc/download?doi=10.1.1.510.4000&rep=rep1&type=pdf [retrieved 18 July, 2017].

[12] Carr, T.D., and Gulkis, S., “Radio Rotation Period of Jupiter,” American Association for the Advancement of Science [online], Vol. 154, No. 3746, 15 Oct, 1966, pp. 257-259, http://www.jstor.org/stable/1719307 .

[13] Ed, V.I. M.., “Working Model of the Atmosphere and Near Planetary Space of Jupiter,” NASA NTM 75564, Oct. 1978, https://ntrs.nasa.gov/archive/nasa/casi.ntrs.nasa.gov/19790002813.pdf .

[14] Kerley, G. I., “Structures of the Planets Jupiter and Saturn,” A Kerley Technical Services Research Report [online], Dec. 2004, https://arxiv.org/ftp/arxiv/papers/1307/1307.3094.pdf [retrieved 8 Oct, 2017.]

[15] Yelle, R. V., Young, L. A., Vervack, R. J., Young, R., Pfister, L., and Sandel, B. R., “Structure of Jupiter's Upper Atmosphere: A Prediction for Galileo”, Journal of Geophysical

sciences [online], Vol. 101, No. E1, 25 Jan. 1996, pp. 2149-2161, http://www.lpl.arizona.edu/~yelle/eprints/Yelle96a.pdf .

[16] Hunten, D., “The Upper Atmosphere of Jupiter”, Journal of the Atmospheric Sciences, [online], Vol. 26, No. 5, 9 June 1969, pp.826-834, http://journals.ametsoc.org/doi/pdf/10.1175/1520-0469%281969%29026%3C0826%3ATUAOJ%3E2.0.CO%3B2 .

[17] Seiff, A., Kirk, D.B., Knight, T.C.D., Young, R.E., Mihalov, J. D., Young, L. A., Milos, F. R., Schubert, G., Blanchard, R. C., and Atkinson, D., “Thermal structure of Jupiter's atmosphere near the edge of a 5μm hot spot in the north equatorial belt”, Journal of Geophysical sciences [online], Vol. 103, No. E10, 25 Sept. 1998, pp. 22, 857- 22, 889, http://onlinelibrary.wiley.com/doi/10.1029/98JE01766/epdf .

[18] “Jupiter’, NASA [online], https://solarsystem.nasa.gov/planets/jupiter/in-depth/ [retrieved 11 Aug. 2017].

[19] “Science Overview”, Jupiter Orbit Insertion Online Press Kit [online], https://www.jpl.nasa.gov/news/press_kits/juno/science/ [retrieved 9 Sept. 2017].

[20] Ingersoll, A. P., “Inertial Taylor Columns md Jupiter's Great Red Spot”, Journal of Atmospheric Sciences [online], Vol. 26, 4 Feb. 1969, pp. 744 - 752, https://authors.library.caltech.edu/3988/1/INGjas69a.pdf .

[21] “Jupiter”, NASA Gallery [online], https://solarsystem.nasa.gov/planets/jupiter/galleries/?page=0&per_page=25&order=created_at+desc&search=&condition_1=1%3Ais_in_resource_list&category=51&tags=jupiter&fancybox=true&href_query_params=category%3Dplanets_jupiter&button_class=big_more_button [retrieved 5 Nov. 2017].

Chapter 3 - Jupiter's Magnetosphere and its effect on the spacecraft

3.1 Introduction

The mission design to Jupiter is immensely influenced by its magnetosphere and the extreme conditions lie in it. The Jovian magnetosphere greatly affects the performance and the structural integrity of the spacecraft in its vicinity. The spacecraft can be damaged entirely or can suffer critical problems while passing through the magnetosphere.

The Jovian magnetosphere is the space around Jupiter in which magnetic field of Jupiter dominates. Jupiter’s magnetosphere is the largest magnetosphere in the solar system. The average width of the magnetosphere is nearly 5.3 million kilometers (3.3 million miles) which is 150 times larger than Jupiter itself and approximately 15 times bigger than the Sun [1]. The trailing end of the magnetosphere reaches beyond the orbit of Saturn. To put in perspective, the Jupiter’s magnetosphere would cover 2°of sky if it can be seen at Earth from half-a-billion miles away while the Sun would occupy 0. 5°of sky only [10]. In addition to its largest size, Jupiter’s magnetosphere is strongest in the solar system. The magnetic field of Jupiter is 16 to 54 times stronger compared to Earth’s magnetic field [23]. Therefore, the Jovian magnetosphere is much more influential and spans to very far distances compared to the Earth’s magnetosphere.

Jupiter’s magnetic field rotates at a very high speed; its periodicity (~ 9 h 55 min) is described using the system III rotational system. Its fast rotation provides energy to the magnetosphere. Jupiter has similar characteristics to that of a pulsar due to its high spin rate and the strong magnetic field [10]. A pulsar is a neutron star which discharges radio emissions periodically after a millisecond or a second difference and emits particles along its magnetic pole [24]. However, the rotational speed and magnetic field of Jupiter is weaker compared to a pulsar; therefore, it does not fall into the category of pulsars [10]. Nonetheless, high intensity of the magnetic field accelerates moving particles in the magnetosphere and causes them to emit radio waves which aid in the study of Jupiter and its magnetosphere using spectroscopy technique.

The Jovian magnetosphere is filled with a huge number of energetic particles. Majority of the particles in the magnetosphere are confined to the plasma sheet located in the equatorial plane of

the planet. The plasma sheet differentially rotates with the magnetic field of Jupiter. The high-speed rotating plasma generates strong current systems in the magnetosphere under the effect of the magnetic field. The region with the concentrated current systems is known as the current sheet which is also located with the plasma sheet in the equatorial plane. The current sheet takes the complex shape at greater distances from the planet under the effect of solar wind.

Jupiter's magnetosphere is mainly divided into three regions: inner, middle, and outer magnetosphere. The inner magnetosphere is a home to highly intense radiation belts and a tenuous ring system. The radiation belts can cause acute damage to the spacecraft by ejecting or displacing electrons from its surface and components. The radiation dose can degrade the performance of the spacecraft by misleading the instruments to act on false commands. The protective measures like hardening of the spacecraft material and circuits along with shielding of the components are extremely crucial to reduce the severe effects on the spacecraft in the magnetosphere. Given the serious threats to the safety of the spacecraft in the Jovian environment, it is important to understand the nature and structure of the Jupiter's magnetosphere along with its effects on the spacecraft.

3.2 Jovian Magnetosphere

The Jovian magnetosphere is extremely complex and powerful. It extends from 600,000 miles to 2 million miles (1-3 million km) towards Sun side which 14 R_J to 42 R_J where R_J is the equatorial radius of Jupiter (1 R_J = 71,492 km). The nightside extent of the Jovian magnetosphere is 600 million miles (~1 billion km) approximately which reaches Saturn's orbit [23]. The magnetosphere is stretched to greater distances by the outflowing plasma under the effect of centrifugal force, and the outward moving plasma drags magnetic field with it [10]. The intensity of the Jovian magnetosphere is nearly 4 Gauss, and its magnetic moment is 20,000 times larger than the magnetic moment of Earth [2], [3]. The main features of Jupiter's magnetosphere include bow shock, magnetosheath, magnetopause, magnetotail, plasma sheet, and current sheet. The Jovian magnetosphere is divided into three regions: inner, middle, and outer magnetosphere. The inner magnetosphere traps and accelerates the charged particles by imparting high energy to them which results in the creation of extreme radiation belts [23].

The plasma sheet is replenished by unloading material from the satellites of Jupiter through surface eruption in addition to the plasma contribution from solar wind and Jovian ionosphere. The satellite Io adds a large amount of particles to the magnetosphere; therefore, Io is the major plasma contributor to the magnetosphere. The inner magnetosphere corotates with the planet, and at the middle magnetosphere the rotation of plasma slows down. The speed of the plasma at the outer magnetosphere becomes significantly out of sync from the rotation of the planet because of smaller centrifugal force acting on the plasma at greater distances. The solar wind merges with the Jovian magnetosphere in the outer region.

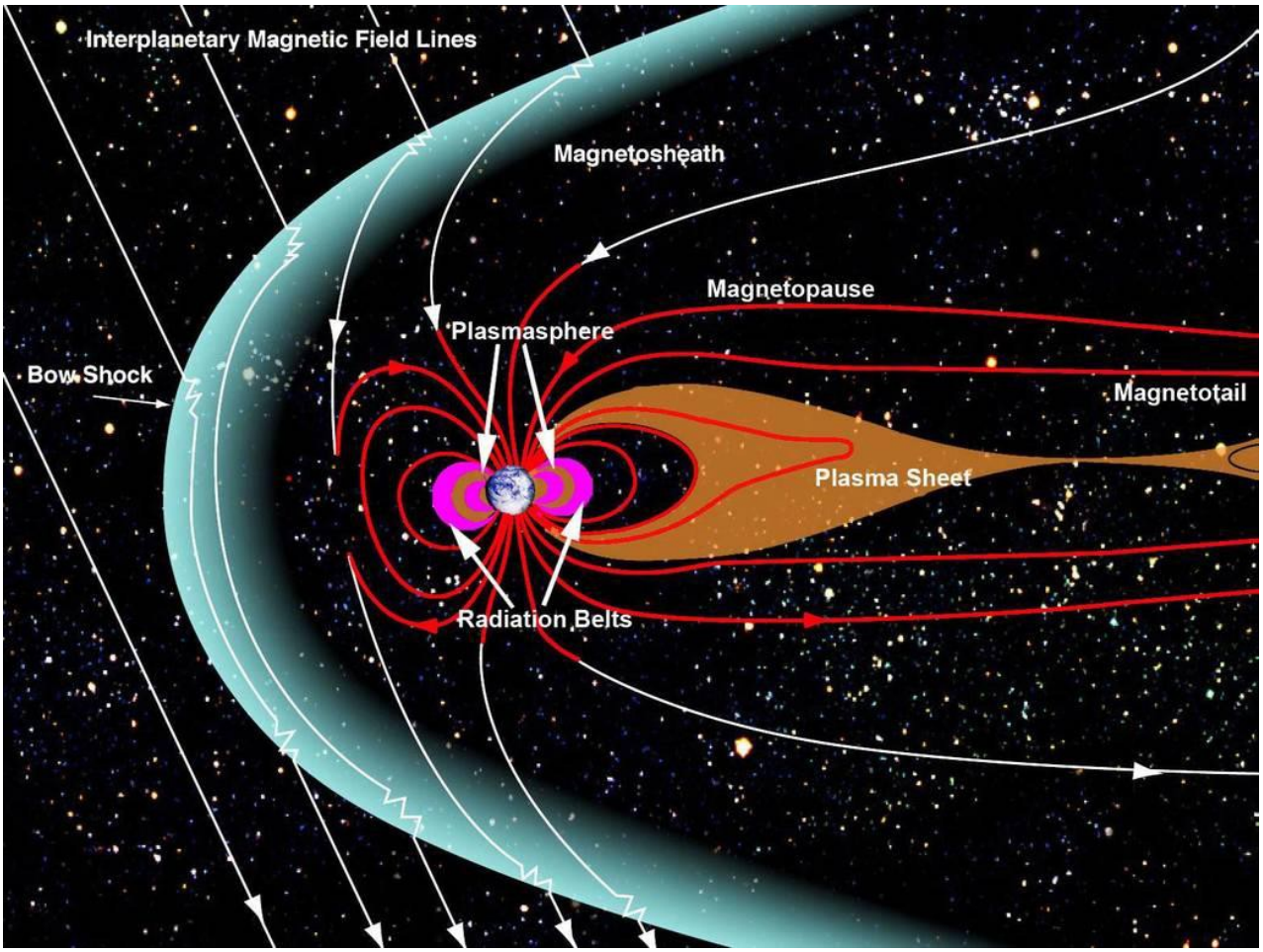

Fig.1: Configuration of Jupiter's magnetosphere [4]

3.2.1 Bow Shock

The magnetosphere of Jupiter protects the planet from the solar wind. When solar wind moving at supersonic speed encounters Jupiter's magnetosphere, a bow shock is created as a result of this

the interaction. The bow shock diverts the high speed moving solar wind away from the planet. The incoming solar wind impacts the Jovian magnetosphere with the approximate speed of 400 km/s (1,440,000 km/h) [10]. Due to this interaction between the extremely powerful magnetic field and the high-speed solar wind, an immensely strong bow shock forms in front of Jupiter which provide the dayside boundary to the Jovian magnetosphere. The location of the bow shock is not fixed; it depends upon the solar wind pressure at a particular time.

3.2.2 Magnetosheath

The region between the boundaries of bow shock and magnetopause is called the magnetosheath. As magnetosheath includes the downstream region of the bow shock, the mix of solar and the planetary plasma exists in the magnetosheath. Jupiter's magnetosheath was studied through the samples taken by several visiting spacecraft over the years. Phillips et al. [5] discuss the nature of the plasma found in the magnetosheath based on the data obtained from Pioneer 10 and 11, and Voyager 1 and 2 flybys of Jupiter. The results indicated the presence of the hot and cold plasma in the magnetosheath. The low energy protons were found in the temperature range of 2×10^5 K to 1×10^6 K, and the high energy "suprathermal protons" were also detected at temperatures greater than 10^6 K. The suprathermal particles are created when hot plasma has excessive kinetic energy and the mean free path between the particles is very large, and the "kinetic effects" become a dominant factor in the plasma motion and produce wave fluctuation [6]. The "wave-particle interactions replace Coulomb collisions and enhance dispersive effects" which heat the particles, as a result, the suprathermal particles are formed [7]. The electrons with energy between 50 eV to 200 eV were discovered in the magnetosheath as well. The electrons at temperatures from 2×10^5K to7×10^5K had "flat-topped distribution" in the Jovian magnetosheath which is similar to the magnetosheath of Earth [5]. The magnetopause boundary layer was sensed where plasma properties progressively changed from "magnetosheath-like" plasma to magnetospheric plasma [5]. Richardson [8] notes in the paper "The magnetosheaths of the outer planets" that the dayside sampling of Jupiter's magnetosheath by Voyager 1 and 2 indicated the hot plasma incorporated 20 - 50 percent of the total plasma in the magnetosheath, and the corresponding temperature of the hot plasma was 6-10 times higher than the cold plasma temperature [8]. Thus, the magnetosheath hosts both cold and hot plasma, and it serves as a transitioning region from solar to magnetospheric plasma.

3.2.3 Magnetopause

The magnetopause is the region of the magnetosphere which differentiates between low density hot plasma and the highly dense cold plasma. Depending upon the solar wind pressure, the magnetopause can be found between $45R_J$ and $100R_J$ at dayside of Jupiter [2]. The magnetopause separates the incoming solar plasma from the internal plasma residing in the magnetosphere.

3.2.4 Magnetotail

The stretched part of the magnetosphere at opposite side of the bow shock is called the magnetotail of Jupiter. Solar wind drags the magnetosphere with it to greater distances which results in the creation of the magnetotail. Thus, "A magnetotail forms downstream of a magnetized planet as a direct consequence of momentum transfer between the magnetosphere and the solar wind" [2]. The shape and dynamics of the magnetotail depend on the interaction between the viscous forces and solar wind which dictates the open or closed shape of the magnetosphere. A closed magnetosphere involves the viscous encounter of the solar wind plasma, and it conforms to the smaller size and in teardrop shape [2]. For the open magnetosphere, the solar wind enters in the magnetosphere and plays a significant role in the dynamics of the magnetosphere. The solar wind also stretches the magnetosphere to larger distances. The magnetotail of the open magnetosphere gets divided into two lobes which sandwich the current sheet in between them [2]. The lobes reduce the thickness of the current sheet through compression.

Jupiter's magnetosphere is of the open magnetosphere type with the extremely long magnetotail. The length of the Jupiter's magnetotail is nearly 7,000 R_J, and Voyager 2 sensed it near the Saturn's orbit [2]. Voyager 1 and 2 explored the dawn side of the magnetotail at the approximate distance of 100 R_J from the planet. The current sheet thickness in the magnetotail is 2 R_J approximately, and the lobes surrounding the current are deficient in plasma. The rate of field magnitude decay in the lobes is predicted as the function of the power law with a power of -1.4 i.e. $x^{-1.4}$ which is faster field reduction rate compared to the field decay in the Earth's lobes in

the magnetotail [2]. The solar wind enters in the Jovian magnetotail and interacts with the magnetic field and plasma, and it dictates the shape and dynamics of the magnetotail.

3.2.5 Io torus

The satellite Io is the major supplier of the plasma in the Jovian magnetosphere. A doughnut-shaped plasma ring circles the Io's orbit. Volcanic eruptions from Io's surface eject gases to the outer space where they are dissociated into ions. Sulfur dioxide (SO_2) is the main gas which escapes from Io's surface through volcanic activities and gets ionized to several charged states of sulfur (S) and oxygen (O) ions. The rate of plasma unloading from the Io surface to the Jovian magnetosphere is nearly 1 ton/s (6×10^{29} amu/s) [2]. The observations from Pioneer 10 and 11 and Voyager 1 and 2 spacecraft indicate fluctuations in the plasma density over time which seems to be associated with the level of volcanic activity on Io [10]. The Io torus extends from 5.2 R_J to nearly 10 R_J [2]. The Io torus is mainly energized from the rotational energy of Jupiter. The rotation of the magnetic field with the planet makes the ionized particles spin with it, and the velocity of the particles increases when moving radially outwards from the planet [10]. Hence, Jupiter's rotational energy is imparted to the Io torus through acceleration of the plasma.

The Io torus consists cold and hot plasma; therefore, it is divided into two regions: "inner cold region" and "outer warm torus region" [2]. The temperature of the inner cold plasma lies in the range of ~ 2 eV to 10 eV while the warm torus plasma can be at the temperature of 60 eV approximately. The low temperature of the ions signals that these ions are present in the inner torus region from a relatively long period where it is subjected to cooling over time. The colder plasma diffuses inwards and the warm plasma moves outwards under the effect of the centrifugal force of the planet [2]. Thus, the Io torus contributes a huge amount of plasma to the Jovian magnetosphere.

3.2.6 Plasma sheet

The Jovian magnetosphere is rich with energetic particles and ionized gases which are known as plasma. Majority of the plasma in the Jovian magnetosphere resides in a thin layer called plasma sheet which is located close to the equatorial plane of the magnetic dipole. The average thickness of the plasma sheet is between ±2 R_J to 5 R_J approximately [10]. The concentration of the

plasma to a thin disk region is due to the magnetic mirror force aligned with the field lines which acts on the gyrating particles having the magnetic moment [2]. The Io torus plasma experiences the centrifugal force because of co-rotation with the magnetic field. As the temperature of the inner Io torus plasma is below 10 eV, the cold plasma experiences relatively less magnetic mirror force [2]. The cold plasma comes to rest at the most distant point from the planet's spin axis due to the smaller magnetic mirror force acting on it, "Thus, the plasma is confined to a surface called the centrifugal equator, which is defined by the loci of points where each field line has reached its maximum distance from the rotational axis of Jupiter" [2]. The location of the plasma sheet with centrifugal equator near Io torus was confirmed by Voyager 1 data [2]. The plasma sheet traps most of the particles present in the Jovian magnetosphere in a relatively thin disk.

3.2.7 Current sheet

The condensed rotating plasma under the effect of strong magnetic field generates electrical current throughout the magnetosphere. The current sheet is the region in which bulk of the current is concentrated. It is located in the same equatorial region as the plasma sheet. Therefore, the terms current sheet and plasma sheet are sometimes used interchangeably in reference to the plasma rich region parallel to the magnetic dipole equator. However, "The changing field and plasma environment in the magnetosphere ensures that the current sheet is neither planar nor constant in its thickness" [2]. At dawn side, the half thickness of equatorial current is estimated to be 2.5 R_J, and the energy density of ions approximated from the pressure balance is found to be $\geq$ 30 keV [9]. Given the high energy density of particles, the strength of the equatorial current sheet is believed to exceed 160 MA (160 million Amperes) [2]. The current sheet contains the current systems resulted from high-speed plasma rotation. Therefore, the current sheet is the region involving high-intensity current systems.

3.3 Inner magnetosphere

The region of the magnetosphere closer to Jupiter (within 10 R_J) is known as the inner magnetosphere. The plasma sheet in this region co-rotates with the planet's magnetic field. The inner magnetosphere is most heavily populated with the plasma compared to the rest of the magnetosphere. The high energy radiation belts and the dust ring system are also a part of the inner magnetosphere.

The Io torus is a part of inner magnetosphere as well which keeps it filled with the plasma. The other sources of plasma include solar wind and the ionospheres of Jupiter and other Jovian satellites. The inner magnetosphere hosts both hot and cold plasma in it, which is bound to the centrifugal equator [2]. The distribution of the Io torus plasma is greatly affected by the magnetic field due to high field strength and low temperature of the inner torus plasma. As highly dense cold plasma rotates under the effect of intense magnetic field, the "ratio of the particle energy density to the magnetic energy density" is less than 0.2 making the magnetic field dominant on the plasma. Thus, the plasma gets confined to the plasma sheet under the effect of the dominant magnetic field. When a charged particle moves across the magnetic field, it experiences the Lorentz force; therefore, the moving charged particles tend to align themselves with the field lines which come to rest at the centrifugal equator, the farthest location from the spin axis of the planet [2]. The plasma sheet coincides with the centrifugal equator.

The main species of particles in the inner magnetosphere include ions of sulfur (S), sodium (Na), and oxygen (O) which are believed to be originating from the satellite Io [10]. In addition to the Io torus as a plasma supplier, the Jovian magnetosphere gets restocked with the particles from other sources including Sun and the ionosphere of Jupiter and Jovian satellites. The solar wind influx to Jupiter's magnetosphere makes less than 1% of the plasma which translates to nearly 100 kg/s [2]. The ionosphere of Jupiter adds hydrogen ions (H_2^+ and H^+) to the magnetosphere through plasma transportation along field lines. The ionospheric flux depends on the several aspects such as "the temperature variations of the ionosphere with the solar zenith angle, other factors such as the auroral precipitation of ions and electrons and the ionospheric heating from Pedersen currents" [2]. The Pedersen currents are the ionospheric current which flows parallel to the electric field [11]. The Jovian ionospheric plasma contribution to the magnetosphere is estimated close to 20 kg/s. The ionospheres of Jovian moons also add less than 20 kg/s plasma to the magnetosphere [2]. Forms of energetic hydrogen (H_2 and H_3) were also detected in the magnetosphere. The trihydrogen (H_3) seems to have come from Jupiter's ionosphere. The dihydrogen (H_2) is believed to be emanating from ionospheres of either Jovian satellites or from the ionosphere of Jupiter. The data from Voyager 1 and 2 indicate that the plasma density changes over time which may depend upon the volcanic activity on Io, the amount of solar wind

influx, and on the rate of ionospheric plasma transportation [10]. Thus, the abundance of particles in the magnetosphere is dependent on the dynamic activities of the sources at any given time.

The inner magnetosphere is richest in plasma compared to the other parts of the magnetosphere; most of the particles are concentrated in the Io torus due to the high influx of particles from the moon. Nonetheless, the boundaries of the Io torus are not precise. A considerable drop in plasma density at certain distances provides the estimation of the Io torus boundaries [10]. The approximate boundaries of the Io torus lie between 5.2 R_J and 10 R_J [2]. Similarly, the transition from the inner magnetosphere to middle magnetosphere is gauged from the population decrease of particles.

3.4 Middle magnetosphere

Magnetosphere ranging from 10 R_J to 40 R_J is defined as the middle magnetosphere. The rate of the plasma rotation with respect to the magnetic field starts to decrease in the middle magnetosphere. The rotating plasma lags the magnetic field by a factor of 2 or less in the middle magnetosphere [10]. The radial currents produce aurorae in the Jupiter's ionosphere through "large field-aligned potentials" [2]. The shape and location of the current sheet are rearranged in the middle magnetosphere. From 30 R_J onwards, current sheet is found in between the magnetic dipole equator and the centrifugal equator because of the force balance of centrifugal and thermal pressure [2]. The current sheet takes a complex form because the solar wind pressure also plays a significant role in this region. The ratio of particle energy density to magnetic energy density surpasses 1 because of decreased plasma population in the middle magnetosphere compared to the inner region. Voyager 1 data indicated the decline of plasma density from 2,000 particles/cm^3 in the Io torus to 0.2 particles/cm^3 near 35 R_J [2]. In the middle magnetosphere, the strength of magnetic field and plasma density becomes smaller compared to the inner magnetosphere.

3.5 Outer magnetosphere

Beyond 40 R_J, the magnetosphere is termed as the outer magnetosphere. The plasma further lags the magnetic field in the outer magnetosphere. The rotational speed of the plasma reduces by a factor of 2 or more relative to the magnetic field rotation [2]. In addition, solar wind makes its

way into the outer magnetosphere; therefore, the magnetospheric plasma becomes a mix of solar wind particles and the Jovian plasma. Solar wind seems to contribute ions of helium (He), carbon (C), nitrogen (N), oxygen (O), neon (Ne), manganese (Mn), silicon (Si), and iron (Fe) to the outer magnetosphere [10]. The current sheet becomes parallel to the solar wind beyond 60 R_J under the effect of solar wind pressure [2]. The nightside of the outer magnetosphere includes an additional current system which bridges the currents of magnetic disk and magnetopause together. This current system elongates the magnetotail to 7,000 R_J approximately and divides the magnetotail into two lobes above and below the current sheet [2]. The outer magnetosphere is influenced by solar wind which plays a significant in its dynamics and structure.

3.6 Radiation belts

The inner magnetosphere of Jupiter includes a region of highly intense radiation belts that emit synchrotron radiations to the outer space. The strong electric fields power the inward diffusing plasma which causes the generation of the radiation belts [2]. The diffusion of plasma within 10 R_J is believed to be mainly driven by electric field corresponding to the ionospheric winds, and at the distances greater than 10 R_J, “magnetic perturbations, electric fields associated with magnetospheric convection, or interchange instabilities driven by thermal plasma gradients may drive the diffusion” [12]. The most intense part of the radiation belts is the inner portion of the radiation belts from 1 R_J to 2 R_J, and this region consists nearly one half of the peak radiation density found beyond 2 R_J [13]. The radiation belts are in a relatively compact region and exhibit extremely harsh environment.

The Cassini spacecraft studied Jovian radiation belts during its flyby of Jupiter. The radio emission data collected by Cassini suggested that the high energy particles are moving at speeds close to the speed of light. “Cassini's radar instrument, operating in a listen-only mode, measured the strength of microwave radio emissions at a frequency of 13.8 gigahertz (13.8 billion cycles per second or 2.2centimeter wavelength)” [14]. Cassini observations also indicated the wobbling of the radiation belts with respect to the planet due to magnetic dipole tilt relative to the geographical poles. The synthesis of the Cassini data concluded that Jovian radiation belts exhibit most severe environment in the entire solar system [14]. Thus, Jovian radiation belts

consist of extremely high speed moving plasma and present most hazardous environment to the spacecraft.

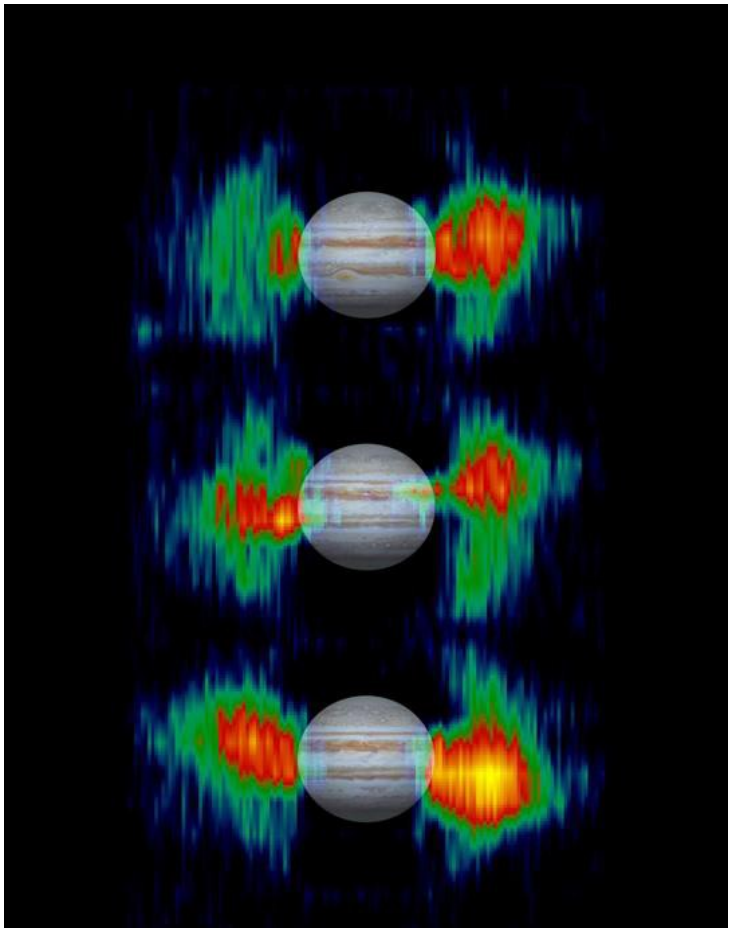

Fig. 2: Jovian radiation belts at three different instances during one rotation of Jupiter [14]

3.7 Rings

A faint dust ring system encircles Jupiter. The existence of Jovian rings was not known until Voyager 1 discovered them in the year of 1979. These rings could only be seen behind Jupiter when Sunlight hit them, or they are visible in the infrared region of the spectrum due to their dim appearance [15]. The rings are composed of small dust particles.

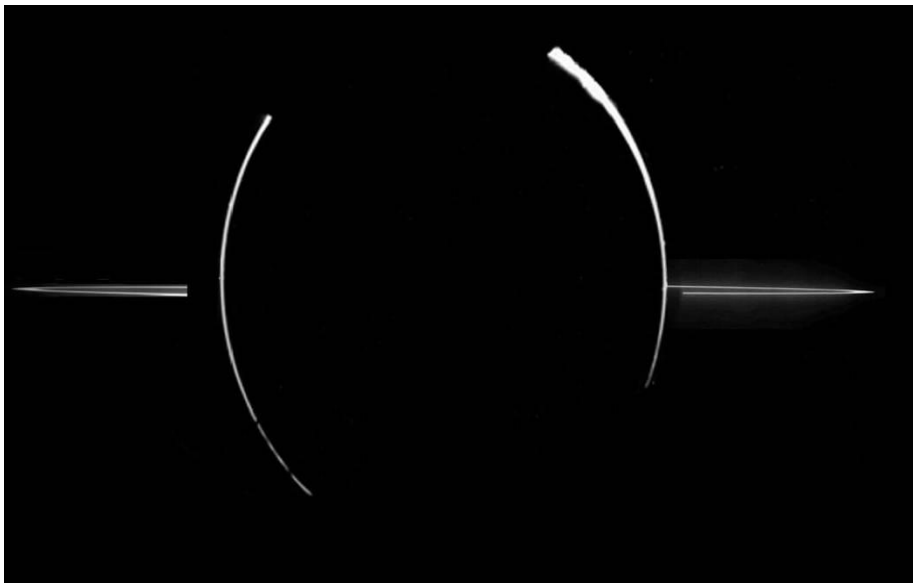

Fig. 3: illuminated rings in the sunlight taken by Galileo during the solar eclipse by Jupiter [18]

The entire ring system is divided into three main regions: a pair of outer rings (gossamer rings), the main ring, and the doughnut-shaped halo ring. The rings are found in the vicinity of the inner Jovian moons, and the dust particles in the rings are believed to have come from these moons. The outermost gossamer ring is located along the orbit of Thebe satellite. The second gossamer ring is found along Amalthea moon's orbit [16]. The gossamer rings are extended from 1.81 R_J to 3.2 R_J [17]. The flattened main ring resides between the orbits of Andrasta and Metis moons. The width of the main ring is 6,500 km (4,000 miles) approximately which ranges from 1.72 R_J to 1.82 R_J [16], [17]. Lastly, the innermost halo ring extends from 1.40 R_J to 1.72R_J [17]. The halo ring is thicker than other rings because of electromagnetic forces from the Jovian magnetosphere. The thickness of halo ring falls in the range of 20,000 km to 40,000 km (12,400 miles to 25,000 miles). However, most of the particles in the halo ring stay closer to the ring plane within few hundred kilometers [16]. The micrometeoroid impacts at the surfaces of Jovian moons eject dust particles which are captured into the orbit around Jupiter; therefore, the moons are believed to be the main source of the ring material. Without the replenishment of dust particles from the Jovian moons, the rings are expected to diminish over time. Thus, the input of dust particles from Jovian moons sustains the rings.

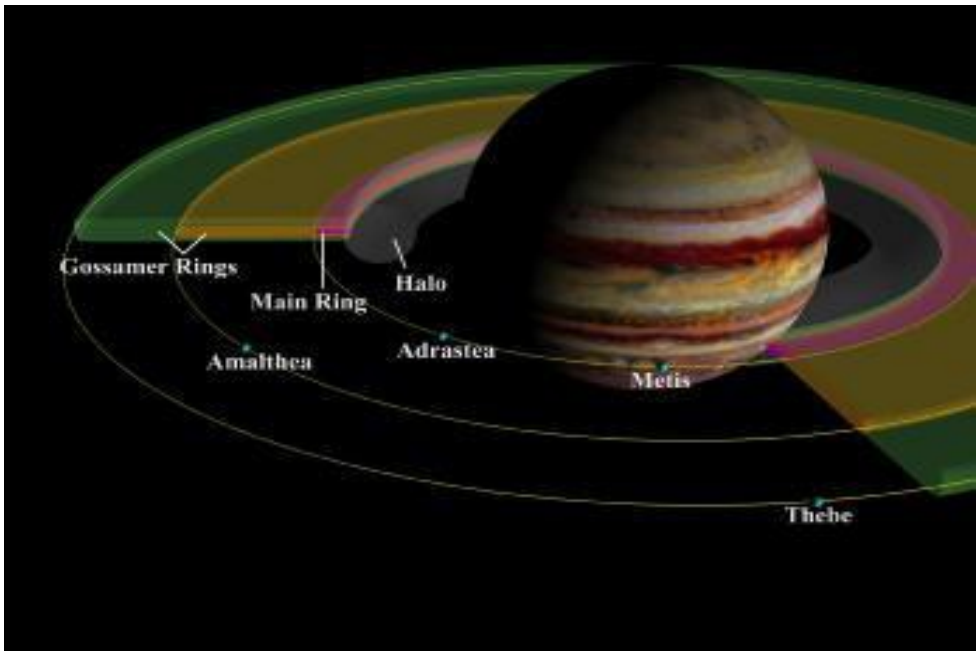

Fig. 4: Jupiter's ring system [15]

3.8 Hazards to the spacecraft

The presence of enormously intense environment in Jupiter's surroundings poses several critical threats to the visiting spacecraft for Jovian missions. In addition to the harshest radiation belts encircling the planet, Jupiter has most powerful magnetic field and largest magnetosphere in the solar system. The high energy radiations can cause severe damage to the spacecraft outer body and can create malfunctions in the electrical components and science equipment such as sensors and particle analyzer instruments stored inside the spacecraft. The main issues include long-term ionization effects, displacements effects, and transient interference effects [22]. The temporary interference effects disappear after the radiation exposure ends while the long-term ionization effects create permanent irregularities in the electronic components. The high speed moving ions can knock out the electrons from the surface of the spacecraft by breaking the molecular bonds of the material through the ionization effect. These particles can displace the electrons in the crystal lattice which cause the imbalance of electrons and holes, "The endgame for any spacecraft that enters this doughnut-shaped field of high-energy particles is an encounter with the harshest radiation environment in the solar system" [19]. Even outside of the radiation belts, the magnetosphere consists of high speed rotating plasma accompanied by the immensely powerful magnetic field which can cause harm to the spacecraft.

The Galileo spacecraft on a mission (1989-2003) to study Jupiter and its moon encountered several problems due to the presence of intense conditions there, “Almost all of the science instruments and several engineering systems suffer from problems caused by increasing noise when pushed deep into the Jovian particle environment” [20]. Due to the lack of onboard dosimeter, the radiation dose for Galileo had to be calculated using the particle detector data. The resulting calculations showed that spacecraft was exposed to 600 krads of radiation dose over mass per unit area of 2.2 g/cm^2 in 33 orbits around Jupiter while the spacecraft was designed to endure only 150 krads of dose [20]. Figure 5 shows the computed dose rate model from data indicating cumulative dosage getting close to 600 krads after 31st orbit.

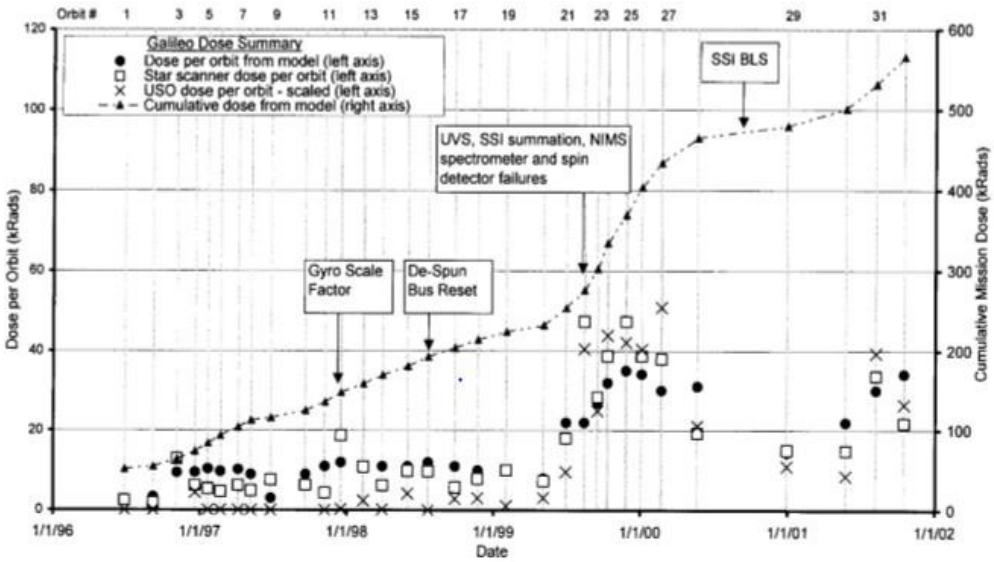

Fig. 5: Radiation dose approximation encountered by Galileo spacecraft [20]

The spacecraft suffered severe problems in its instruments after radiation dose surpassed 150 krads limit [20]. The issues caused by harmful radiations included high detector noise, quartz oscillator phase shift in the frequency, power anomalies probable from arcing dielectrics, instrument failures resulted from current leakage due to increased radiation dose, problems in the optical elements, and few other irregularities [20]. Galileo spacecraft entered safe mode after falsely detecting a signal for “Power-on-reset”, and nearly all the data was lost from orbits 16, 18, and 33 because of the safe mode activation. Moreover, Galileo experienced anomalies in the

pair of its gyros [20]. Numerous problems experienced by Galileo spacecraft in its electrical components and scientific instruments indicate the severity of the Jovian environment.

Current mission to Jupiter by spacecraft Juno to map the entire planet is also accumulating radiation dose during each pass through the magnetosphere. According to mission Juno's project manager (JPL Pasadena, CA), Rick Nybakken, the cumulative radiation dose encountered by Juno will be "equivalent of over 100 million dental X-rays" during the lifetime of the mission [19]. Such a high radiation exposure to Juno spacecraft is expected despite its polar orbit which is away from the intense equatorial region of Jovian magnetosphere. Hence, the consideration of protective measures for the spacecraft is extremely critical to deal with the potential threats in the Jovian magnetosphere.

3.9 Possible protection techniques

The spacecraft and its instruments require vigorous protective measures to survive in the high radiation Jovian environment. Numerous protective techniques like device hardening, inherent shielding through proper component placement, circuit hardening, external shielding, and so on are used to ensure spacecraft safety from acute Jovian conditions [22]. Individual devices can be hardened against radiation dose by layering them with the insulating coat and with the material selection for the device which is less sensitive to the radiation dose. Similarly, the circuits can be hardened physically and logically to make them radiation tolerant. Physical hardening of the circuits is achieved by manufacturing chips on "insulating substrates" in place of the regular semiconductor wafers. Most insulating substrates include Silicon on Insulator (SOI) and Silicon on Sapphire [21]. The logical radiation hardening is done by using error correcting memory, employing redundant components, installing watchdog timer, and so on. The error correcting memory technique is based on the coded instructions to confront data anomalies; it involves three main steps: reading the data, inspection of the data consistency by looking for errors and writing the necessary correction to the random-access memory (RAM) [21]. The watchdog timer is used as the ultimate option after other preventative methods become insufficient. The watchdog timer is also a check on the functioning of the system because the software schedules instructions write to the watchdog after a specific time which indicates that the system is operational. In case of anomalies in the system due to radiation effects, there is a high possibility

that the system becomes unable to pass the write instructions to the watchdog timer. Therefore, the watchdog timer will run out of time which enforces hard reset of the system [21]. Redundancies in data taking methods help to affirm consistency of the data, as well as, they provide the assurance of data collection if one of the components is damaged. The insulating coating at the outer surface of the spacecraft protects it in the high radiation environment. Placing most sensitive components under relatively robust components minimizes radiation effects on the delicate instruments. Encasing the sensitive instruments in the insulated shield is desired to protect the devices from harm.

The spacecraft Juno is furnished with the high-quality shield and protective equipment to reduce the radiation effects on the spacecraft. Juno's onboard electrical wiring is radiation hardened and the sensors are secured under protective shielding. Its most delicate components such as flight computer and the vital elements of science instruments are enclosed in a "first-of-its-kind titanium vault" which weighs nearly 172 kg (400 pounds). This "highest profile piece of armor" will minimize the radiation dose to inner electronics by 800 times compared to the radiation dose encountered by the outer titanium casing [19]. These protective measures will help Juno sustain in the Jovian surroundings for its mission life by slowing the rate of the damage to the spacecraft from high-speed moving particles. Thus, the protective measures are a crucial part of the spacecraft survival and the mission success in the Jovian magnetosphere.

3.10 Conclusion

Jupiter's magnetosphere is not only the strongest and largest magnetosphere; it also has the harshest environment in the solar system. It is a home to most severe radiation belts in the solar system. The high-speed charged particles moving nearly at the speed of light form powerful current systems throughout the magnetosphere. The Jovian moons along with other sources like solar wind replenish plasma in the magnetosphere to keep it dynamically active. A ring system consisting of tiny dust particles surrounds Jupiter. All these conditions: high-speed moving plasma, strong current systems, radiation belts, intense magnetic field, and dust particles in the rings poses major challenges to the mission design for Jupiter. Therefore, vigorous safety measures are required to sustain the spacecraft in this environment. Hence, a thorough study of Jovian surroundings was essential to plan a mission to Jupiter.

3.11 References

[1] “Jupiter’s Magnetosphere”, NASA [online], https://www.missionjuno.swri.edu/jupiter/magnetosphere/ [retrieved 08 Aug. 2017].

[2] Khurana, K. K., Kivelson, M.G., Vasyliunas, V. M., Krupp, N., Woch, J., Lagg, A., Mauk, B. H., and Kurth, W. S., “The Configuration of Jupiter’s Magnetosphere”, *Jupiter: The Planet, Satellites and Magnetosphere*, Cambridge University, 2004, http://www.igpp.ucla.edu/people/mkivelson/Publications/279-Ch24.pdf.

[3] “Do other solar system planets have protective magnetospheres?”, NASA, [online], https://genesismission.jpl.nasa.gov/science/module4_solarmax/solarmax_planets.html [retrieved 10 Nov. 2017].

[4] “Magnetospheres of the Outer Planets Group”, University of Colorado Boulder [online], http://lasp.colorado.edu/home/mop/resources/graphics/graphics/?doing_wp_cron=1515888639.94015789031982421875 00 [retrieved 15 Oct. 2017].

[5] Phillips, J. L., Bame, S.J., Thomsen, M. E., Golstein, B. E., Smith, and E. J., “Ulysses Plasma Observations in the Jovian Magnetosheath”, *Journal of Geophysical Research* [online], Vol. 98 No. A12, 1 Dec. 1993, pp 21,189-21,202, doi: 10.1029/93JA02592.

[6] Lazar1, M. Schlickeiser, R., and Poedts, S., “Suprathermal Particle Populations in the Solar Wind and Corona”, intechopen.com [online], http://cdn.intechopen.com/pdfs/32539/InTech-Suprathermal_particle_populations_in_the_solar_wind_and_corona.pdf [retrieved 02 Nov. 2017].

[7] Lazar, M., Schlickeiser, R., and Poedts, S., “Suprathermal Particle Populations in the Solar Wind and Corona”, [online], http://cdn.intechopen.com/pdfs/32539/InTech-Suprathermal_particle_populations_in_the_solar_wind_and_corona.pdf [retrieved 9 Nov. 2017].

[8] Richardson, J. D., “The magnetosheaths of the outer planets”, *USA Planetary and Space Science* [online], No. 50, 2002, pp 503-517, http://citeseerx.ist.psu.edu/viewdoc/download?doi=10.1.1.6.9904&rep=rep1&type=pdf.

[9] Khurana, K. K., and Schwarzl, H., “Global structure of Jupiter's magnetospheric current sheet”, *Journal of Geophysical research: Space Physics*, Vol. 110, No. A07227, 23 July 2005, http://onlinelibrary.wiley.com/doi/10.1029/2004JA010757/full.

[10] Yeates, C. M., Johnson, T. V., Colin, L., Fanale, F. P., Frank, L., and Hunten, D. M., “Galileo: Exploration of Jupiter’s System”, NASA SP-479, Washington, DC, 1985, https://ntrs.nasa.gov/archive/nasa/casi.ntrs.nasa.gov/19860001670.pdf.

[11] Cowley, S. W. H., “Magnetosphere-Ionosphere Interactions' A Tutorial Review”, Department of Physics and Astronomy, University of Leicester, Leicester, UK [online], http://www.uio.no/studier/emner/matnat/fys/FYS3610/h13/cowley2000.pdf [retrieved 27 Oct. 2017].

[12] Brice, N., and Mcdonough, T. R., “Jupiter's radiation belts”, *Icarus*, Vol. 18, Issue 2, Feb. 1973, pp 206-219, https://www.sciencedirect.com/science/article/pii/0019103573902042.

[13] Degioanni, J. J. C., “The Radiation Belts of Jupiter”, NASA N73 - 25878, Urbana, Illinois, 1973, https://ntrs.nasa.gov/archive/nasa/casi.ntrs.nasa.gov/19730017151.pdf .

[14] “Inner Radiation Belts of Jupiter”, NASA [online], https://www.nasa.gov/mission_pages/juno/multimedia/pia03478.html [retrieved 14 Nov. 2017].

[15] “How did Jupiter's Rings Form?”, NASA [online], https://www.nasa.gov/centers/goddard/multimedia/largest/rings.html [retrieved 08 Oct. 2017].

[16] “Jupiter’s Rings”, NASA [online], https://www.missionjuno.swri.edu/jupiter?show=hs_jupiter_story_jupiters-rings [retrieved 28 Oct. 2017].

[17] Throop, H. B., Porco, C. C., West, R. A., Burns, J. A., Showalter, M. R., and Nicholson, P. D., “The jovian rings: new results derived from Cassini, Galileo, Voyager, and Earth-based observations”, *ICARUS* [online], No. 172, 8 Mar. 2004, pp 59-77, http://ciclops.org/media/sp/2007/2687_7449_0.pdf.

[18] “Jupiter's Rings Revealed”, NASA [online], 23 Mar. 2008, https://www.nasa.gov/multimedia/imagegallery/image_feature_995.html

[19] “NASA’s Juno Spacecraft to Risk Jupiter’s Fireworks for Science”, NASA [online], Release 16-063, 16 June 2016, https://www.nasa.gov/press-release/nasa-s-juno-spacecraft-to-risk-jupiter-s-fireworks-for-science

[20] Fieseler, P. D., Ardalan, S. M., and Frederickson, Dr. R. A., “The Radiation Effects on Galileo Spacecraft Systems at Jupiter”, Jet Propulsion Laboratory, Pasadena, Ca, https://web.archive.org/web/20110719204111/http://trs-new.jpl.nasa.gov/dspace/bitstream/2014/11661/1/02-0220.pdf [retrieved 15 Nov. 2017].

[21] Yu, F., Liu, J., Huang, Z., Luo, H., and Lu, Z., “Overview of Radiation Hardening Techniques for IC Design”, *Information Technology Journal* [online], No. 9, 10 June 2010, pp. *1068-1080*, http://scialert.net/fulltext/?doi=itj.2010.1068.1080

[22] Van Lint, V. A. J., Raymond, J. P., Hart, A. R., and Price, M. L., “Radiation Design Book”, NASA CR 152011, 7 May 1977, https://ntrs.nasa.gov/archive/nasa/casi.ntrs.nasa.gov/19770081915.pdf.

[23] “Jupiter”, NASA [online], https://solarsystem.nasa.gov/planets/jupiter/in-depth/ [retrieved 12 Aug. 2017].

[24] “Neutron Stars”, NASA [online], Mar. 2017, https://imagine.gsfc.nasa.gov/science/objects/neutron_stars1.html.

Chapter 4: Aerobraking Analysis and Results

Nomenclature

Symbol	Definition
A	Area of the spacecraft
a	Semi-major axis of the orbit
a_d	Acceleration due to drag
a_g	Acceleration due to gravity
a_{SC}	Total spacecraft acceleration
a_x, a_y, a_z/$\ddot{x}, \ddot{y}, \ddot{z}$	Components of acceleration vectors
C_D	Coefficient of drag
dm	Infinitesimal change in mass
dt	Infinitesimal change in time
e	Eccentricity of the orbit
G	Universal gravity constant
g_o	Sea level acceleration due to gravity
h	Angular momentum per unit mass
ht	Altitude above surface
I_{SP}	Specific impulse
Δm	Small change in mass
$\dot{m}_e$	Rate of mass flow
m_J	Mass of Jupiter
m_{SC}	Mass of the spacecraft
r	Arbitrary position vector
$\dot{r}$	Time derivative of position
$\ddot{r}$	Second time derivative of position
r_a	Apoapsis radius
r_p	Periapsis radius
R_J	Radius of Jupiter
r_{oSC}	Initial position vector
r_{SC}	Position Vector of the spacecraft
T	Period of the orbit
Δt	Small change in time
T_f	Thrust force
x, y, z	Components of position vectors
v_{atm}	Velocity of the atmosphere
v_{oSC}	Initial velocity vector
v_p	Periapsis velocity

v_{relSC}	Relative Velocity of the spacecraft w.r.t atmosphere
v_{SC}	Spacecraft velocity
$v_x, v_y, v_z/\dot{x}, \dot{y}, \dot{z}$	Components of position vectors
θ	True Anomaly
ρ	Atmospheric density
μ	Product of universal gravitational constant and mass of Jupiter
ω_J	Orbital speed of Jupiter

4.1 Introduction

Several missions to Jupiter are in their planning phase to study its small moon Europa which is one of the few moons in the solar system with potential signs of life. The orbit insertion with the pure propulsive burn is highly expensive. Current mission to Jupiter (Mission Juno) reserved 1,232 kg of propellant (810 kg of hydrazine and 422 kg of oxidizer) for the 35-minute burn for orbit insertion which would reduce the orbital period from 53.5 days to 14 days [2], [4]. The total mass of the Juno spacecraft was 3,625 kg at launch [2]. Therefore, nearly 34 percent of the spacecraft total mass at launch was dedicated to the reserve fuel for the orbit insertion burn. The Leros 1b engine of the Juno spacecraft has the specific impulse of 317s; therefore, the engine would use 447 kg of fuel during the 35-minute burn [3], [2]. If aerobraking can be employed for the orbit insertion around Jupiter, the Jovian mission can be made economical by saving required fuel for the propulsive burn. Hence, the scenario of similar period reduction as of Juno's using aerobraking is studied in this chapter to get the idea of fuel and cost savings in terms of numbers from the implementation of the technique.

4.2 Theory

The orbit of the spacecraft is affected by atmospheric drag which results in the degradation of the orbit size. Atmospheric drag can be used to shrink the orbit from a larger elliptical orbit to a smaller orbit without using fuel through the propulsive burn. Atmospheric drag works against the motion of the spacecraft and thus, reduces its velocity which results in the smaller apoapsis compared to the original apoapsis altitude.

The periapsis of the orbit is placed in the upper atmosphere of the planet. The consecutive passes through the atmosphere gradually reduces the apoapsis altitude of the orbit; therefore, it decreases the size of the orbit.

The relative velocity of the spacecraft would be the difference between the velocity of the atmosphere and spacecraft.

Relative velocity of the spacecraft with respect to the atmosphere is given by:

$$v_{relSC} = v_{SC} - v_{atm} \tag{4.1}$$

Velocity of the atmosphere:

$$v_{atm} = \omega_J \times r_{SC} \tag{4.2}$$

Therefore, spacecraft relative velocity:

$$v_{relSC} = v_{SC} - \omega_J \times r_{SC} \tag{4.3}$$

From Newton's 2nd law for the spacecraft:

$$-\frac{Gm_J m_{SC}}{r^2} - \frac{1}{2}\rho v_{relSC}^2 C_D A = m_{SC} a \tag{4.4}$$

$$-\frac{Gm_J m_{SC}}{r^2} - \frac{1}{2}\rho \dot{r}_{relSC}^2 C_D A = m_{SC} \ddot{r} \tag{4.5}$$

Solving the dynamics of the spacecraft, the net change in velocity (Δv) due to atmospheric drag is determined after each pass.

4.3 Assumptions

- Other perturbing forces like the solar pressure or J_2 perturbations are assumed to be negligible
- No significant change in the velocity of the spacecraft due to winds
- The lower atmosphere is in hydrostatic equilibrium i.e. pressure decreases with height
- The upper atmospheric properties can be determined by assuming the mixture of gases have the properties of the calorically perfect gas i.e. specific heat constants (c_v and c_p) depend on the temperature only and are independent of pressure and enthalpy
- Flow through the engine nozzle:
    - Is isentropic i.e. no addition of irreversibilities in the flow
    - The fuel and oxidizer are well mixed
    - No additional forces acting on the flow

4.4 Procedure

The goal of this analysis was to determine Δv savings when the period of the orbit is reduced from 54.2 days to 14 days through aerobraking. The initial state vector was determined based on

the knowledge of the periapsis altitude and initial period. Next, the dynamics of the system is analyzed using MATLAB by considering the major forces acting on the system.

4.4.1: Determination of state vector

Radius of Jupiter, $R_J = 7142\ km$

Altitude above surface, $ht = 350km$

$$G = 6.67\ e - 20\ \frac{km^3}{kg.s^2}$$

$$\mu = G * m_J = 1.2661e + 08\ \ \frac{km^3}{s^2}$$

$$T = 54.2\ days$$

$$T = \frac{2\pi}{\sqrt{\mu}} a^{\frac{3}{2}}$$

Semi-major axis, a:

$$a = \left(\frac{T\sqrt{\mu}}{2\pi}\right)^{\frac{2}{3}} = \left(\frac{54.2 * \sqrt{1.2661e + 80}}{2\pi}\right)^{\frac{3}{2}} = 4{,}128{,}171\ km$$

Radius of periapsis, r_p

$$r_p = R_J + ht = 71492 + 350 = 71{,}842\ km$$

Initial radius of apoapsis, r_a:

$$r_a = 2a - r_p = 2 * 4128171 - 71842 = 8.1845e + 06\ km$$

Eccentricity of the orbit, e:

$$e = \frac{r_a - r_p}{r_a - r_p} = \frac{8.1845e + 06 - 71842}{8.1845e + 06 + 71842} = 0.983$$

Angular momentum, h:

$$h = \sqrt{r_p \mu (1 + e)} = \sqrt{71842 * 1.2661e + 08 * (1 + 0.983)} = 4.2195e + 06\ \ \frac{km^2}{s}$$

Periapsis velocity, v_p:

$$v_p = \frac{h}{r_p} = \frac{4.2195e+06}{71842} = 59.11\ \frac{km}{s}$$

Position vector at periapsis, r_{oSC}:

$$r_{oSC} = \frac{h^2}{\mu}\frac{1}{(1+ecos\theta)}\begin{matrix}0\\ \cos(\theta)\\ \sin(\theta)\end{matrix} = \frac{4.2195e+06^2}{1.2661e+08}\frac{1}{(1+0.983*\cos(0)}\begin{matrix}0\\ \cos(0)\\ \sin(0)\end{matrix}$$

$$r_{oSC} = [0\ 71842\ 0]\ km$$

vector at periapsis, v_{oSC}:

$$v_{oSC} = \frac{\mu}{h}\begin{bmatrix}0\\ -\sin(\theta)\\ e+\cos(\theta)\end{bmatrix} = \frac{1.2661e+08}{\cancel{4.2195e+06}}\begin{bmatrix}0\\ -\sin(0)\\ 0.983+\cos(0)\end{bmatrix}$$

$$v_{oSC} = [0\ 0\ 59.11]\ \frac{km}{s}$$

Initial state vector:

$$r_{oSC} = [0\ 71842\ 0]\ km$$

$$v_{oSC} = [0\ \ 0\ \ 59.11]\ \frac{km}{s}$$

<u>4.4.2</u> <u>: Dynamics</u>

The motion of the spacecraft under gravitational and atmospheric drag in the orbit is studied by transforming the second order differential equation into the first order differential equation.

$$r_{SC} = [x\ y\ z]$$

$$v_{SC} = [v_x\ v_y\ v_z] = [\dot{x}\ \dot{y}\ \dot{z}]$$

$$a_{SC} = [a_x\ a_y\ a_z] = [\ddot{x}\ \ddot{y}\ \ddot{z}]$$

$$a_{SC} = a_g + a_d$$

$$a_g = -\frac{Gm_J m_{SC}}{|r^3|_{SC}}\begin{matrix}x\\ [y]\\ z\end{matrix}$$

$$a_d = -\frac{1}{2|v_{rel}|}\rho|v_{relSC}^2|C_D A\begin{matrix}\dot{x}\\ [\dot{y}\ ]\\ \dot{z}\end{matrix}$$

The data retrieved from the Galileo probe was used to model the atmosphere of the planet. The data is available from 871.2 km downwards to -137.2km. The density above 871.2 km is estimated by extrapolation of the data due to the absence of available data.

The MATLAB code for the simulation and atmospheric modeling is documented in the appendix section.

4.4.3 : Aerobraking phases

The orbit insertion of the spacecraft around Jupiter via aerobraking is studied in the three phases: walk-in phase, main phase, and walk-out phase. The simulation of these phases was performed and the resulting reduction in velocity and period were extracted from the output.

4.4.4 : Propellant savings

The propellant savings from the aerobraking maneuvers can be determined by applying Newton's second law of motion:

Momentum change during interval $t + \Delta t -$ momentum at time t = net external impulse [1]

Mass flow rate through the nozzle = $\dot{m}_e$

According to mass conservation, rate of mass change in the nozzle is equal to mass flow rate though the nozzle.

$$\frac{dm}{dt} = -\dot{m}_e$$

$$\Delta m = \dot{m}_e \Delta t$$

From thrust equation:

$$\frac{dm}{dt} = -\frac{T_f}{I_{SP}\, g_o}$$

$$\Delta m = -\frac{T_f}{I_{SP}\, g_o}\Delta t$$

Burn time, Δt = 35 minutes

Thrust of Leros 1b engine, T_f = 635 N

Specific Impulse of the engine, I_{SP} = 317 s

Sea level acceleration of gravity, g_o= 9.8 m/s

$$\Delta m = -\frac{635}{317*9.8} 35 * 60 = 429.25\ kg$$

The value for g_o is used as the sea level acceleration of gravity on Earth because the performance of the engine is tested on the Earth, and based on these tests, the specifications of the engine performance are published for the engine data.

4.4.5 : Cost analysis

Propellant mass saving from aerobraking = 429.25 kg

Amount of fuel (Hydrazine) = 192 kg

Amount of oxidizer (Nitrogen Tetraoxide) = 103.25 kg

The propellant prices are taken from the list published by the Department of Logistics under "Aerospace energy standard prices" for its customers and government agencies for the fiscal year 2018 [5].

The cost of hydrazine = $323.13/kg ($146.57/lb.)

The cost of nitrogen tetraoxide = $334.95/kg ($151.93/lb.)

Total cost of hydrazine = $62,041.30

Total cost of nitrogen tetraoxide = $34,583.44

The cost to put 1 kg of payload to low Earth orbit can be $10,000 or more depending on the launch vehicle [6]. To estimate the cost of launching 295.25 kg, $10,000 per kg is used as the reference cost.

The cost to launch 295.25 kg of fuel to low Earth orbit = $2,952,500

The total cost saving including propellant price and launch cost = $3,048,789.80

4.5 Results

The simulation of the spacecraft making passes into the Jupiter's atmosphere was performed using parameters listed in the table 4.5.1. The resulting radius of periapsis and apoapsis along

with change in the spacecraft velocity after each pass is shown in table 4.5.2. The change in the shape of the orbit at the end of each phase is reflected in figures 4.5a to 4.5e.

Table 4.5.1: Parameters

Parameter	**Value**	**Unit**
Universal Gravitational constant, G	$6.67e-20$	$\frac{km^3}{kg.s^2}$
Radius of Jupiter, R_J	71492	km
Orbital velocity of Jupiter, ω_J	$1.878e-04$	$\frac{rad}{s}$
Mass of Jupiter, m_J	1898.19e+24	kg
Mass of Spacecraft, m_{SC}	3625	kg
Surface area of the spacecraft, A	33.47	m^2
Coefficient of Drag, C_D	2.2	-
Periapsis altitude, ht	350	km
Initial period, T_{in}	54.2	days
Final period, T_f	14	days

Table 4.5.2: Resulting orbit properties after each pass

Pass	r_p **(km)**	r_a **(km)**	Δ**v (km/s)**
1	71842	7.73e+06	0.01
2	71842	7.46e+06	0.01
3	71842	7.20e+06	0.01
4	71842	7.46E+06	0.01
5	71842	6.96e+06	0.01
6	71842	6.74e+06	0.01

7	71842	6.63e+06	0.01
8	71842	6.33e+06	0.01
9	71842	6.25e+06	0.01
10	71842	6.15e+06	0.01
11	71842	5.81e+06	0.01
12	71842	5.50e+06	0.01
13	71842	5.36e+06	0.01
14	71842	5.22e+06	0.01
15	71842	5.10e+06	0.01
16	71842	4.98e+06	0.01
17	71842	4.86e+06	0.01
18	71842	4.75e+06	0.01
19	71842	4.64e+06	0.01
20	71842	4.54e+06	0.01
21	71842	4.44e+06	0.01
22	71842	4.35e+06	0.01
23	71842	4.30e+06	0.01
24	71842	4.26e+06	0.01
25	71842	4.17e+06	0.01
26	71842	4.01e+06	0.01
27	71842	3.94e+06	0.01
28	71842	3.86e+06	0.01
29	71842	3.79e+06	0.01
30	71842	3.72e+06	0.01
31	71842	3.66e+06	0.01
32	71842	3.59e+06	0.01
33	71842	3.53e+06	0.01
34	71842	3.47e+06	0.01
35	71842	3.41e+06	0.01
33	71842	3.36e+06	0.01

36	71842	3.30e+06	0.01

Table 4.5.3: Δv savings after each phase

Phase	**Δv (km/s)**
Walk-in Phase	0.026
Main Phase	0.3511
Walk-out Phase	- 0.0411

Table 4.5.4: Net Δv and fuel savings

Net Δv saving	0.336 km/s
Net fuel saving	429.25 kg

Table 4.5.5: Cost savings resulted from fuel savings

Type	Cost saving
Fuel (Hydrazine)	$62,041.30
Oxidizer (Nitrogen Tetraoxide)	$34,583.44
Total propellant	$96,289.80
Launch cost of propellant (295.25 kg)	$2,952,500
Total cost (launch + fuel prices)	$3,048,789.80

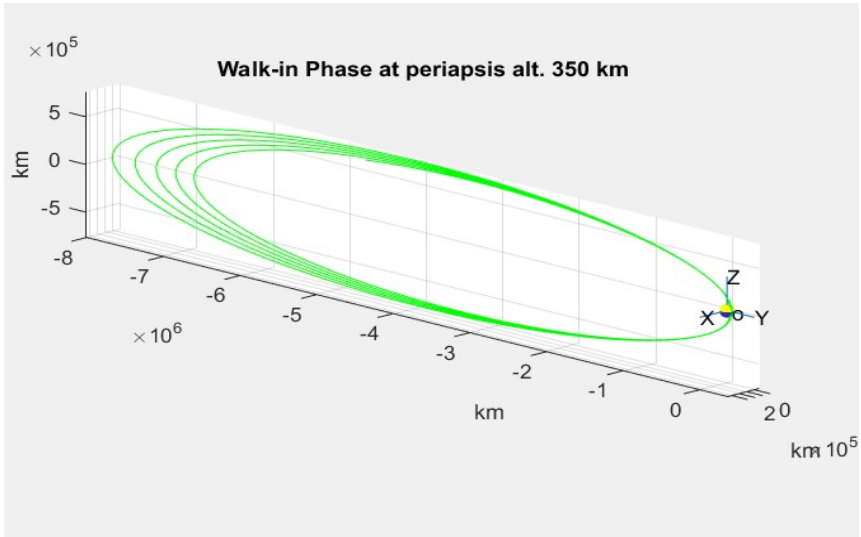

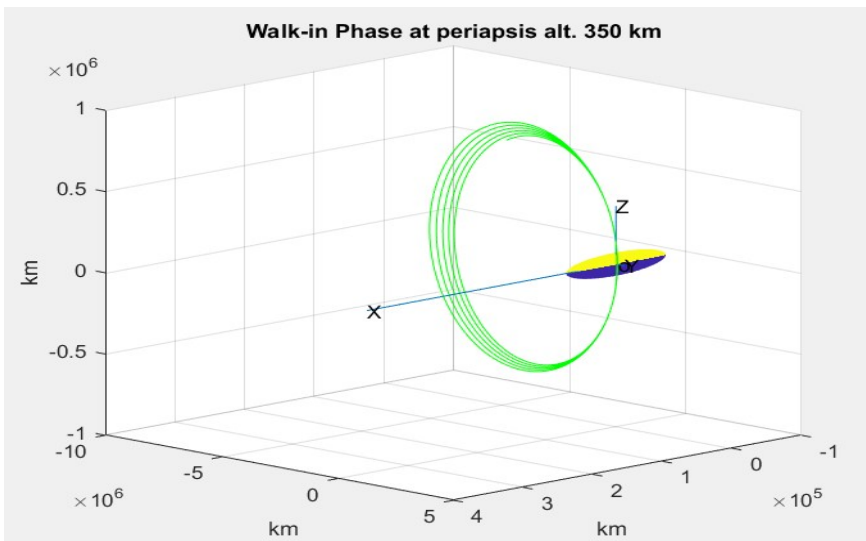

Fig. 4.5 a & b: Walk-in phase visualization

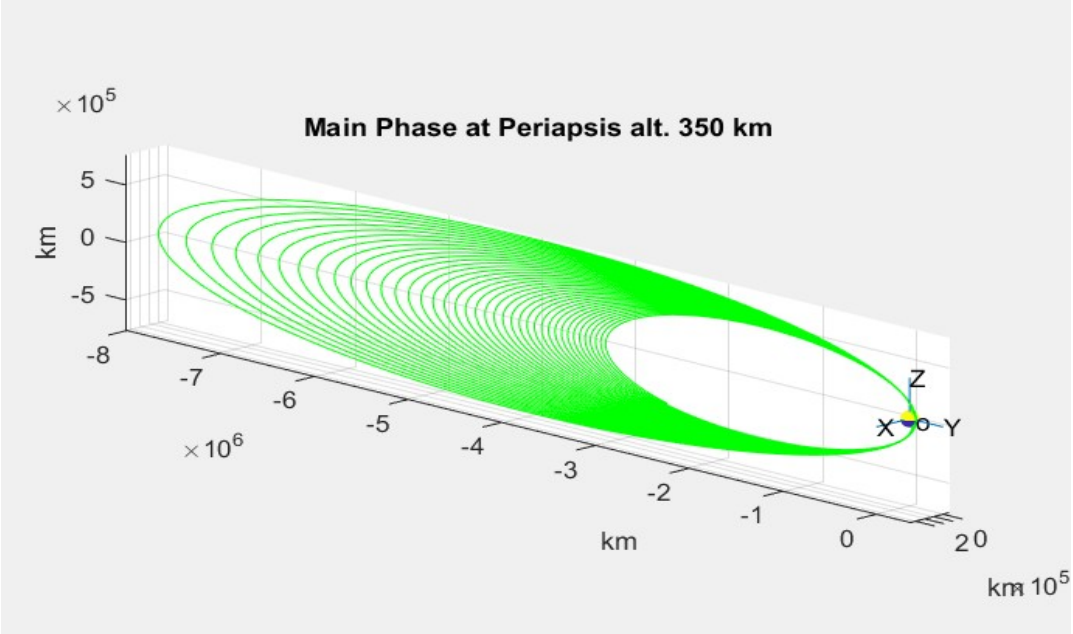

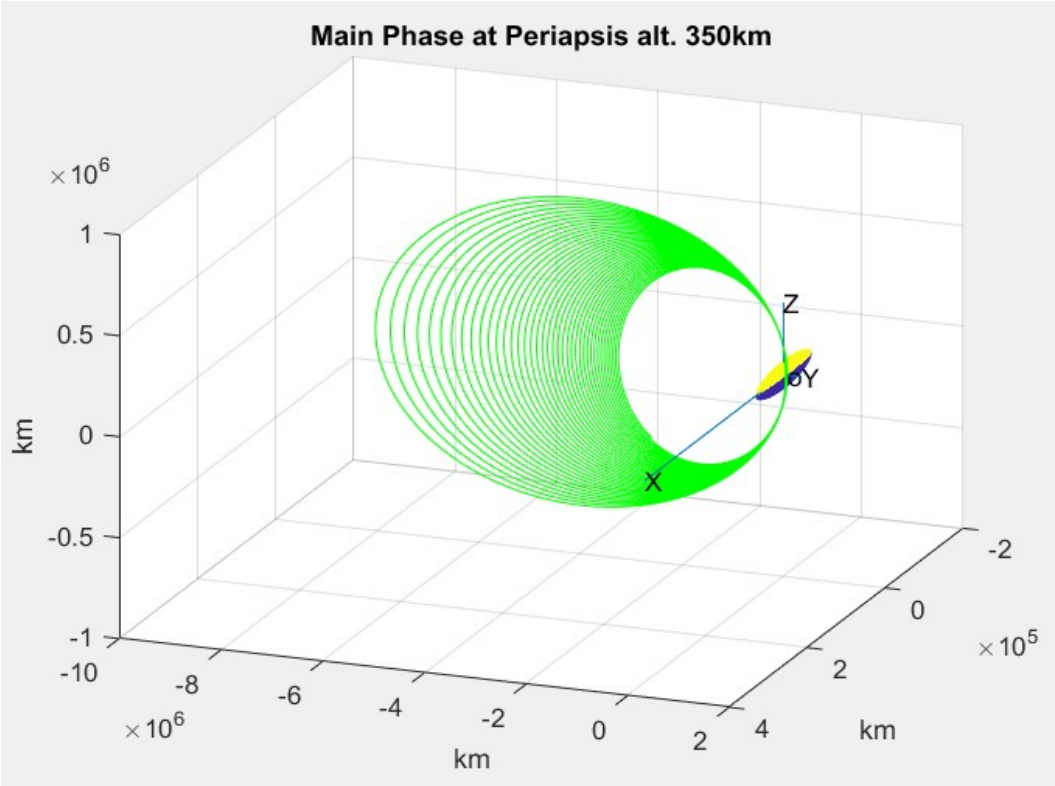

Fig. 4.5c & d: Main phase visualization

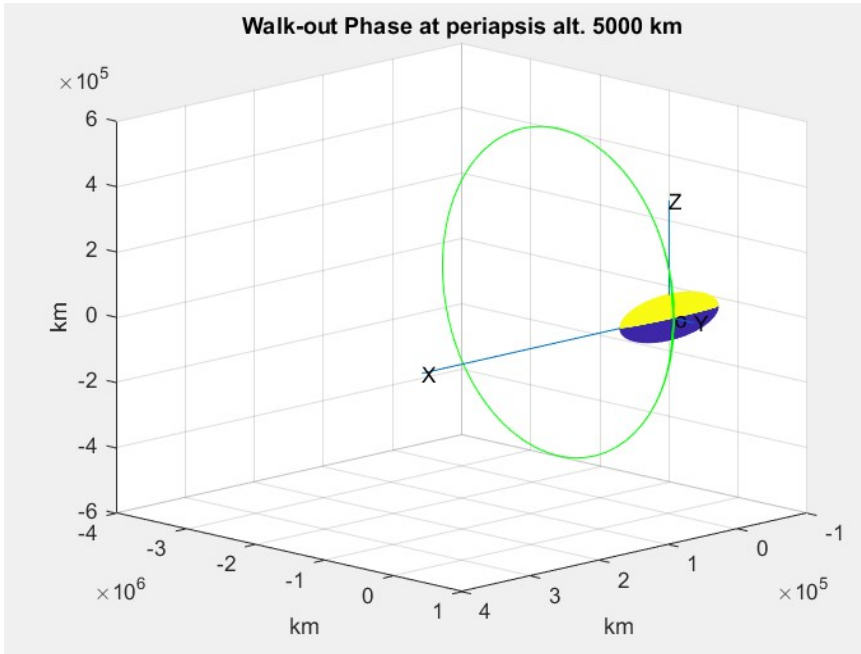

Fig. 4.5e: Walk-out phase visualization

4.6 Discussion

Aerobraking was initiated at 350 km above the assumed surface of Jupiter at 1 bar pressure level with the period of 54.2 days. The walk-in phase resulted in 0.026 km/s decrease in the velocity. After the walk-in phase, the main phase included rest of the passes. The consecutive passes further decreased the orbit. At the end of the main-phase, the change in velocity amounted to 0.351 km/s, and the period of the orbit reduced to 54.2 days to 14 days. After the completion of the main phase, periapsis was raised to the higher altitude so that the orbit no longer gets affected by the drag. The periapsis altitude was raised to 5,000 km from 350 km. The burn at apoapsis to bring the periapsis altitude to 5,000 km would result in the Δv deficit of 0.041 km/s. Hence, the net Δv saving after the three phases is found to be 0.336 km/s.

For Juno mission, a 35 minutes burn was planned to lower the 53.5 day period to 14-day period [2]. The spacecraft would have used 447 kg of fuel during the burn. Analyzing the similar period reduction of the orbit around Jupiter resulted in 429.25 kg of propellant saving which is comparable to the fuel required to adjust the period of the orbit for Juno. Aerobraking resulted in the lesser fuel saving in comparison to the propulsive burn for Juno because the walk-in phase requires a burn to raise the periapsis at the end of the operation. Therefore, a smaller burn is

required for aerobraking as well. Nonetheless, the amount of propellant saving is approximately 1 order higher than fuel required for the burn needed for the walk-out phase. Hence, the orbit insertion around Jupiter through aerobraking saves 429.25 kg of propellant for the case studied in this chapter.

In terms of cost, the fuel savings are translated to $3,048,789.80 of savings. The propellant price for space missions is high. According to the standard price list for aerospace energy issued by Department of Logistics for its customers and government agencies, the cost of fuel is $323.13/kg, and for oxidizer, it is $334.95/kg [5]. The gross price for the propellant turns out to be $96,289.80. Furthermore, it is very costly to launch the payload to space. It could cost more than $10,000 to transport 1 kg of mass to low Earth orbit [6]. Assuming $10,000/kg as the launch cost, $2,952,500 can be saved by reducing 295.25 kg of propellant from the mission. Overall, the mission cost can be reduced by more than 3 million dollars from the fuel savings resulted from aerobraking.

The initial periapsis altitude is chosen to be 350 km after running several scenarios with periapsis at higher altitudes. For example, the walk-in phase was studied with the initial periapsis altitude of 700 km, 600 km, 500 km, and 400 km. The effect of the drag is seen on the spacecraft orbit during these atmospheric passes; however, this effect is much less compared to the atmospheric passes at 350 km due to the lower density at higher altitudes. The smaller effect of drag force on the orbit means the greater number of passes are required to achieve the desired reduction in the period of the orbit. Given that Jupiter is surrounded by tremendously powerful magnetic and extremely harmful radiation belts, the excessive passes to attain the desired science orbit can cause problems to the spacecraft performance and its instruments. Therefore, the minimal number of passes are beneficial for proper functionality of the spacecraft. On the other hand, dipping further into the atmosphere can also be troublesome for the spacecraft. Moving down in the Jovian atmosphere, the temperature, pressure, and density increase as discussed in the “Jupiter’s magnetosphere and its effects on the spacecraft” report. The higher values of atmospheric properties like temperature and density may cause higher perturbations and heat transfer to the spacecraft body. In addition, the gravitational pull of Jupiter may cause the spacecraft to impact the planet with the increased amount of drag at lower altitudes. Thus, the

periapsis altitude of 350 km is chosen to be the intermediate choice between the greater number of passes at higher altitudes and a large amount of drag and heat transfer to the spacecraft at lower heights.

To reduce the period for the stated problem, 350 km is determined to the suitable periapsis altitude for aerobraking based on the required period adjustments for the minimum number of atmospheric passes. As a result, 429.25 kg of fuel saving is predicted via aerobraking to do the orbit insertion around Jupiter.

4.7 Conclusion

Aerobraking around Jupiter results in 0.336 km/s of Δv and 429.25 Kg of propellant savings which translate $3,048,789.80 of cost savings. The Δv results look promising in terms of fuel and cost savings. However, Jupiter is a unique planet with harshest conditions in the vicinity of the planet in the entire solar system. The other factors like heat transfer to the spacecraft are needed to be considered to determine if aerobraking is a feasible operation for the Jovian mission.

4.8 References

[1] Curtis, H. D., “Rocket Vehicle Dynamics”, Orbital Mechanics for Engineering Students, 3rd ed., Waltham, MA, November 8, 2013, pp. 619-640.

[2] “Quick Facts”, Mission Juno [online], Jet Propulsion Laboratory, CA, https://www.jpl.nasa.gov/news/press_kits/juno/facts/ [retrieved 04 Dec. 2017].

[3] “Upper Stage Engines”, MOOG Inc. [online], Niagara Falls, NY, 2013, http://www.moog.com/literature/Space_Defense/Spacecraft/Propulsion/Upper_Stage_Engines_Rev_0913.pdf .

[4] “Mission Overview”, Mission Juno [online], Jet Propulsion Laboratory, CA, https://www.jpl.nasa.gov/news/press_kits/juno/overview/ [retrieved 01 Dec. 2017].

[5] “Aerospace Energy Standard Prices for DOD customers Effective 1 Oct 2017”, Department of Logistics [online], Oct. 2017, http://www.dla.mil/Portals/104/Documents/Energy/Standard%20Prices/Aerospace%20Prices/E_2017Oct1AerospaceStandardPrices_170913.pdf?ver=2017-09-13-145335-477 .

[6] Zapata, E., “The State of Play US Space Systems Competitiveness”, Presentation to the Future In-Space Operations (FISO) Seminar [online], NASA, 11 Oct. 2017, https://ntrs.nasa.gov/archive/nasa/casi.ntrs.nasa.gov/20170009967.pdf .

4.9 Appendices

4.9.1 Appendix A - MATLAB code

4.9.1.1 Main script

```
clear all
close all
clc
% Hour to sec (s)
hr = 3600;
% Universal gravitational Constant (km^3/kgs^2)
G = 6.67*10^-20;
% Mass of Jupiter (kg)
mj = 1898.19*10^24;
% Radius of Jupiter (km)
Rj =71492;
% Mass of the Spacecraft (kg)
msc =3625;
mu1 = G*(mj+msc);

% Initial state vector
ro = 1.0e+04 *[0 7.1842 0];
vo = [0 0 59.1100];
yo = [ro vo]';

to =0; % Intial time (s)
tf =19*54.3*24*hr; % Final time (s)
tspan =(to:3600:tf5); % Time interval

% Tolerance and ode setting adjustment
tol = 1e-12;

options=odeset('RelTol',tol,'AbsTol',[tol tol tol tol tol tol]);

[t,y]=ode113('dEq51',tspan,yo,options);

% Plot of surface of the planet
s1 = [t,y];
[xx1,yy1,zz1]=sphere(1000);
surf(Rj*xx1,Rj*yy1,Rj*zz1)
colormap('default')
caxis([-Rj/100 Rj/100])
shading interp

line([0 5*Rj], [0 0], [0 0]); text(5*Rj,0,0,'X')
line([0 0], [0 5*Rj], [0 0]); text(0,5*Rj,0,'Y')
line([0 0], [0 0], [0 5*Rj]); text(0,0,5*Rj,'Z')

hold on

%Simulation
for i = length(t)
```

```
    plot3(y(1:i,1), y(1:i,2),y(1:i,3),'g')
    drawnow
end

xlabel('km')
ylabel('km')
zlabel('km')
title('Main Phase')
line([0 ro(1)], [0 ro(2)], [0 ro(3)])
text( y(1,1), y(1,2), y(1,3), 'o')
```

4.9.1.2 Differential equation

```
function dfdt = dEq295B(t,f5)
% Position vector (km)
r = f5(1:3)';
rn = norm(r);

% Velocity vector (km/s)
v = f5(4:6)';

% Orbital velocity of Jupiter (rad/s)
wJ = [0;0;1.8268e-04];

% Relative velocity of the spacecraft w.r.t atmosphere (km/s)
vr = v - cross(wJ,r);

% Magnitude of relative velocity (km/s)
vrmag = norm(vr);
% Unit velocity vector
uv = vr/vrmag;

% Universal graviatational Cconstant (km^3/kgs^2)
G = 6.67*10^-20;

% Mass of Jupiter (kg)
mj = 1898.19*10^24;

% Radius of Jupiter (km)
Rj =71492;

% Mass of the Spacecraft (kg)
msc =3625;

mu = G*(mj+msc);

% Coefficient of drag for spacecraft
CD =2.2;

% Area of the Spacecraft (m^2)
A = 33.4711;
```

```
% Altitude at each position (km)
alt = rn - Rj;

% Density at each altitude (kg/m^3)
rhoJ = atm51(alt);

% Components of acceleration due to gravity (km/s^2)

ad = -CD*A/msc*rhoJ*(1000*vrmag)^2/2*uv;

a = -mu*r/rn^3;

atot = a+ad/1000;
dfdt = [v atot]';
end
```

4.9.1.3 Density calculation function at each point

```
function rhoJ = atm295B(zz)

% Altitude (km)
z = [-134.7 -118 -98 -78 -58 -38 -18 0 2 22 42 62 82 102 122 142 162
182 202 222 242 262 282 302 322 342 362 382 402 422 442 462 482 502
522 542 562 582 602 622 642 662 682 702 722 742 762 782 802 822 842
862 871.2 881 901 921 941 961 981 1001 1021 1041 1042 1043];

% density at the above altitudes (kg/m^3)
rho_o = [0.07945 0.003335 0.009915 0.03168 0.001261 0.000571 0.0002325
0.16 0.000102 4.98e-5 2.206e-5 9.878e-6 4.41e-6 2.012e-6 8.713e-7
3.417e-7 1.629e-7 8.251e-8 3.892e-8 1.917e-8 1.023e-8 6.989e-9 4.27e-9
3.058e-9 2.455e-9 1.937e-9 1.451e-9 1.114e-9 9.053e-10 7.562e-10
6.39e-10 5.364e-10 4.506e-10 3.757e-10 3.113e-10 2.567e-10 2.117e-10
1.759e-10 1.487e-10 1.272e-10 1.101e-10 9.638e-11 8.502e-11 7.539e-11
6.700e-11 5.948e-11 5.264e-11 4.635e-11 4.057e-11 3.535e-11 3.082e-11
2.711e-11 2.575e-11 2.4239889*10^-11 2.31447825*10^-11 1.83882607*10^-
11 1.54317389*10^-11 1.24752171*10^-11 9.5186953*10^-12 6.5621735*10^-
12 3.6056517*10^-12 6.491299*10^-13 0 0];


% Corresponding scale height, Hs (km) [Hs = (k*T)/(m*g)]
Hs = [19.01690229 17.52576982 18.99334475 22.29206767 24.52366002
23.25123718 24.92816483 27 26.20318247 24.47837484 24.61767988
24.47794291 24.27062917 23.57371192 23.9013278 27.88221815 30.70879836
31.75918808 37.62505054 47.78796389 62.20804221 66.77646033
83.01818832 92.91115618 93.522481 95.94834225 104.879345 113.8800791
118.1323146 119.5602983 119.8434676 120.9547474 122.2195614
124.6704474 128.5572063 133.9299006 140.4993831 147.1618975
152.4881568 156.6924695 159.682461 161.243726 161.5055009 160.9916901
160.0448426 159.106962 159.6067468 158.980608 160.2980833 162.6303783
```

```
165.23003 166.5985742 166.0877434 166.6 166 166 166 166 166 166 166
166 166 166];

% Out-of-bound altitude adjustments for density calculation
if zz > 1042
     zz = 1042;
elseif zz < 0
    zz = 0;
end

% Iterations set-up
for jj = 1:63
    if zz >= z(jj) && zz < z(jj+1)
        ii = jj;
    end
end

if zz == 1042
  ii = 63;

end

% Density calcultaion as exponential function of scale height,
altitude,
% and density corespponding to scale height
rhoJ = rho_o(ii)*exp(-(zz - z(ii))/Hs(ii));

end
```

4.9.2 Appendix B – Aerobraking at different altitudes

Aerobraking at initial periapsis altitude of 700 km, 600 km, 500 km, 400 km, and 350 km

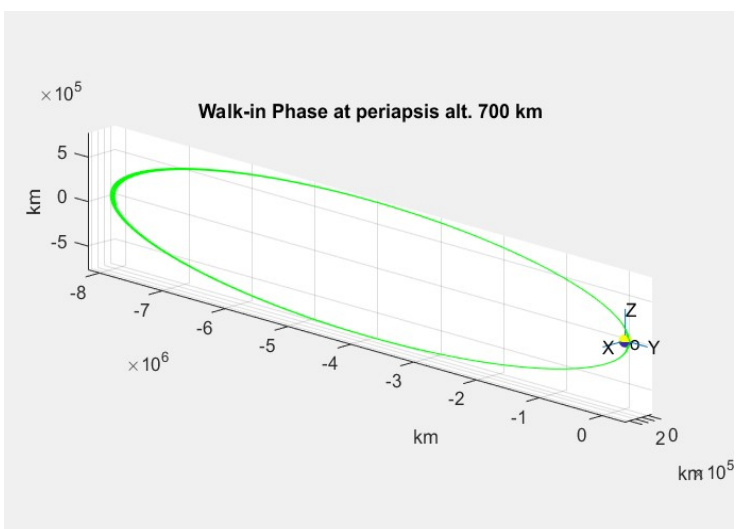

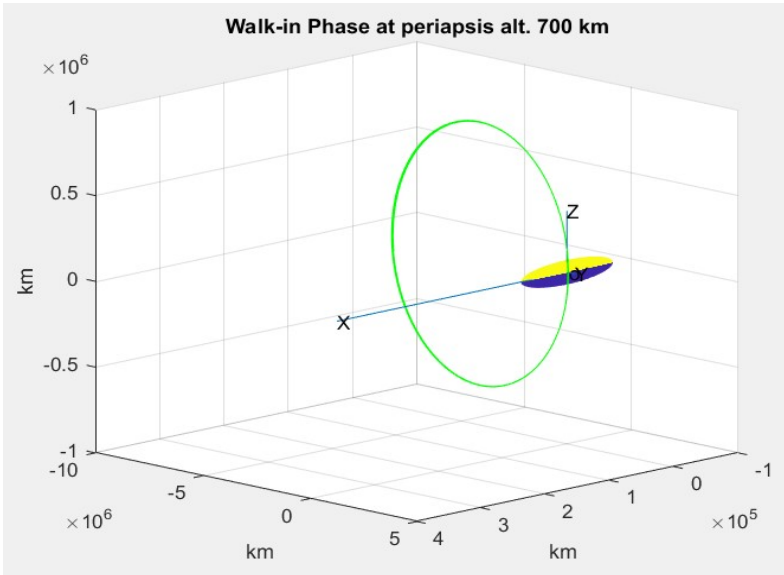
Walk-in Phase at periapsis alt. 700 km
×10^6
1
0.5
0
-0.5
-1
km
Z
X
-10
-5
0
5
×10^6
km
4
3
2
1
0
-1
×10^5
km

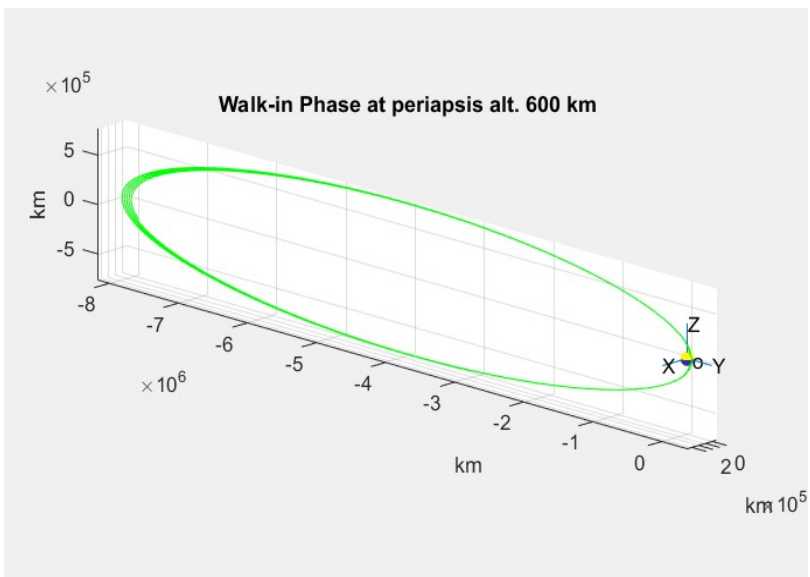
×10^5
Walk-in Phase at periapsis alt. 600 km
5
0
-5
km
-8
-7
-6
-5
-4
-3
-2
-1
0
×10^6
km
Z
X
Y
2
0
km
×10^5

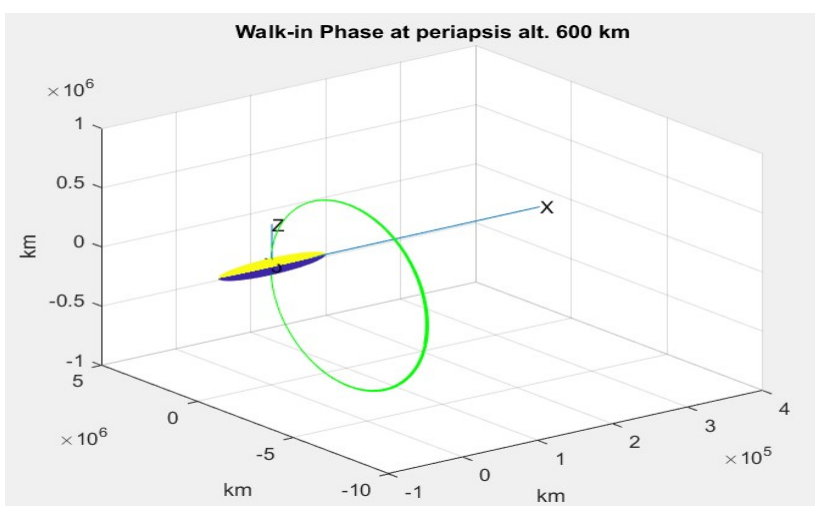
Walk-in Phase at periapsis alt. 600 km
×10^6
1
0.5
0
-0.5
-1
km
Z
X
5
0
-5
-10
×10^6
km
-1
0
1
2
3
4
×10^5
km

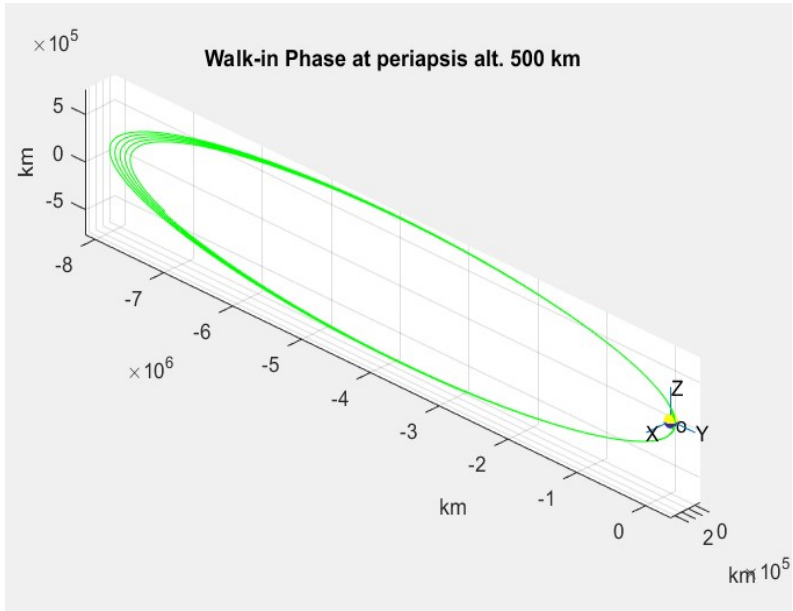
Walk-in Phase at periapsis alt. 500 km
×10^5
5
0
-5
km
-8
-7
-6
×10^6
-5
-4
-3
-2
-1
0
km
Z
X
Y
0
2
km
×10^5

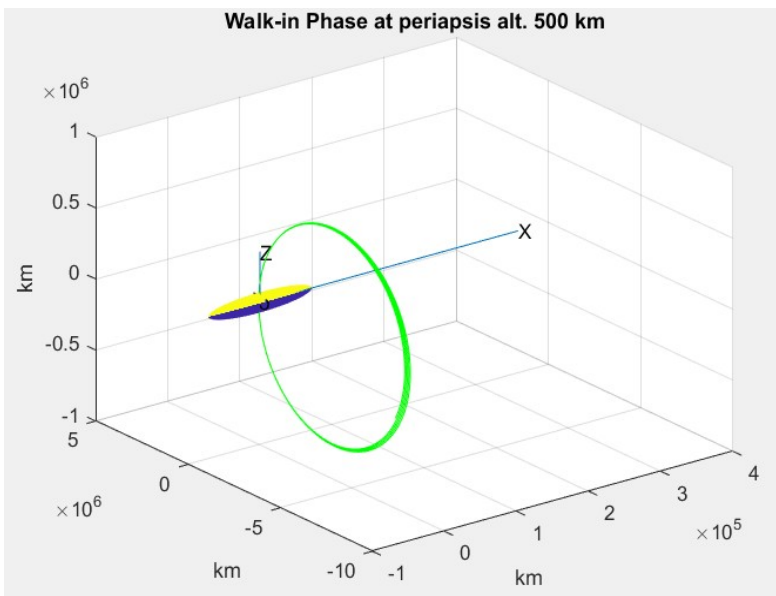
Walk-in Phase at periapsis alt. 500 km
×10^6
1
0.5
0
-0.5
-1
km
Z
X
5
0
-5
-10
×10^6
km
-1
0
1
2
3
4
×10^5
km

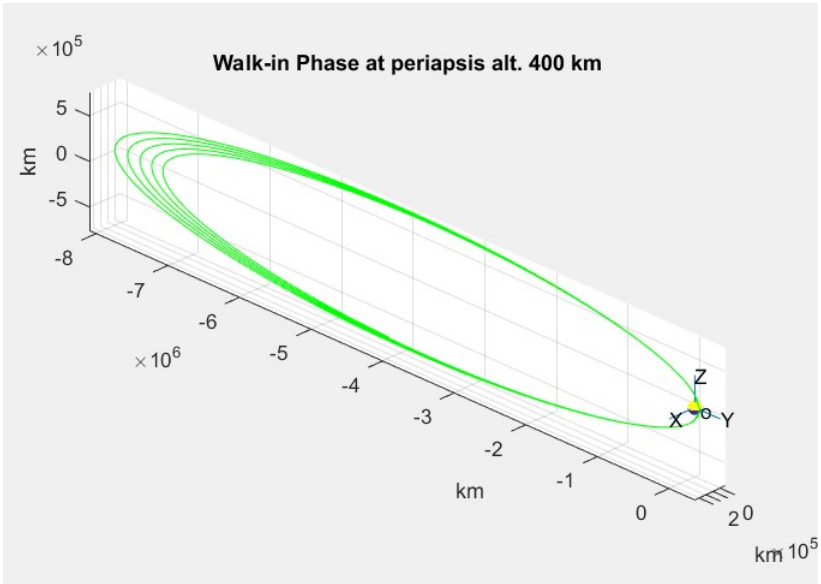
Walk-in Phase at periapsis alt. 400 km
×10^5
5
0
-5
km
-8
-7
-6
×10^6
-5
-4
-3
-2
-1
0
km
Z
X
o
Y
2
0
km
×10^5

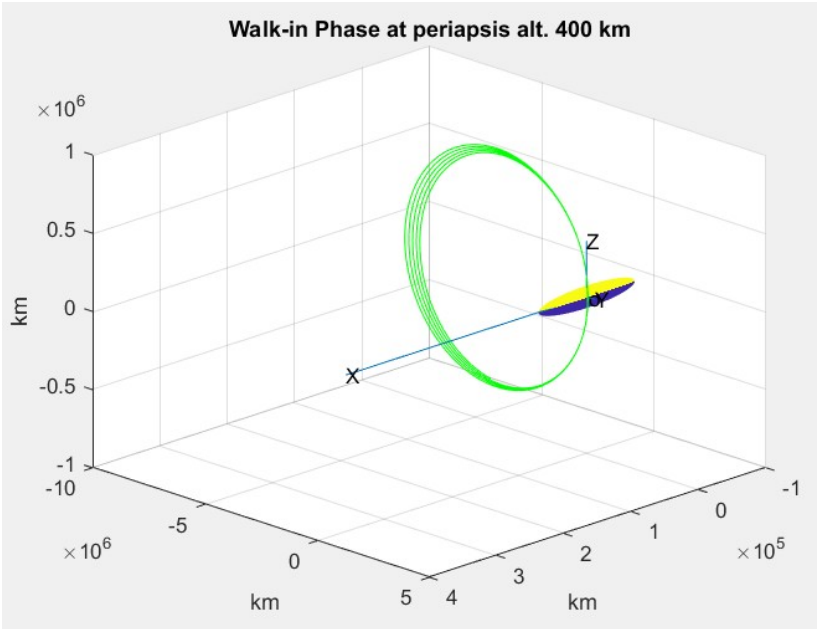
Walk-in Phase at periapsis alt. 400 km
×10^6
1
0.5
0
-0.5
-1
km
Z
X
-10
-5
0
5
×10^6
km
4
3
2
1
0
-1
×10^5
km

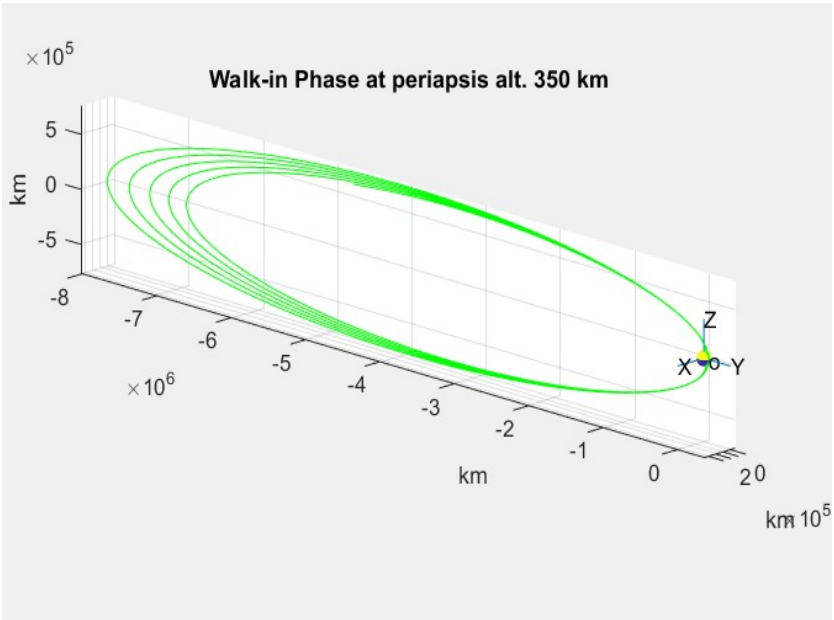
Walk-in Phase at periapsis alt. 350 km
×10^5
5
0
-5
km
-8
-7
-6
-5
-4
-3
-2
-1
0
×10^6
km
Z
X
Y
2
0
-2
km
×10^5

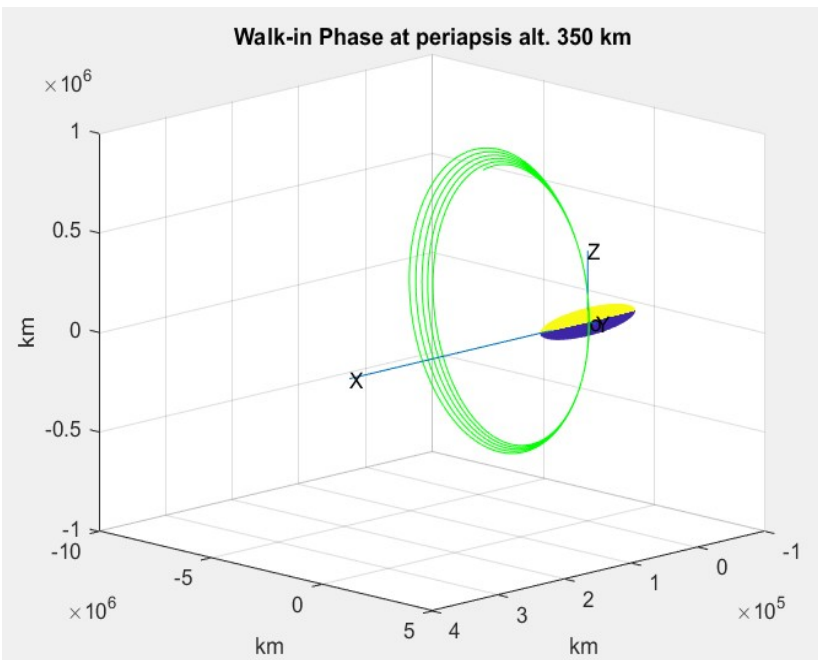
Walk-in Phase at periapsis alt. 350 km
×10^6
1
0.5
0
-0.5
-1
km
Z
Y
X
-10
-5
0
5
×10^6
km
4
3
2
1
0
-1
×10^5
km

Chapter 5: Heat Transfer Analysis on the Spacecraft During Aerobraking

Nomenclature

Symbol	Definition
h_1	Freestream sensible enthalpy per unit mass
h_2	Downstream sensible enthalpy per unit mass of the normal shock
h_{aw}	Adiabatic enthalpy per unit mass
h_w	Sensible enthalpy per unit mass at the wall (surface)
P_1	Freestream Pressure
P_2	Downstream Pressure of the normal shock
Pr	Prandtl number
q_w	Heat transfer at the wall (surface)
T_1	Freestream temprature
T_2	Downstream temprature of the normal shock
u_1	Freestream velocity
u_2	Downstream velocity of the normal shock
u_e	Velocity at the edge of the boundary layer
ρ_1	Freestream density
ρ_2	Downstream density of the normal shock
ρ_e	Density at the edge of the boundary layer
μ_e	Dynamic viscosity at the edge of the boundary layer

5.1 Introduction

While moving at high-speed through the atmosphere, the spacecraft encounters a shock wave in front of it. To find the heat flux to the surface of the spacecraft, it is essential to determine the conditions behind the shock layer. The flow behind the shock layer is inviscid, and the effects of viscosity are seen inside the boundary layer. The effects of the viscosity are assumed negligible at the edge of the boundary layer. Therefore, the flow conditions inside the boundary are different than the flow properties outside it. The temperature at the wall of the body increases due to the conversion of kinetic energy to heat. The conditions behind the shock layer are assigned as the edge flow conditions of the boundary layer. The edge flow conditions are needed to solve the boundary layer equations to calculate the conditions at the surface of the spacecraft. Therefore, the estimate of the temperature, pressure, density, viscosity, and heat transfer to the spacecraft body are made from the boundary layer equations. The surface temperature and heat transfer to the body are extremely important quantities to design the heat shield for the spacecraft.

5.2 Theory

At the stagnation point, the flow velocity becomes nearly zero. For the viscous case, the flow will have a finite velocity after the shock, and at the wall of the body, the flow comes to rest due to the presence of viscosity. At the stagnation point, the heat transfer is inversely proportional to the nose radius of the body [1]. Therefore, the blunt bodies are preferred for the atmospheric entry. For a blunt body, the shock layer will be nearly straight at the stagnation point. Therefore, the shock layer can be treated as the normal shock in front of the spacecraft at the stagnation point. Outside the boundary layer, the flow is inviscid.

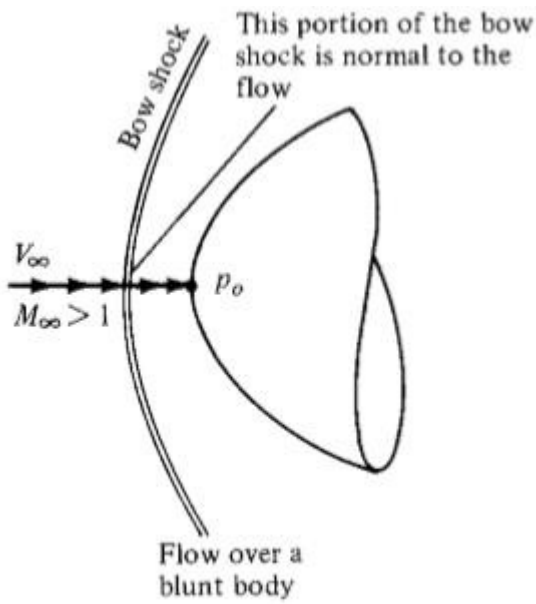

Fig. 5.2a: High-speed flow at stagnation point [1]

For the atmospheric pass, the velocity of the spacecraft is very high, and the flow behind the shock layer and inside the boundary layer can be in non-equilibrium conditions. The gases of the atmosphere can be chemically reactive, and the gases can dissociate and ionize due to high-temperature effects for the atmospheric entry at large velocities. To account for the chemical reactions, dissociation, and ionizations factors, the simulation tools like Computational Fluid Dynamics (CFD) are required to solve the conditions behind the shock layer and the boundary layer. For the preliminary estimate of heat transfer, the equilibrium flow conditions can be assumed. Therefore, the normal shock equations for the inviscid flow in thermochemical equilibrium case are used for the first approximation of the temperature outside the boundary layer at the stagnation point. In thermochemical equilibrium, there is a local equilibrium exists at each point along the flow. For the thermodynamically equilibrium flow, the internal energy depends on the local temperature. For the flow which is in the chemical equilibrium, the local chemical composition of the gases can be deduced from the equilibrium chemical equations [2]. Therefore, in the thermodynamically equilibrium, both thermodynamic and chemical equilibrium exist.

The flow properties behind the normal shock can be determined using the numerical technique based on the Navier Stokes equations which include continuity, momentum, and energy

equations. The Navier Stokes equations state that mass, momentum, and energy of the system is conserved.

For the normal shock, the freestream conditions are known, and the conditions behind the shock can be calculated using the numerical scheme applied to the equations stated below. The freestream conditions are denoted with subscript 1, and the flow properties behind the shock are given the subscript 2.

From the continuity equation:

$$\rho_1 u_1 = \rho_2 u_2 \tag{5.2.1}$$

$$u_2 = \frac{\rho_1}{\rho_2} u_1 \tag{5.2.2}$$

From the momentum equation:

$$P_1 + \rho_1 u_1^2 = P_2 + \rho_2 u_2^2 \tag{5.2.3}$$

Substituting u_2 in the equation (5.2.3) and rearranging:

$$P_2 = P_1 + \rho_1 u_1^2 \left(1 - \frac{\rho_1}{\rho_2}\right) \tag{5.2.4}$$

From the energy equation:

$$h_1 + \frac{u_1^2}{2} = h_2 + \frac{u_2^2}{2} \tag{5.2.5}$$

Substituting u_2 in the equation (5.2.5) and rearranging:

$$h_2 = h_1 + \frac{u_1^2}{2}\left[1 - \left(\frac{\rho_1}{\rho_2}\right)^2\right] \tag{5.2.6}$$

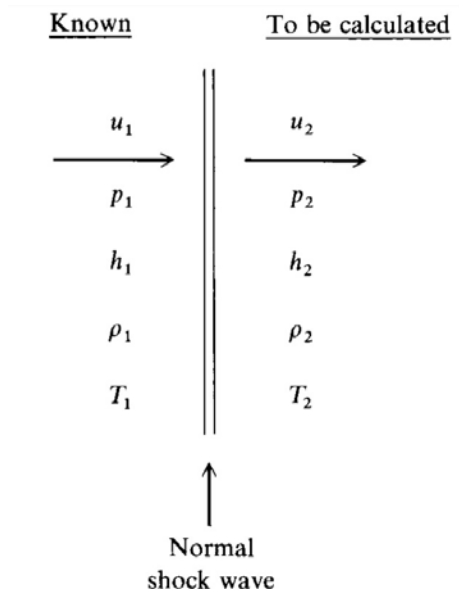

Fig. 5.2b: Normal shock visualization

At hypersonic speeds, the heat transfer at the stagnation point can be determined from the laminar boundary equation solution.

For the sphere the heat transfer at the stagnation point can be calculated from the equation shown below:

$$q_w = 0.763 Pr^{-0.6} (\rho_e \mu_e)^{1/2} \sqrt{\frac{du_e}{dx}} (h_{aw} - h_w) \qquad (5.2.7)$$

The wall conditions can be determined from the numerical scheme by assuming the thermochemical equilibrium to make the preliminary guess.

5.3 Assumptions

- The front area of the spacecraft is assumed to be spherical in shape to reduce the heat transfer to the body compared to the sharp nose
- At stagnation point, the shock is normal to the blunt body
- For the normal shock calculation:
    - The flow is inviscid i.e. no viscosity
    - The flow is in thermochemical equilibrium
- For heat transfer calculation at stagnation point:

- The boundary layer at stagnation point is laminar i.e. no disturbance in the streamlines.

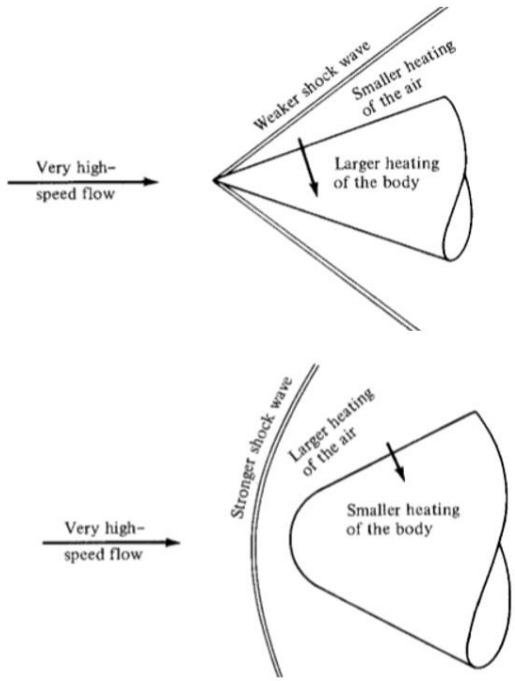

Fig. 5.3a: Heating of sharp vs. blunt body at high speed

5.4 Procedure

The procedure to calculate the flow properties behind the normal shock is listed below:

- The initial value of density ratio is assumed
  $\frac{\rho_1}{\rho_2} = 0.07$
- The assumed density ratio is substituted in the equations (5.2.4) and (5.2.6) along with the known freestream conditions to solve for the pressure and enthalpy behind the normal shock.
- The calculated values of pressure and enthalpy are used as input values in the “Chemical Equilibrium Application” software, also known as CEA, developed by NASA.
- The mixture of gases with the initial known composition is specified in the CEA.
- After executing the simulation for the specified problem, the thermodynamic properties of the flow behind the shock such as density, temprature, internal energy, and so on are found.

- Using the new value of density behind the normal shock, the updated density ratio is calculated.
- The updated density ratio is used in the calculation of the pressure and enthalpy downstream of the shock.
- The simulation in the CEA is repeated with the updated values of pressure and enthalpy values.
- The iterative process is repeated until the density value converges.
- From the converged iteration in CEA, the flow properties are taken as the final downstream flow conditions of the normal shock.

The downstream flow properties behind the normal shock serve the edge conditions of the boundary layer. The same process in the CEA is repeated to find the temprature and enthalpy at the wall of the spacecraft by using properties behind the normal shock as input values. Once the conditions at the edge of the boundary layer and wall enthalpy are known, the equation (5.2.7) is used to find the heat transfer at the stagnation point of the spacecraft.

5.5 Results

The results from the iterative process of calculating downstream conditions of the normal shock are noted below:

Table 5.5.1: Freestream conditions

Name	Value
Pressure (P_1)	0.03865 Pa
Temprature (T_1)	570.1 K
Velocity, (u_1)	59.11 km/s
Density (ρ_1)	1.78×10^{-9} kg/m^3
Sensitive enthalpy (h_1) (From CEA)	3,810,100 J/kg

Table 5.5.2: Composition of the gases in the atmosphere at 350 km

Species	Number of moles	Mole fraction
Hydrogen (H_2)	3.75×10^{-3}	0.9716

Helium (He)	9.99×10^{-5}	0.02569
Monoatomic Hydrogen (H)	1.04×10^{-5}	0.002696
Methane (CH_4)	4.18×10^{-10}	1.08×10^{-7}

Table 5.5.3: Downstream conditions of the normal shock at the stagnation point

Iteration	P_2 (Pa)	h_2 (J/kg)	ρ_2 (kg/m^3)	T_2 (K)
1	5.79	1742245869	1.8235×10^{-8}	39981.93
2	5.62	1734122319	1.7721×10^{-8}	39934.64
3	5.60	1733018199	1.766×10^{-8}	39928.9
4	5.60	1733020213	1.7661×10^{-8}	39928.18
5	5.60	1733020213	1.7661×10^{-8}	39928.2
6	**5.60**	**1733020213**	$\mathbf{1.7661 \times 10^{-8}}$	**39928.2**

5.6 Discussion

From the aerobraking analysis, the speed of the spacecraft for the first atmospheric pass is 59.11 km/s which is extremely large for the atmospheric entry. At this speed, the atmospheric gases will turn into the reacting mixture, and the dissociation and ionization effects can also be present. Therefore, Computational Fluid Dynamics will be needed to solve for flow properties behind the shock for the high-speed flow to account for reactions, dissociation, and ionization effects. However, the preliminary estimate of the temperature behind the shock can be made based on the simple case. Therefore, the thermochemical equilibrium case is studied here to make the initial approximation about the temperature behind the shock.

For most cases, the temperature will be the highest at the stagnation point. Thus, it is extremely important to determine the temperature and heat transfer at the stagnation point because it will set the standard for heat shield design for the spacecraft. The shock becomes normal at the nose of the blunt body; therefore, the normal shock relations are used to calculate the flow properties at the stagnation point.

The results from CEA indicate extremely high temperature behind the normal shock at the stagnation point. The freestream velocity of the spacecraft is very large at periapsis altitude

which is used in the calculation of pressure and enthalpy behind the normal shock using equations (5.2.4) and (5.2.6). Therefore, the pressure and enthalpy become large downstream of the shock. The pressure at 350 km is very low, 0.0386 μbar (0.00386 Pa), the downstream increases to 0.056 mbar (5.60 Pa) which is small as well. The enthalpy value rises from 3,810,100 J/kg to downstream value of 1,733,020,213 J/kg which is 4 orders higher than the upstream enthalpy. The enormously high value of enthalpy results in very large temperature downstream of the shock. The normal shock calculations for the thermochemical equilibrium case results in the temperature of 39,928.2 K behind the shock. This temperature becomes the edge condition for the boundary layer on the surface of the body.

The results from CEA are fitted to the thermodynamic properties calculations for the temperature limit of 20,000 K. This indicates that the solution becomes unstable due to much larger input values which are dependent on the very high velocity of the spacecraft at the periapsis altitude. The enormously large values of flow properties point out that Computational Fluid Dynamics may solve the flow properties at such a high speed. However, the simulation tools like CEA and CFD software are limited to handle the results to a certain order which includes the order of flow properties encountered in the typical hypersonic scenarios. Therefore, the velocity of the spacecraft maybe too large for the simulation tools to predict the downstream conditions because there are so many uncertainties exist at high-speed flows, and the flow becomes very turbulent and chaotic to predict the nature of the flow properties.

Even with the fitted results for the thermodynamic properties obtained from CEA, the downstream temperature is so large that the gases will become radiative, and the body will melt away. At high-temperature flows, the fluid parcels start to emit energy through radiation, or it could absorb energy from radiation absorption [2]. Hence, the enthalpy becomes variable due to the heat addition or lose by the fluid through radiation emission/absorption. The heat transfer to the body includes radiative heat addition term as well at hypersonic speeds. The air becomes radiative at 10,000 K [2]. For Galileo probe entry in the Jupiter’s atmosphere, nearly 95% of the heat transfer to the body was due to radiative heating as a result of the high speed and large temperature behind the shock layer [2]. The obtained temperature is much higher; thus, the heat

transfer cannot be calculated using the simplified equations as the solution becomes unstable, and the input quantities such as enthalpy for the simulation no longer stay constant.

The calculated temperature is so high that the heat protection to the body becomes impractical. The temperature of the surface of the Sun is around 5,811 K [3]. The temperature of the space shuttle can reach 1,921 K approximately during atmospheric entry [4]. The obtained temperature from the equilibrium case is tremendously higher than the temperature at Sun's surface and the surface of the Space Shuttle during entry.

5.7 Conclusion

To investigate the temperature effects and the heat transfer to the spacecraft during atmospheric passes, a preliminary estimate was made using simplified case of thermochemical equilibrium. The results obtained from Chemical Equilibrium Applications indicate very large temperature 39,928.2 K. The large value of temperature is a result of the extremely high velocity of the spacecraft through the atmosphere. The resulting temperature will melt the spacecraft body, and the heat protection can be insufficient at such high temperatures.

5.8 References

[1] Anderson, J. D. Jr., *Fundamentals of Aerodynamics*, 5th ed., McGraw-Hill companies, New York, 2011, pp. 11, 839-876.

[2] Anderson, J. D. Jr., *Hypersonic and High-Temprature Gas Dynamics*, edited by J. A. Schetz, 2nd ed., AIAA, Reston, Virginia, 2006, pp. 261-341, 449-558, 599-646, 759-781.

[3] "The Sun", NASA [online], edited by B. Dunbar, 3 Aug. 2017, https://www.nasa.gov/sun .

[4] "Thermal Protection System", NASA [online], https://www.nasa.gov/centers/johnson/pdf/584728main_Wings-ch4b-pgs182-199.pdf [retrieved 02 Apr. 2018].

5.9 Appendix: The Screenshots of CEA

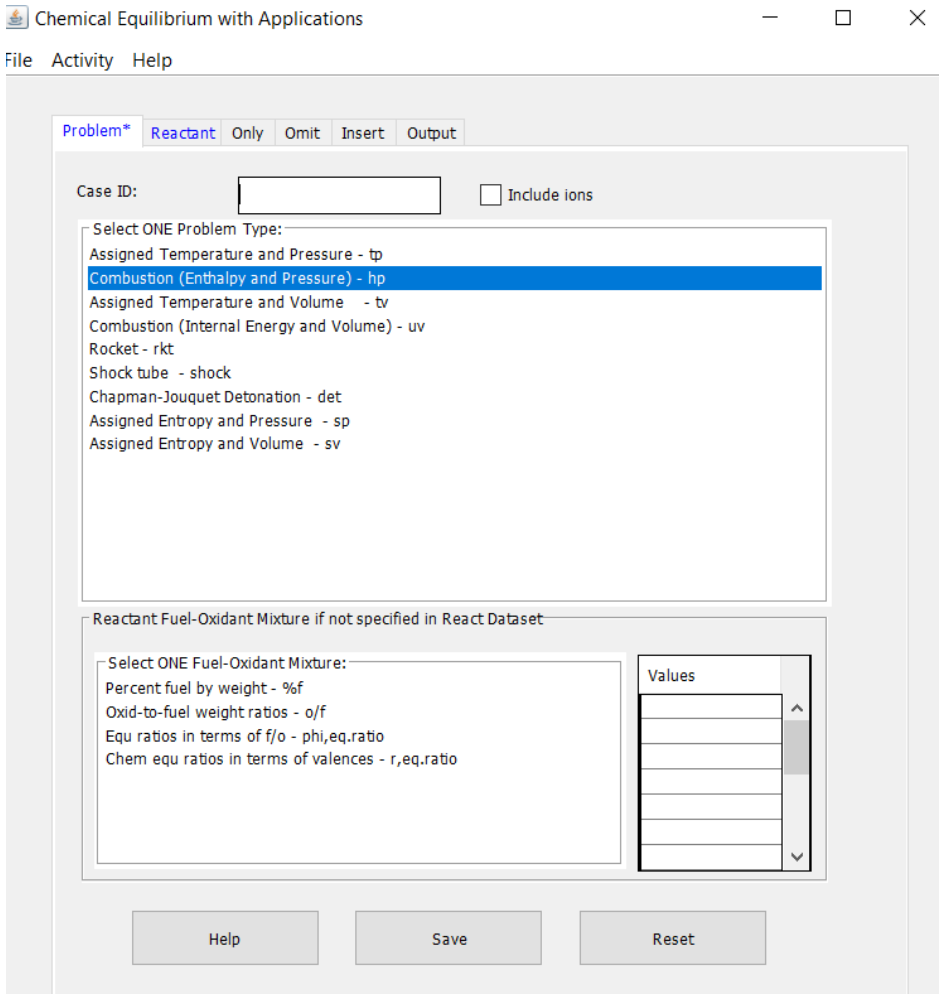

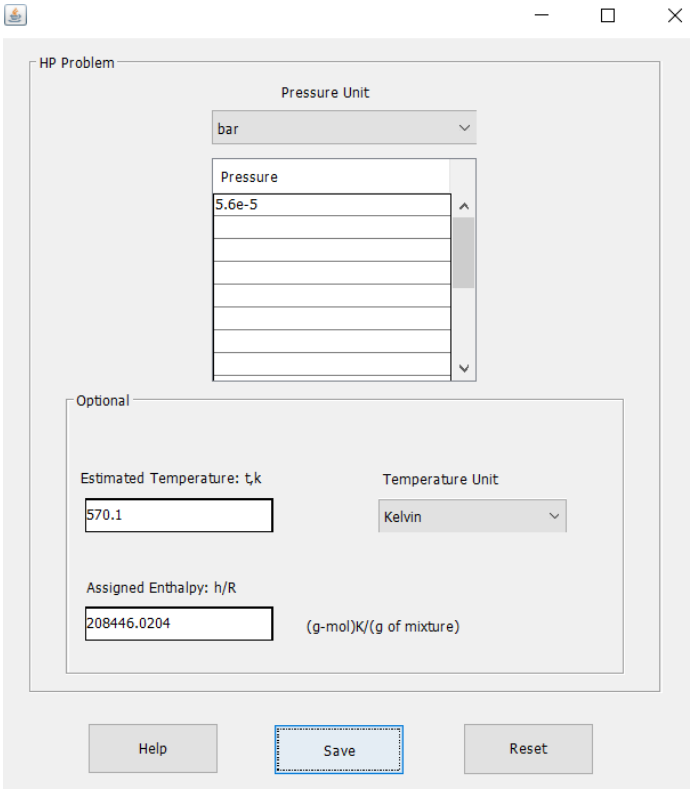
HP Problem
Pressure Unit
bar
Pressure
5.6e-5
Optional
Estimated Temperature: t,k
570.1
Temperature Unit
Kelvin
Assigned Enthalpy: h/R
208446.0204
(g-mol)K/(g of mixture)
Help
Save
Reset

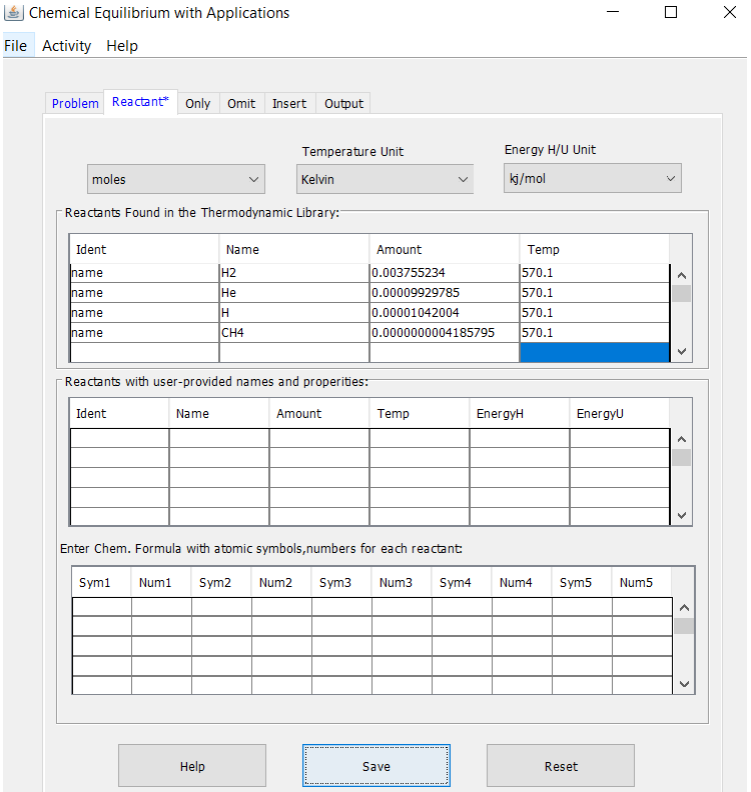
Chemical Equilibrium with Applications
File
Activity
Help
Problem
Reactant*
Only
Omit
Insert
Output
moles
Temperature Unit
Kelvin
Energy H/U Unit
kJ/mol
Reactants Found in the Thermodynamic Library:
Ident
Name
Amount
Temp
name
H2
0.003755234
570.1
name
He
0.00009929785
570.1
name
H
0.00001042004
570.1
name
CH4
0.0000000004185795
570.1
Reactants with user-provided names and properities:
Ident
Name
Amount
Temp
EnergyH
EnergyU
Enter Chem. Formula with atomic symbols,numbers for each reactant:
Sym1
Num1
Sym2
Num2
Sym3
Num3
Sym4
Num4
Sym5
Num5
Help
Save
Reset

Chapter 6: Viability of Aerobraking Technique for the Orbit Insertion Around Jupiter

6.1 Introduction

The fuel and cost savings from aerobraking analysis look promising. More than 3 million dollars can be saved in terms of fuel price and launch cost by using aerobraking. However, the aerobraking maneuvers require a long time to shrink the orbit. The temperature behind the normal shock at the stagnation point obtained from the preliminary estimation turned out to be very large. Therefore, the factors like time and heat transfer to the body need to be considered in addition to the cost savings associated with the aerobraking technique.

6.2 Summary of the aerobraking and heat analysis results

The results obtained from aerobraking analysis and the temprature effects on the spacecraft during aerobraking at Jupiter are listed below:

6.2.1 Aerobraking analysis results

Table 6.5.1: Parameters for aerobraking

Parameter	Value	Unit
Universal Gravitational constant, G	$6.67\ e-20$	$\frac{km^3}{kg.s^2}$
Radius of Jupiter, R_J	71492	km
Orbital velocity of Jupiter, ω_J	$1.878e-04$	$\frac{rad}{s}$
Mass of Jupiter, m_J	1898.19e+24	kg
Mass of Spacecraft, m_{SC}	3625	kg
Surface area of the spacecraft, A	33.47	m^2
Coefficient of Drag, C_D	2.2	-
Periapsis altitude, ht	350	km
Initial period, T_{in}	54.2	days

Final period, T_f	14	days

Table 6.5.2: Δv savings after each phase

Phase	**Δv (km/s)**
Walk-in Phase	0.026
Main Phase	0.3511
Walk-out Phase	- 0.0411

Table 6.5.3: Net Δv and fuel savings

Net Δv saving	0.336 km/s
Net fuel saving	429.25 kg

Table 6.5.4: Cost savings resulted from fuel savings

Type	Cost saving
Fuel (Hydrazine)	$62,041.30
Oxidizer (Nitrogen Tetraoxide)	$34,583.44
Total propellant	$96,289.80
Launch cost of propellant (295.25 kg)	$2,952,500
Total cost (launch + fuel prices)	$3,048,789.80

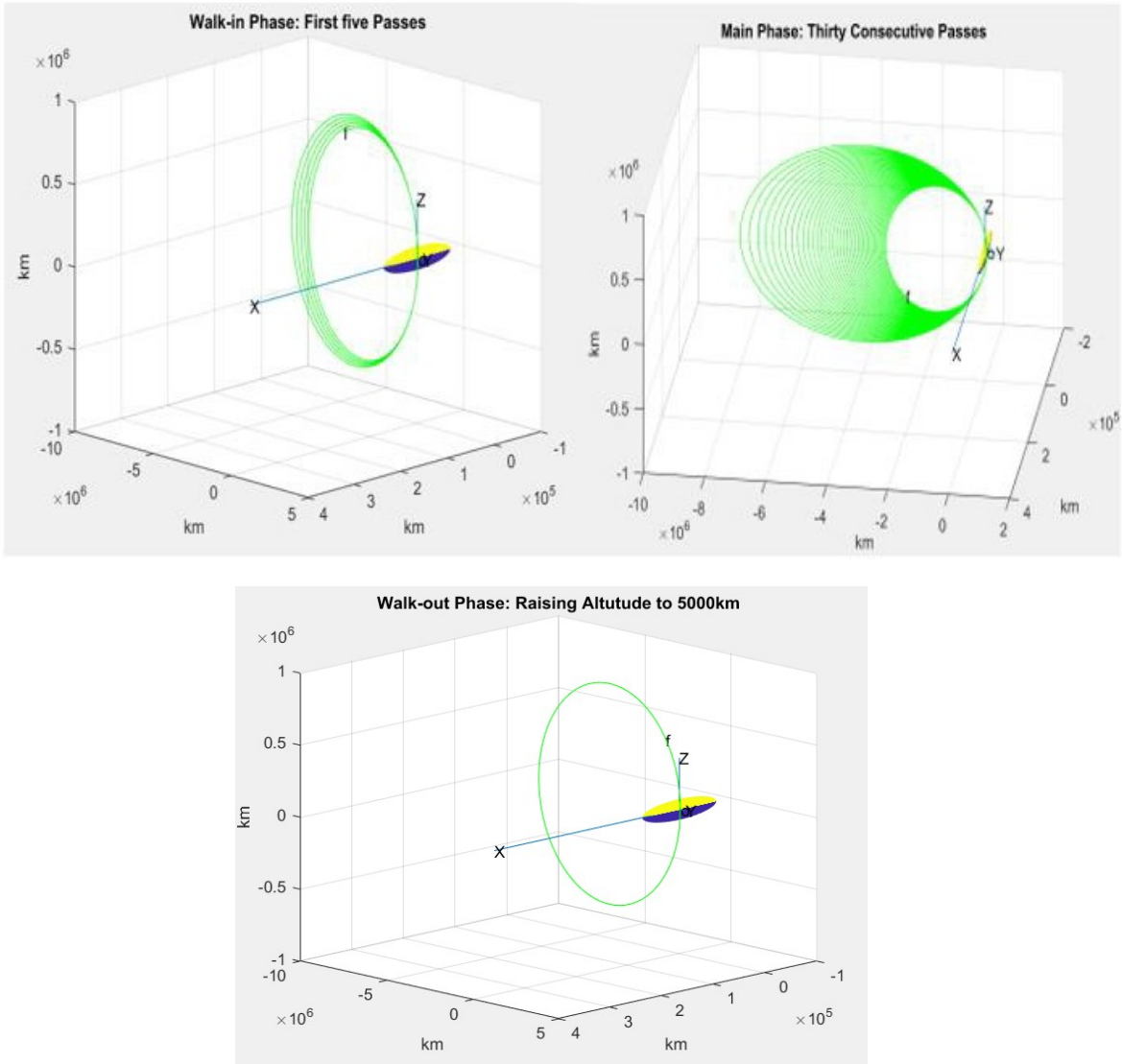

Fig. 1: Aerobraking phase visualization in MATLAB

6.2.2 Heat analysis on the spacecraft during the atmospheric pass

Table 6.2.2.1: Freestream conditions

Name	Value
Pressure (P_1)	0.03865 Pa
Temprature (T_1)	570.1 K
Velocity, (u_1)	59.11 km/s
Density (ρ_1)	1.78×10^{-9} kg/m^3

Sensitive enthalpy (h_1) (From CEA)	3,810,100 J/kg

Table 6.2.2.2: Composition of the gases in the atmosphere at 350 km

Species	Number of moles	Mole fraction
Hydrogen (H_2)	3.75×10^{-3}	0.9716
Helium (He)	9.99×10^{-5}	0.02569
Monoatomic Hydrogen (H)	1.04×10^{-5}	0.002696
Methane (CH_4)	4.18×10^{-10}	1.08×10^{-7}

Table 6.2.2.3: Downstream conditions of the normal shock at the stagnation point

Iteration	P_2 (Pa)	h_2 (J/kg)	ρ_2 (kg/m^3)	T_2 (K)
1	5.79	1742245869	1.8235×10^{-8}	39981.93
2	5.62	1734122319	1.7721×10^{-8}	39934.64
3	5.60	1733018199	1.766×10^{-8}	39928.9
4	5.60	1733020213	1.7661×10^{-8}	39928.18
5	5.60	1733020213	1.7661×10^{-8}	39928.2
6	**5.60**	**1733020213**	$\mathbf{1.7661 \times 10^{-8}}$	**39928.2**

6.3 Discussion

Aerobraking replaces propulsive burn to make the orbit smaller; however, the procedure takes a long to bring the orbit to its final shape. Therefore, it is a trade-off between time and money. A few hour burn is replaced by many months of the orbit reshaping via aerobraking. If the mission goal is to achieve the final orbit around the planet economically, and the time constraint is not a crucial factor for the mission timeline, aerobraking can be an appropriate choice given the operations can be carried out safely at the target planet. For the missions which have a relatively short timeline to achieve its goal, the aerobraking may not be the best method to choose. The orbit insertion around Jupiter using aerobraking to reduce the 54.2 days period to 14 days which was studied through this project takes nearly 3 years to complete the orbit reshaping using aerobraking. It is not suitable to take a long time to achieve the desired orbit in case of the Jovian mission because the intense radiation belts and the powerful magnetosphere can cause enough

harm to the spacecraft during this time. Thus, the spacecraft may not be able to perform the actual science for the mission objectives after being exposed to the harsh conditions around the planet during aerobraking. Typically, the science operations are not performed during aerobraking maneuvers because it might be very risky to do that. Hence, the aerobraking is not a good choice for a Jovian mission from the point of view of time requirement for orbit reshaping.

The preliminary analysis to find the temperature behind the normal shock at the stagnation point shows very large temperature values. At these temperatures, the gases will be radiative and heat transfer to the body will be dominated by the radiative heat from the extremely hot gases. It is not practical to cool the surface of the spacecraft at this temperature because the material from the spacecraft could melt in this scenario. The ablative material cannot be used as well because the ablation will become unstable at such a high temperature, and the ablation method for numerous atmospheric passes is not feasible due to mass loss from the surface which also affects the aerodynamics of the spacecraft. Thus, the atmospheric entry at 39,928.2 K is not feasible because the spacecraft can burn up in the atmosphere due to the high heat flux.

Aerobraking for the Jupiter mission include drawbacks like the long time for the orbit reshaping and a very high temperature generation during the atmospheric entry.

6.4 Conclusion

The conditions at Jupiter such as harmful radiation belts, powerful current systems, immensely powerful magnetic field, and the particles moving nearly at the speed of light pose challenges to the Jovian mission design. Making numerous passes for the orbit shaping means to increase the radiation dose for the spacecraft along with increasing the probability of the particle impact rate on the spacecraft. The time needed to perform the aerobraking for the Jovian mission is not practical because of the presence of harsh conditions around the planet. The heat analysis also shows the unrealistic temperature generation downstream of the shock at the stagnation point. Hence, the aerobraking at Jupiter is not feasible due to the harmful conditions at the planet, a large time requirement for the maneuvers, and the extremely high heat transfer to the spacecraft body.